On the effect of disorder on band structures

An analytical study of the effects of disorder on the BHZ Hamiltonian and an extended BHZ Hamiltonian

Marnix Huibers

Delft University of Technology
Faculty of Applied Sciences

with supervision of R. J. Skolasinski (MSc.), Dr. A. R. Akhmerov and Dr. M. T. Wimmer

July 23, 2017

Master Thesis

TU Delft

Contents

1 Introduction

A conductor in practice (almost) always has imperfections, such as foreign atoms substituting for atoms of the crystal, vacancies due to missing atoms or dislocations in the crystal. These defects will scatter electrons in the conductor. The effect on the electron motion of such imperfections, can be modelled by defining a potential which deviates from that of an ideal crystal. When a crystal contain impurities, it is usually impossible to know what the exact potential landscape is. Therefore, are experimental observations often best modelled by calculating ensemble averages. Assumptions are made about properties of the impurities. Then, the members of the ensemble, which typically all have a different disorder configuration, are generated and subsequently averaged. The averaged potentials can be used to alter the Hamiltonian and study the difference between clean and disordered systems.

Finding new topologically non-trivial states of matter is an important goal in condensed matter physics[1]. The quantum Hall state was the first example of such a state[2],[3],[4],[5]. Another proposed state is the quantum spin hall (QSH) insulator[1],[6]. The QSH insulator is invariant under time reversal and the 2D bulk is gapped. There are topologically protected edge states that lie inside the bulk insulating gap. These edge states are helical, which means that at a given edge there are two[1] states with opposite spin-polarization counter propagating. The two counter propagating modes are time-reversed partners of each other and because their wave functions are orthogonal, there is no scattering between these two states. If an electron would be reflected, its spin must be flipped. However, such a spin-flip is forbidden, because it would break time reversal symmetry. The BHZ Hamiltonian[6] can be used to describe the QSH insulator. The effect of average disorder on the BHZ Hamiltonian is investigated in this research. By altering the Hamiltonian in order to take the averaged potentials into account (see previous paragraph), the disordered band structure can be calculated and subsequently compared to the clean one.

Symmetry plays a central role in quantum mechanics and in physics in general. When a symmetry is present, a feature of the system remains unchanged under some transformation, such as a rotation or inversion in space or time. Mathematically, the operators associated with these transformations are called symmetry operators and commute or anti-commute with the Hamiltonian. By using the commutation relations, the constraints, which the presence of symmetries impose on the Hamiltonian, can be found. By starting from a 3-band basis and imposing symmetry constraints, an extended BHZ Hamiltonian can be derived[7]. The effect of average disorder is studied on the band structure of the aforementioned Hamiltonian.

Section 2.1 introduces the Green's function, which tells how a system reacts to an impulse response. The role of the Green's function in quantum mechanics is discussed and specifically how it relates to the Hamiltonian. The objective of this section is to introduce the equations governing the Green's functions, which are later used to capture the effect of disorder.

Section 2.2 introduces the tight-binding approach. The objective of this section is to show how the connection is made from continuous functions to computer simulations. It involves defining a lattice that can have any shape. Operators and functions are discretized and the quantities of the system are only defined on the lattice points.

In section 2.3, the diagrammatic impurity-average technique is presented. After stating assumptions about the disorder properties, theory from the previous two sections is used to find an analytical expression for the impurity averaged Green's function. The concept of the self-energy is introduced and eventually the first order self-consistent Born equation is derived.

In section 3.1, the first order self-consistent Born approximation is tested on relatively simple Hamiltonians. By considering for example an infinite quantum well, its validity can be assessed. The effect the disorder has on the band structure is discussed.

In section 3.2, the theory is applied to the more interesting BHZ Hamiltonian and an extended BHZ Hamiltonian. It is visualized how the disorder influences the band structure of the aforementioned Hamiltonians and it is discussed how the disorder changes the transport properties of a sample. It is shown that by plotting the disordered band structures, the results of a transport calculation can be qualitatively predicted.

[1] When there is an even number of pairs of helical edge states, interactions can open a gap and the system is topologically trivial. However, when there is an odd number of pairs of helical edge states, interactions can not open a gap unless time reversal symmetry is broken. For simplicity it is assumed here that there is one pair of helical edge states at each edge.

In this work the software package Kwant[8] is extensively used. It is a free (open source) Python package for numerical calculations on tight-binding models. With Kwant, one can among other things calculate dispersions, wave functions, Green's functions and transport properties.

During my studies I became interested in condensed matter physics. I would like to thank Dr. A. R. Akhmerov and Dr. M. T. Wimmer for giving me the opportunity to work in their group and in this field. On many occasions I have benefited from their guidance. In addition, I would like to express my gratitude to R. J. Skolasinski (MSc). We had many discussions and I thank him for sharing his programming knowledge as well as proofreading drafts.

2 Theory

2.1 Green's functions

2.1.1 General discussion of Green's functions

The theory in section 2.1 is based on [9], [10] and [11]. The Green's function gives the response of a system at every position $\bar{r}$, and every time t, due to a delta peak forcing at a certain position $\bar{r}'$, and at a certain time t'. Consider the general differential equation and the equation for the Green's function

$$\hat{\mathcal{L}}\left\{\psi(\bar{r},t)\right\} = f(\bar{r},t), \tag{2.1.1a}$$

$$\text{then: } \hat{\mathcal{L}}\left\{G(\bar{r},t;\bar{r}',t')\right\} = \delta(\bar{r}-\bar{r}')\delta(t-t'), \tag{2.1.1b}$$

where $\hat{\mathcal{L}}$ is a linear operator, $G(\bar{r},t;\bar{r}',t')$ is the Green's function and $f(\bar{r},t)$ is the source term of the differential equation. Since the source term, $f(\bar{r},t)$, can be seen as a superposition of delta forcings, the solution involves a sum over the Green's functions. This superposition principle only holds if $\hat{\mathcal{L}}$ is a linear operator. This intuitive notion can be shown more clearly by doing

$$\int\int_V \hat{\mathcal{L}}\left\{G(\bar{r},t;\bar{r}',t')\right\} f(\bar{r}',t')d^3\bar{r}'dt' = \int\int_V \delta(\bar{r}-\bar{r}')\delta(t-t')f(\bar{r}',t')d^3\bar{r}'dt' = f(\bar{r},t) = \hat{\mathcal{L}}\left\{\psi(\bar{r},t)\right\}.$$

Now use that $\hat{\mathcal{L}}$ in the most left part of the the equation above, only operates on $\bar{r}$ and t and therefore it can be taken out of the integral

$$\hat{\mathcal{L}}\left\{\int\int_V G(\bar{r},t;\bar{r}',t')f(\bar{r}',t')d^3\bar{r}'dt'\right\} = \hat{\mathcal{L}}\left\{\psi(\bar{r},t)\right\},$$

which suggests

$$\psi(\bar{r},t) = \int\int_V G(\bar{r},t;\bar{r}',t')f(\bar{r}',t')d^3\bar{r}'dt'.$$

The derivation above is not rigorous, usually there are additional terms involving an integral over the Green's function, which account for the the boundary and initial conditions. The boundary and initial conditions can also be viewed as forcings on the solution. When the linear operator $\hat{\mathcal{L}}$ is known, usually Green's second identity can be used to find the solution as a function of the Green's function. As an example a derivation, where the solution for the three dimensional non-homogeneous wave equation is expressed in terms of several integrals over the Green's function, can be found in appendix A.2. In this derivation is used that the Green's function is symmetric under exchange of $\bar{r}$ and $\bar{r}'$. This symmetry is called Maxwell's reciprocity and it is proven for the time-independent case in appendix A.1. Intuitively this symmetry makes sense; if the space is isotropic, it does not matter whether you excite the system at position $\bar{r}'$ and measure at $\bar{r}$ or excite at position $\bar{r}$ and measure at $\bar{r}'$.

When solving a differential equation with non-homogeneous boundary conditions, the Green's function always satisfies homogeneous boundary conditions. The Green's function is defined as the response of the system to a delta forcing only and therefore there should be no forcing from the boundaries. An advantage of the use of Green's functions is that when the source term of the differential equation, the boundary condition or the initial state of the system are changed, it is not necessary to repeat an entire calculation as long as the linear operator $\hat{\mathcal{L}}$ stays the same. The general solution of the differential equation is expressed as integrals over the Green's function, which involve the forcing function, the boundary condition and the initial state of the system. By simply adjusting the integrands of the integrals, the changes in the forcing function, the boundary or initial conditions can be incorporated.

There are two kinds of solutions to the equation for the Green's function: the retarded and the advanced Green's function[2]. Let $\hat{G}^+(\bar{r},t;\bar{r}',t')$ be the retarded Green's function and $\hat{G}^-(\bar{r},t;\bar{r}',t')$ the advanced

[2]Besides the retarded and advanced Green's function also the greater and the lesser Green's function are often defined. These Green's functions will not be used in this work.

Green's function, with the following properties

$$\hat{G}^+(\bar{r},t;\bar{r}',t') = 0 \quad \text{for} \quad t < t', \tag{2.1.2a}$$

$$\hat{G}^-(\bar{r},t;\bar{r}',t') = 0 \quad \text{for} \quad t > t'. \tag{2.1.2b}$$

As the retarded Green's function, $\hat{G}^+(\bar{r},t;\bar{r}',t')$, can only take on non-zero values for times after the delta forcing has taken place, the retarded Green's function is causal. It can then also be seen that the advanced Green's function, $\hat{G}^-(\bar{r},t;\bar{r}',t')$, is anti-causal, because it has only non-zero values before the excitation occurs.

From now on the the Green's function is considered to be an operator, so that

$$\hat{\mathcal{L}}\ \hat{G}(t;t') = \delta(t-t')\hat{I}. \tag{2.1.3}$$

The Green's function can then be viewed as the right inverse of $\hat{\mathcal{L}}$.

2.1.2 Green's functions in quantum mechanics

In the case of the Schrödinger equation

$$\left(i\hbar\frac{\partial}{\partial t} - \hat{H}\right)|\psi(t)\rangle = 0, \tag{2.1.4}$$

the linear operator $\hat{\mathcal{L}}$ is equal to $\left(i\hbar\frac{\partial}{\partial t} - \hat{H}\right)$. The solution to this equation is

$$|\psi(t)\rangle = e^{-\frac{i}{\hbar}\hat{H}(t-t')}\,|\psi(t=t')\rangle = \hat{U}(t,t')\,|\psi(t')\rangle\,, \tag{2.1.5}$$

where $\hat{U}(t,t')$ is the time evolution operator. The equation for the Green's function is

$$\left(i\hbar\frac{\partial}{\partial t} - \hat{H}\right)\hat{G}^{\pm}(t;t') = \hat{\mathcal{L}}\ \hat{G}^{\pm}(t;t') = \delta(t-t')\hat{I}. \tag{2.1.6}$$

Only the time or energy dependence of the Green's functions are written throughout section 2.1, but the Green's functions are also functions of position, momentum or wavevector depending on the chosen basis, for example: $\langle\hat{p}|\,\hat{G}^{\pm}(t;t')\,|\hat{p}'\rangle = G^{\pm}(\bar{p},t;\bar{p}',t')$.

The solution to equation (2.1.6) for the retarded and advanced Green's function is

$$\hat{G}^+(t;t') = \begin{cases} -\frac{i}{\hbar}e^{-i\hat{H}(t-t')/\hbar} & \text{for } t > t' \\ 0 & \text{for } t < t' \end{cases} \quad = \quad -\frac{i}{\hbar}\hat{U}(t,t')\Theta(t-t'), \tag{2.1.7}$$

$$\hat{G}^-(t;t') = \begin{cases} 0 & \text{for } t > t' \\ \frac{i}{\hbar}e^{-i\hat{H}(t-t')/\hbar} & \text{for } t < t' \end{cases} \quad = \quad \frac{i}{\hbar}\hat{U}(t,t')\left(1-\Theta(t-t')\right), \tag{2.1.8}$$

where $\Theta(t-t')$ is the Heaviside step function. It can be verified that these are the solutions by substituting them into equation (2.1.6) and using $\left[\hat{H},\hat{U}(t,t')\right] = 0$.

Inverting equations (2.1.7) and (2.1.8) give

$$\hat{U}(t,t') = \begin{cases} i\hbar\hat{G}^+(t;t') & \text{for } t > t' \\ -i\hbar\hat{G}^-(t;t') & \text{for } t < t'. \end{cases} \tag{2.1.9}$$

Equation (2.1.9) can be presented equivalently as $\hat{U}(t,t') = i\hbar(\hat{G}^+(t;t') - \hat{G}^-(t;t'))$. Besides the time evolution operator, this operator is also known as the spectral function

$$A(t,t') \equiv i\hbar(\hat{G}^+(t;t') - \hat{G}^-(t;t')). \tag{2.1.10}$$

Using equations (2.1.5) and (2.1.9), the solution of the Schrödinger equation is written in terms of the retarded and advanced Green's function

$$|\psi(t)\rangle = \begin{cases} i\hbar\hat{G}^{+}(t;t')\,|\psi(t')\rangle & \text{for } t > t' \\ -i\hbar\hat{G}^{-}(t;t')\,|\psi(t')\rangle & \text{for } t < t'. \end{cases} \tag{2.1.11}$$

It can be seen from $|\psi(t)\rangle = i\hbar\hat{G}^{+}(t;t')\,|\psi(t')\rangle$ for $t > t'$, that the retarded Green's function propagates the wave function. The wave function at a certain time is used to calculate the wave function for a later time, while from $|\psi(t)\rangle = -i\hbar\hat{G}^{-}(t;t')\,|\psi(t')\rangle$ for $t < t'$, it is seen that the advanced Green's function is used to calculate the wave function at a certain time from the wave function in the future.

Further the Hermitian conjugate of $\hat{G}^{+}(t;t')$ is equal to $\hat{G}^{-}(t';t)$:

$$\left(\hat{G}^{+}(t;t')\right)^{\dagger} = \frac{i}{\hbar}e^{i\hat{H}^{\dagger}(t-t')/\hbar}\Theta(t-t') = \frac{i}{\hbar}e^{-i\hat{H}(-(t-t'))/\hbar}\left[1-\Theta(-(t-t'))\right] = \hat{G}^{-}(-t;-t') = \hat{G}^{-}(t';t). \tag{2.1.12}$$

So far time-dependent Green's functions were considered. The time-independent Green's functions can be obtained by taking the Fourier transform of the time-dependent ones (equation (2.1.7) and (2.1.8)):

$$\hat{G}^{+}(E) = \mathcal{F}_{\epsilon}\left\{\hat{G}^{+}(t;t')\right\} = \int_{-\infty}^{\infty}\hat{G}^{+}(t;t')e^{iE(t-t')/\hbar}e^{-\epsilon(t-t')/\hbar}dt = \int_{t'}^{\infty}\hat{G}^{+}(t;t')e^{iE(t-t')/\hbar}e^{-\epsilon(t-t')/\hbar}dt, \tag{2.1.13a}$$

$$\hat{G}^{-}(E) = \mathcal{F}_{\epsilon}\left\{\hat{G}^{-}(t;t')\right\} = \int_{-\infty}^{\infty}\hat{G}^{-}(t;t')e^{iE(t-t')/\hbar}e^{+\epsilon(t-t')/\hbar}dt = \int_{-\infty}^{t'}\hat{G}^{-}(t;t')e^{iE(t-t')/\hbar}e^{\epsilon(t-t')/\hbar}dt. \tag{2.1.13b}$$

The infinitesimal small number $\epsilon > 0$ is introduced to make sure the integrals converge. The integrals in equations (2.1.13a) and (2.1.13b) can be evaluated as

$$\hat{G}^{+}(E) = \int_{t'}^{\infty} -\frac{i}{\hbar}e^{-i\hat{H}(t-t')/\hbar}e^{iE(t-t')/\hbar}e^{-\epsilon(t-t')/\hbar}dt = \frac{\hat{I}}{E+i\epsilon-\hat{H}}, \tag{2.1.14a}$$

$$\hat{G}^{-}(E) = \int_{-\infty}^{t'} \frac{i}{\hbar}e^{-i\hat{H}(t-t')/\hbar}e^{iE(t-t')/\hbar}e^{\epsilon(t-t')/\hbar}dt = \frac{\hat{I}}{E-i\epsilon-\hat{H}}. \tag{2.1.14b}$$

Clearly from (2.1.14a) and (2.1.14b)

$$\left[\hat{G}^{+}(E)\right]^{\dagger} = \hat{G}^{-}(E). \tag{2.1.15}$$

In the steps above, the Hamiltonian can be replaced by $\hat{H}_0$, which contains only the kinetic part of the full Hamiltonian. The retarded and advanced Green's function are then denoted by $\hat{G}_0^{\pm}(t;t')$ or in the time-independent case $\hat{G}_0^{\pm}(E)$. For clarity and later references equations (2.1.7), (2.1.8), (2.1.14a) and (2.1.14b) are repeated for the free Green's functions:

$$\hat{G}_0^{+}(t;t') = \begin{cases} -\frac{i}{\hbar}e^{-i\hat{H}_0(t-t')/\hbar} & \text{for } t > t' \\ 0 & \text{for } t < t' \end{cases} = -\frac{i}{\hbar}\hat{U}_0(t,t')\Theta(t-t'), \tag{2.1.16}$$

$$\hat{G}_0^{-}(t;t') = \begin{cases} 0 & \text{for } t > t' \\ \frac{i}{\hbar}e^{-i\hat{H}_0(t-t')/\hbar} & \text{for } t < t' \end{cases} = \frac{i}{\hbar}\hat{U}_0(t,t')\left(1-\Theta(t-t')\right), \tag{2.1.17}$$

$$\hat{G}_0^{+}(E) = \frac{\hat{I}}{E+i\epsilon-\hat{H}_0}, \tag{2.1.18a}$$

$$\hat{G}_0^{-}(E) = \frac{\hat{I}}{E-i\epsilon-\hat{H}_0}. \tag{2.1.18b}$$

2.1.3 Lippmann-Schwinger equation

The Lippmann-Schwinger equation gives the relation between the free and the full Green's function. We start from the Schrödinger equation for the free and full Hamiltonian

$$\left(i\hbar\frac{\partial}{\partial t} - \hat{H}_0\right)|\psi(t)\rangle = 0,$$
$$\left(i\hbar\frac{\partial}{\partial t} - \hat{H}_0 - \hat{V}\right)|\psi(t)\rangle = 0.$$

The equations for the Green's functions are

$$\left(i\hbar\frac{\partial}{\partial t} - \hat{H}_0\right)\hat{G}_0^{\pm}(t;t') = \delta(t-t')\hat{I}, \tag{2.1.20a}$$
$$\left(i\hbar\frac{\partial}{\partial t} - \hat{H}_0 - \hat{V}\right)\hat{G}^{\pm}(t;t') = \delta(t-t')\hat{I}. \tag{2.1.20b}$$

The solution of equation (2.1.20b) can be written as an integral equation

$$\hat{G}^+(t;t') = \hat{G}_0^+(t;t') + \int_{t'}^{t}\hat{G}_0^+(t;\tilde{t})\hat{V}\hat{G}^+(\tilde{t};t')d\tilde{t} = \hat{G}_0^+(t;t') + \int_{t'}^{t}\hat{G}^+(t;\tilde{t})\hat{V}\hat{G}_0^+(\tilde{t};t')d\tilde{t}, \tag{2.1.21a}$$
$$\hat{G}^-(t;t') = \hat{G}_0^-(t;t') + \int_{t}^{t'}\hat{G}_0^-(t;\tilde{t})\hat{V}\hat{G}^-(\tilde{t};t')d\tilde{t} = \hat{G}_0^-(t;t') + \int_{t}^{t'}\hat{G}^-(t;\tilde{t})\hat{V}\hat{G}_0^-(\tilde{t};t')d\tilde{t}. \tag{2.1.21b}$$

It is verified that the presented solution for $\hat{G}^+(t;t')$ in equation (2.1.21a), satisfies the equation for the Green's function, equation (2.1.20b), by substituting it

$$i\hbar\frac{\partial}{\partial t}\hat{G}_0^+(t;t') + i\hbar\frac{\partial}{\partial t}\int_{t'}^{t}\hat{G}^+(t;\tilde{t})\hat{V}\hat{G}_0^+(\tilde{t};t')d\tilde{t} - \hat{H}_0\hat{G}_0^+(t;t') - \hat{H}_0\int_{t'}^{t}\hat{G}^+(t;\tilde{t})\hat{V}\hat{G}_0^+(\tilde{t};t')d\tilde{t} -$$
$$\hat{V}\hat{G}_0^+(t;t') - \hat{V}\int_{t'}^{t}\hat{G}^+(t;\tilde{t})\hat{V}\hat{G}_0^+(\tilde{t};t')d\tilde{t} \stackrel{?}{=} \delta(t-t')\hat{I}.$$

The first and third term are together equal to $\delta(t-t')\hat{I}$ by equation (2.1.20a), further the derivative with respect to time in the second term can be taken into the integral as well as the $\hat{H}_0$ in the fourth term and $\hat{V}$ in the last term

$$\delta(t-t')\hat{I} + \int_{t'}^{t}i\hbar\frac{\partial}{\partial t}\hat{G}^+(t;\tilde{t})\hat{V}\hat{G}_0^+(\tilde{t};t')d\tilde{t} - \int_{t'}^{t}\hat{H}_0\hat{G}^+(t;\tilde{t})\hat{V}\hat{G}_0^+(\tilde{t};t')d\tilde{t} -$$
$$\hat{V}\hat{G}_0^+(t;t') - \int_{t'}^{t}\hat{V}\hat{G}^+(t;\tilde{t})\hat{V}\hat{G}_0^+(\tilde{t};t')d\tilde{t} \stackrel{?}{=} \delta(t-t')\hat{I}.$$

This can be rewritten to

$$\delta(t-t')\hat{I} + \int_{t'}^{t}\left[i\hbar\frac{\partial}{\partial t} - \hat{H}_0 - \hat{V}\right]\hat{G}^+(t;\tilde{t})\hat{V}\hat{G}_0^+(\tilde{t};t')d\tilde{t} - \hat{V}\hat{G}_0^+(t;t') \stackrel{?}{=} \delta(t-t')\hat{I}.$$

Using equation (2.1.20b) for the second term

$$\delta(t-t')\hat{I} + \int_{t'}^{t}\delta(t-\tilde{t})\hat{I}\hat{V}\hat{G}_0^+(\tilde{t};t')d\tilde{t} - \hat{V}\hat{G}_0^+(t;t') \stackrel{?}{=} \delta(t-t')\hat{I},$$

$$\delta(t-t')\hat{I} + \hat{V}\hat{G}_0^+(t;t') - \hat{V}\hat{G}_0^+(t;t') \stackrel{?}{=} \delta(t-t')\hat{I},$$

$$\delta(t-t')\hat{I} = \delta(t-t')\hat{I}.$$

Indeed the presented solution for $\hat{G}^+(t;t')$ satisfies the equation for the Green's function. A similar procedure can be done for $\hat{G}^-(t;t')$.

The set of equations (2.1.21a) and (2.1.21b) are called the time-dependent Lippmann-Schwinger equations. It gives the relation between the free Green's function and the full Green's function. By taking the Fourier transform, $\hat{G}^{\pm}(E) = \mathcal{F}_\epsilon\left\{\hat{G}^{\pm}(t;t')\right\}$, the time-independent counterpart is found

$$\hat{G}^+(E) = \hat{G}_0^+(E) + \int_{t'}^{\infty}\left[\int_{t'}^{t}\hat{G}_0^+(t;\tilde{t})\hat{V}\hat{G}^+(\tilde{t};t')d\tilde{t}\right]e^{iE(t-t')/\hbar}e^{-\epsilon(t-t')/\hbar}dt =$$
$$\hat{G}_0^+(E) + \int_{t'}^{\infty}\left[\int_{t'}^{t}\hat{G}^+(t;\tilde{t})\hat{V}\hat{G}_0^+(\tilde{t};t')d\tilde{t}\right]e^{iE(t-t')/\hbar}e^{-\epsilon(t-t')/\hbar}dt,$$

$$\hat{G}^-(E) = \hat{G}_0^-(E) + \int_{-\infty}^{t'}\left[\int_{t}^{t'}\hat{G}_0^-(t;\tilde{t})\hat{V}\hat{G}^-(\tilde{t};t')d\tilde{t}\right]e^{iE(t-t')/\hbar}e^{\epsilon(t-t')/\hbar}dt =$$
$$\hat{G}_0^-(E) + \int_{-\infty}^{t'}\left[\int_{t}^{t'}\hat{G}^-(t;\tilde{t})\hat{V}\hat{G}_0^-(\tilde{t};t')d\tilde{t}\right]e^{iE(t-t')/\hbar}e^{\epsilon(t-t')/\hbar}dt.$$

The infinitesimal small number $\epsilon > 0$ is introduced in the Fourier transform to make sure the integrals converge. Among other things, interchanging the order of the integrals gives

$$\hat{G}^+(E) = \hat{G}_0^+(E) + \int_{t'}^{t}\left[\int_{t'}^{\infty}\hat{G}_0^+(t;\tilde{t})e^{iE(t-\tilde{t})/\hbar}e^{-\epsilon(t-\tilde{t})/\hbar}dt\right]\hat{V}\hat{G}^+(\tilde{t};t')e^{iE(\tilde{t}-t')/\hbar}e^{-\epsilon(\tilde{t}-t')/\hbar}d\tilde{t} =$$
$$\hat{G}_0^+(E) + \int_{t'}^{t}\left[\int_{t'}^{\infty}\hat{G}^+(t;\tilde{t})e^{iE(t-\tilde{t})/\hbar}e^{-\epsilon(t-\tilde{t})/\hbar}dt\right]\hat{V}\hat{G}_0^+(\tilde{t};t')e^{iE(\tilde{t}-t')/\hbar}e^{-\epsilon(\tilde{t}-t')/\hbar}d\tilde{t},$$

$$\hat{G}^-(E) = \hat{G}_0^-(E) + \int_{t}^{t'}\left[\int_{-\infty}^{t'}\hat{G}_0^-(t;\tilde{t})e^{iE(t-\tilde{t})/\hbar}e^{\epsilon(t-\tilde{t})/\hbar}dt\right]\hat{V}\hat{G}^-(\tilde{t};t')e^{iE(\tilde{t}-t')/\hbar}e^{-\epsilon(\tilde{t}-t')/\hbar}d\tilde{t} =$$
$$\hat{G}_0^-(E) + \int_{t}^{t'}\left[\int_{-\infty}^{t'}\hat{G}^-(t;\tilde{t})e^{iE(t-\tilde{t})/\hbar}e^{\epsilon(t-\tilde{t})/\hbar}dt\right]\hat{V}\hat{G}_0^-(\tilde{t};t')e^{iE(\tilde{t}-t')/\hbar}e^{-\epsilon(\tilde{t}-t')/\hbar}d\tilde{t}.$$

The expressions in the square brackets are equal to $G_0^{\pm}(E)$ or $G^{\pm}(E)$

$$\hat{G}^+(E) = \hat{G}_0^+(E) + \hat{G}_0^+(E)\hat{V}\int_{t'}^{t}\hat{G}^+(\tilde{t};t')e^{iE(\tilde{t}-t')/\hbar}e^{-\epsilon(\tilde{t}-t')/\hbar}d\tilde{t} =$$
$$\hat{G}_0^+(E) + \hat{G}^+(E)\hat{V}\int_{t'}^{t}\hat{G}_0^+(\tilde{t};t')e^{iE(\tilde{t}-t')/\hbar}e^{-\epsilon(\tilde{t}-t')/\hbar}d\tilde{t},$$

$$\hat{G}^-(E) = \hat{G}_0^-(E) + \hat{G}_0^-(E)\hat{V}\int_{t}^{t'}\hat{G}^-(\tilde{t};t')e^{iE(\tilde{t}-t')/\hbar}e^{-\epsilon(\tilde{t}-t')/\hbar}d\tilde{t} =$$
$$\hat{G}_0^-(E) + \hat{G}^-(E)\hat{V}\int_{t}^{t'}\hat{G}_0^-(\tilde{t};t')e^{iE(\tilde{t}-t')/\hbar}e^{-\epsilon(\tilde{t}-t')/\hbar}d\tilde{t}.$$

The last integrals can now be evaluated, giving the time-independent Lippmann-Schwinger equations:

$$\hat{G}^+(E) = \hat{G}_0^+(E) + \hat{G}_0^+(E)\hat{V}\hat{G}^+(E) = \hat{G}_0^+(E) + \hat{G}^+(E)\hat{V}\hat{G}_0^+(E), \tag{2.1.22a}$$
$$\hat{G}^-(E) = \hat{G}_0^-(E) + \hat{G}_0^-(E)\hat{V}\hat{G}^-(E) = \hat{G}_0^-(E) + \hat{G}^-(E)\hat{V}\hat{G}_0^-(E). \tag{2.1.22b}$$

The time-dependent and time-independent Lippmann-Schwinger equations are repeated below for clarity and later reference:

$$\hat{G}^+(t;t') = \hat{G}_0^+(t;t') + \int_{t'}^{t} \hat{G}_0^+(t;\tilde{t})\hat{V}\hat{G}^+(\tilde{t};t')d\tilde{t} = \hat{G}_0^+(t;t') + \int_{t'}^{t} \hat{G}^+(t;\tilde{t})\hat{V}\hat{G}_0^+(\tilde{t};t')d\tilde{t}, \tag{2.1.23a}$$

$$\hat{G}^-(t;t') = \hat{G}_0^-(t;t') + \int_{t}^{t'} \hat{G}_0^-(t;\tilde{t})\hat{V}\hat{G}^-(\tilde{t};t')d\tilde{t} = \hat{G}_0^-(t;t') + \int_{t}^{t'} \hat{G}^-(t;\tilde{t})\hat{V}\hat{G}_0^-(\tilde{t};t')d\tilde{t}, \tag{2.1.23b}$$

$$\hat{G}^+(E) = \hat{G}_0^+(E) + \hat{G}_0^+(E)\hat{V}\hat{G}^+(E) = \hat{G}_0^+(E) + \hat{G}^+(E)\hat{V}\hat{G}_0^+(E), \tag{2.1.24a}$$

$$\hat{G}^-(E) = \hat{G}_0^-(E) + \hat{G}_0^-(E)\hat{V}\hat{G}^-(E) = \hat{G}_0^-(E) + \hat{G}^-(E)\hat{V}\hat{G}_0^-(E). \tag{2.1.24b}$$

2.1.4 Born series and Dyson's equation

As a first approximation (Born approximation) the full Green's functions in the integrals of equations (2.1.23a) and (2.1.23b) can be replaced by free ones

$$\hat{G}^+(t;t') = \hat{G}_0^+(t;t') + \int_{t'}^{t} \hat{G}_0^+(t;\tilde{t})\hat{V}\hat{G}_0^+(\tilde{t};t')d\tilde{t}, \tag{2.1.25a}$$

$$\hat{G}^-(t;t') = \hat{G}_0^-(t;t') + \int_{t}^{t'} \hat{G}_0^-(t;\tilde{t})\hat{V}\hat{G}_0^-(\tilde{t};t')d\tilde{t}. \tag{2.1.25b}$$

By putting equation (2.1.25a) back into (2.1.23a) and (2.1.25b) back into (2.1.23b) the next term of the approximation is obtained. The series that arises when this procedure is continued is called the Born series:

$$\hat{G}^+(t;t') = \hat{G}_0^+(t;t') + \int_{t'}^{t} \hat{G}_0^+(t;\tilde{t})\hat{V}\hat{G}_0^+(\tilde{t};t')d\tilde{t} + \int_{t'}^{t} dt_1 \int_{t'}^{t_1} dt_2\ \hat{G}_0^+(t;t_1)\hat{V}\hat{G}_0^+(t_1;t_2)\hat{V}\hat{G}_0^+(t_2;t') + \dots\ , \tag{2.1.26a}$$

$$\hat{G}^-(t;t') = \hat{G}_0^-(t;t') + \int_{t}^{t'} \hat{G}_0^-(t;\tilde{t})\hat{V}\hat{G}_0^-(\tilde{t};t')d\tilde{t} + \int_{t}^{t'} dt_1 \int_{t_1}^{t'} dt_2\ \hat{G}_0^-(t;t_1)\hat{V}\hat{G}_0^-(t_1;t_2)\hat{V}\hat{G}_0^-(t_2;t') + \dots\ . \tag{2.1.26b}$$

The Born series for the retarded Green's function, equation (2.1.26a), has an intuitive physical interpretation. The full Green's function is a sum of scattering events. The zeroth order term corresponds to no scattering event; there is free propagation from t' to t. The first order term corresponds to free propagation from t' to $\tilde{t}$, then an interaction occurs, followed by free propagation from $\tilde{t}$ to time t. The series continues this way, every higher order term has one more scattering event than the previous term.

Following a similar procedure, the Born series for the time-independent case can be found:

$$\hat{G}^+(E) = \hat{G}_0^+(E) + \hat{G}_0^+(E)\hat{V}\hat{G}_0^+(E) + \hat{G}_0^+(E)\hat{V}\hat{G}_0^+(E)\hat{V}\hat{G}_0^+(E) + \dots\ , \tag{2.1.27a}$$

$$\hat{G}^-(E) = \hat{G}_0^-(E) + \hat{G}_0^-(E)\hat{V}\hat{G}_0^-(E) + \hat{G}_0^-(E)\hat{V}\hat{G}_0^-(E)\hat{V}\hat{G}_0^-(E) + \dots\ . \tag{2.1.27b}$$

The effects of the scattering events can be lumped together using the self-energy:

$$\hat{G}^+(t;t') = \hat{G}_0^+(t;t') + \int_{t'}^{t} dt_1 \int_{t'}^{t} dt_2\ \hat{G}_0^+(t;t_1)\hat{\Sigma}^+(t_1;t_2)\hat{G}^+(t_2;t') = \tag{2.1.28a}$$

$$\hat{G}_0^+(t;t') + \int_{t'}^{t} dt_1 \int_{t'}^{t} dt_2\ \hat{G}^+(t;t_1)\hat{\Sigma}^+(t_1;t_2)\hat{G}_0^+(t_2;t'),$$

$$\hat{G}^-(t;t') = \hat{G}_0^-(t;t') + \int_{t}^{t'} dt_1 \int_{t}^{t'} dt_2\ \hat{G}_0^-(t;t_1)\hat{\Sigma}^-(t_1;t_2)\hat{G}^-(t_2;t') = \tag{2.1.28b}$$

$$\hat{G}_0^-(t;t') + \int_{t}^{t'} dt_1 \int_{t}^{t'} dt_2\ \hat{G}^-(t;t_1)\hat{\Sigma}^-(t_1;t_2)\hat{G}_0^-(t_2;t').$$

Similarly for the time-independent counterpart:

$$\hat{G}^{+}(E) = \hat{G}_0^{+}(E) + \hat{G}_0^{+}(E)\hat{\Sigma}^{+}(E)\hat{G}^{+}(E) = \hat{G}_0^{+}(E) + \hat{G}^{+}(E)\hat{\Sigma}^{+}(E)\hat{G}_0^{+}(E), \tag{2.1.29a}$$

$$\hat{G}^{-}(E) = \hat{G}_0^{-}(E) + \hat{G}_0^{-}(E)\hat{\Sigma}^{-}(E)\hat{G}^{-}(E) = \hat{G}_0^{-}(E) + \hat{G}^{-}(E)\hat{\Sigma}^{-}(E)\hat{G}_0^{-}(E). \tag{2.1.29b}$$

Equations (2.1.28a), (2.1.28b), (2.1.29a) and (2.1.29b) are are all Dyson's equations. Rewriting equation (2.1.29a) and (2.1.29b) leads to

$$\hat{G}^{\pm}(E) = \frac{\hat{I}}{\left[\hat{G}_0^{\pm}(E)\right]^{-1} - \hat{\Sigma}^{\pm}(E)} = \frac{\hat{I}}{E \pm i\epsilon - \hat{H}_0 - \hat{\Sigma}^{\pm}(E)}. \tag{2.1.30}$$

Because $\left[\hat{G}^{+}(E)\right]^{\dagger} = \hat{G}^{-}(E)$ (see equation (2.1.15)) it follows that

$$\left[\hat{\Sigma}^{+}(E)\right]^{\dagger} = \hat{\Sigma}^{-}(E). \tag{2.1.31}$$

2.2 Tight-binding

The theory in this section is based on [11] and [8]. So far, all the functions (e.g. the Green's function and wave function) were represented as continuous functions. Due too the complexity of problems, the system of interest is often studied with a computer simulation and it is therefore necessary to make a discretization. The approach that involves such a discretization is called tight-binding and it involves defining a lattice that can have any shape. Quantities of the system are only defined on the lattice points. Electrons that are localised at a certain site are influenced only by sites that are sufficiently close to them.

The continuous wave function is discretized as follows:

$$|\psi\rangle = \sum_i \psi_i \, |i\rangle \, , \tag{2.2.1}$$

where ψ_i are coefficients and $|i\rangle$ is a vector that corresponds with the i-th lattice site.

The non-interacting many particle Hamiltonian is then given by

$$\hat{H} = \sum_{i,j} H_{ij} \, |i\rangle \, \langle j| \, . \tag{2.2.2}$$

Here, $|i\rangle$ is a column vector, $\langle j|$ is a row vector, called ket and bra and H_{ij} are matrix elements. The diagonal elements of the matrix $\hat{H}$ represent the local chemical potential of the sites, while the off-diagonal elements give the interactions between the sites. These hopping terms are often chosen to be zero for sites that are further apart than nearest or next-nearest neighbours.

In order to clarify the tight binding approach an example is given of a 1D system with a certain potential landscape. The Hamiltonian is

$$\hat{H} = -\frac{\hbar^2}{2m}\frac{d^2}{dx^2} + V(x).$$

For simplicity, the Hamiltonian is discretized on a evenly spaced lattice with lattice constant a. The lattice sites are indicated by index i and thus $x = ia \equiv |i\rangle$.

In the Hamiltonian it can be seen that the second derivative with respect to position is needed. In order to obtain the expression for the second derivative at lattice site i, the discrete first forward derivative and the discrete first backward derivative are calculated first

$$\left.\frac{d\psi}{dx}\right|_{(i+\frac{1}{2})a} = \frac{\psi((i+1)a) - \psi(ia)}{a}, \tag{2.2.3a}$$

$$\left.\frac{d\psi}{dx}\right|_{(i-\frac{1}{2})a} = \frac{\psi(ia) - \psi((i-1)a)}{a}. \tag{2.2.3b}$$

The second derivative at lattice site i then becomes

$$\left.\frac{d^2\psi}{dx^2}\right|_{ia} = \frac{1}{a}\left(\left.\frac{d\psi}{dx}\right|_{(i+\frac{1}{2})a} - \left.\frac{d\psi}{dx}\right|_{(i-\frac{1}{2})a}\right),$$

$$\left.\frac{d^2\psi}{dx^2}\right|_{ia} = \frac{\psi((i+1)a) - 2\psi(ia) + \psi((i-1)a)}{a^2}. \tag{2.2.4}$$

The Hamiltonian acting on the wave function at lattice site i is then

$$\left[\hat{H}\psi\right]_{ia} = -\frac{\hbar^2}{2ma^2}\cdot\{\psi((i+1)a) - 2\psi(ia) + \psi((i-1)a)\} + V(ia). \tag{2.2.5}$$

Rewriting and defining $t = \frac{\hbar^2}{2ma^2}$ gives

$$\left[\hat{H}\psi\right]_{ia} = V(ia) + 2t\psi(ia) - t\left\{\psi((i+1)a) + \psi((i-1)a)\right\}. \tag{2.2.6}$$

Removing the test function (wave function) gives the matrix elements of $\hat{H}$:

$$H_{ij} = \begin{cases} V(ia) + 2t & \text{for } i = j \\ -t & \text{for } i \text{ and } j \text{ are nearest neighbours} \\ 0 & \text{otherwise.} \end{cases} \tag{2.2.7}$$

The tight-binding Hamiltonian thus is

$$\hat{H} = \sum_i (V(ia) + 2t)\left|i\right\rangle\left\langle i\right| - t\left(\left|i+1\right\rangle\left\langle i\right| + \left|i\right\rangle\left\langle i+1\right|\right). \tag{2.2.8}$$

This method can be generalized to higher dimensions. In general the matrix elements of $\hat{H}$ are given by

$$H_{ij} = \begin{cases} V(\bar{r}_i) + qt & \text{for } i = j \\ -t & \text{for } i \text{ and } j \text{ are nearest neighbours} \\ 0 & \text{otherwise,} \end{cases} \tag{2.2.9}$$

where q is the number of nearest neighbours for the chosen dimension.

2.3 Disordered conductors

2.3.1 General discussion disordered conductors

The theory in section 2.3 is based on [11] and [12]. Consider a metallic conductor placed between two leads. The conductor is not clean but disordered; there are foreign atoms that substituted atoms of the crystal, vacancies and other kinds of deviations from the perfect structure. The defects give rise to potentials that will scatter the electrons as they are moving through the conductor.

Take a conductor with N impurities located at $\bar{r}_1, \bar{r}_2, ...\bar{r}_N$ and let V be the volume of the conductor. Assume that all the impurities are of the same kind, which means that the potentials of the impurities are equal. The potential that the electrons feel due to the impurities is the sum of all the individual potentials

$$V(\bar{r}) = \sum_{i=1}^{N} V_{imp}(\bar{r} - \bar{r}_i). \tag{2.3.1}$$

Equation (2.3.1) can be written as an integral by introducing a density function which is a sum of delta functions

$$V(\bar{r}) = \sum_{i=1}^{N} V_{imp}(\bar{r} - \bar{r}_i) = \int_V d^3\bar{r}' V_{imp}(\bar{r} - \bar{r}')\rho(\bar{r}' - \bar{r}_i), \tag{2.3.2}$$

$$\rho(\bar{r}-\bar{r}_i)=\sum_{i=1}^{N}\delta(\bar{r}-\bar{r}_i). \tag{2.3.3}$$

Further a Fourier transform is introduced

$$\mathcal{F}\{f(\bar{r})\}=F(\bar{q})=\int_V d^3\bar{r}e^{-i\bar{q}\cdot\bar{r}}f(\bar{r}), \tag{2.3.4a}$$

$$\mathcal{F}^{-1}\{F(\bar{q})\}=f(\bar{r})=\frac{1}{(2\pi)^3}\int d^3\bar{q}e^{i\bar{q}\cdot\bar{r}}F(\bar{q}), \tag{2.3.4b}$$

where f is a test function. The Fourier transform is applied to the potential

$$V(\bar{q})=\mathcal{F}\{V(\bar{r})\}=\int_V d^3\bar{r}'e^{-i\bar{q}\cdot\bar{r}'}\sum_{i=1}^{N}V_{imp}(\bar{r}'-\bar{r}_i)=$$
$$\int_V d^3\bar{r}'e^{-i\bar{q}\cdot\bar{r}'}V_{imp}(\bar{r}'-\bar{r}_1)+\int_V d^3\bar{r}'e^{-i\bar{q}\cdot\bar{r}'}V_{imp}(\bar{r}'-\bar{r}_2)+\dots\ .$$

Apply a change in variables, $\tilde{r}=\bar{r}'-\bar{r}_i$, in order to evaluate the integrals

$$V(\bar{q})=V_{imp}(\bar{q})\sum_{i=1}^{N}e^{-i\bar{q}\cdot\bar{r}_i}. \tag{2.3.5}$$

The potential only depends on the distance between the electron and the impurity, therefore the argument $\bar{q}$ in equation (2.3.5) represents the difference between the ingoing and outgoing wavevector of the electron.

If the conductor has volume V in which N impurities are embedded, the mean distance between the impurities is equal to $(N/V)^{-1/d}=n^{-1/d}$, where d is the dimension. The conductor can be divided into small cells characterized by the lattice constant a. The lattice constant is usually smaller than the mean distance between the impurities. By letting the lattice constant go to zero, one can go to the continuous limit.

Let $P(\bar{r}_1,\bar{r}_2,...,\bar{r}_N)$ be the probability to have a certain configuration of impurities. If the positions of the impurities are independent then $P(\bar{r}_1,\bar{r}_2,...,\bar{r}_N)=P(\bar{r}_1)P(\bar{r}_2)...P(\bar{r}_N)$. If the probability density as a function of the position is uniform then $P(\bar{r}_i)=1/M$, where M is the total number of cells. If the cells are cubes $P(\bar{r}_i)=a^3/V$ and in the continuous limit $P(\bar{r}_i)=1/V$.

The expectation value of an observable is equal to the sum of the probability to get a certain configuration times the value of the observable for that configuration. For the continuous case, the expectation value of a variable F is given by

$$\langle F\rangle=\int_V P(\bar{r}_1,\bar{r}_2,...,\bar{r}_N)F(\bar{r}_1,\bar{r}_2,...,\bar{r}_N)\prod_{i=1}^{N}d^3\bar{r}_i. \tag{2.3.6}$$

For the independent random case in the continuous limit this simplifies to

$$\langle F\rangle=\frac{1}{V^N}\int_V F(\bar{r}_1,\bar{r}_2,...,\bar{r}_N)\prod_{i=1}^{N}d^3\bar{r}_i. \tag{2.3.7}$$

If a lattice would be considered, the pre-factor is changed to $\frac{a^{3N}}{V^N}$ and the integral would become a summation over all the lattice sites

$$\langle F\rangle=\frac{a^{3N}}{V^N}\prod_{i=1}^{N}\sum_{\{\bar{r}_i\}}F(\bar{r}_1,\bar{r}_2,...,\bar{r}_N). \tag{2.3.8}$$

In equation (2.3.8), $\{\bar{r}_i\}$ means that the coordinate of the i-th impurity is swept over all the lattice sites.

So far it was assumed that all the impurities were of the same kind. This can be a good approximation for certain systems, alternatively it can be assumed that the potentials of the impurities have a delta shape of

which the amplitudes are independently generated from a distribution with zero mean and that the positions in the conductor are random. Also in this case the conductor has N impurities located at $\bar{r}_1, \bar{r}_2, ..., \bar{r}_N$ and volume V. One impurity potential then has the form $\alpha_i \delta(\bar{r} - \bar{r}_i)$, where α_i is the generated value from a distribution and $\delta(\bar{r} - \bar{r}_i)$ gives the random position in the conductor. The chosen distribution, for the amplitudes of the delta potentials, can for example be uniform or Gaussian. The notation $U_{imp}(\bar{r} - \bar{r}_i)$ is used instead of $V_{imp}(\bar{r} - \bar{r}_i)$ in order to prevent confusion with the case where the impurity potentials were equal. The total potential is the sum of all the individual impurity potentials and is equal to

$$U(\bar{r}) = \sum_{i=1}^{N} U_{imp}(\bar{r} - \bar{r}_i). \tag{2.3.9}$$

The same definition of the Fourier transform as in the equal impurity case is chosen: $\mathcal{F}\{f\} = F(\bar{q}) = \int_V d^3\bar{r}' e^{-i\bar{q}\cdot\bar{r}'} f(\bar{r}')$. The impurity interactions only result in a change of the wavevector of the electrons, therefore $\bar{q} = \bar{k}_{new} - \bar{k}_{old}$. The Fourier transform of the impurity potentials only depends on $\bar{q}$

$$U(\bar{q}) = \int_V d^3\bar{r}' e^{-i\bar{q}\cdot\bar{r}'} \alpha_1 \delta(\bar{r}' - \bar{r}_1) + \int_V d^3\bar{r}' e^{-i\bar{q}\cdot\bar{r}'} \delta(\bar{r}' - \bar{r}_2) + ... + \int_V d^3\bar{r}' e^{-i\bar{q}\cdot\bar{r}'} \alpha_N \delta(\bar{r}' - \bar{r}_N),$$

$$U(\bar{q}) = \sum_{i=1}^{N} \alpha_i e^{-i\bar{q}\cdot\bar{r}_i}. \tag{2.3.10}$$

The impurity amplitudes are drawn from a distribution with first moment $\tilde{U}_1$ equal to zero, second moment equal to $\tilde{U}_2$, third moment equal to $\tilde{U}_3$ etc. The average over all the generated values is denoted by $\mathbb{E}$, which for the first and second moment of $U(\bar{q})$ yield

$$\mathbb{E}\left[U(\bar{q})\right] = \mathbb{E}\left[\sum_{i=1}^{N} \alpha_i e^{-i\bar{q}\cdot\bar{r}_i}\right] = \sum_{i=1}^{N} \mathbb{E}\left[\alpha_i\right] e^{-i\bar{q}\cdot\bar{r}_i} = 0, \tag{2.3.11}$$

$$\mathbb{E}\left[U(\bar{q})U(\bar{q}')\right] = \mathbb{E}\left[\sum_{i=1}^{N} \alpha_i e^{-i\bar{q}\cdot\bar{r}_i} \sum_{i=1}^{N} \alpha_i e^{-i\bar{q}'\bar{r}_i}\right] = \sum_{i,j=1}^{N} \mathbb{E}\left[\alpha_i\alpha_j\right] e^{-i\left(\bar{q}\cdot\bar{r}_i + \bar{q}'\cdot\bar{r}_j\right)}.$$

When $i \neq j$, then $\mathbb{E}\left[\alpha_i\alpha_j\right] = \mathbb{E}\left[\alpha_i\right]\mathbb{E}\left[\alpha_j\right] = 0$ because the amplitudes are independently generated. When $i = j$, then $\mathbb{E}\left[\alpha_i\alpha_j\right] = \mathbb{E}\left[\alpha_i^2\right] = \tilde{U}_2$ and therefore

$$\mathbb{E}\left[U(\bar{q})U(\bar{q}')\right] = \sum_{i,j=1}^{N} \mathbb{E}\left[\alpha_i\alpha_j\right] e^{-i\left(\bar{q}\cdot\bar{r}_i + \bar{q}'\cdot\bar{r}_j\right)} = \begin{cases} \tilde{U}_2 \sum\limits_{\tilde{i}=1}^{N} e^{-i\left(\bar{q}+\bar{q}'\right)\cdot\bar{r}_{\tilde{i}}} & \text{for } i = j \\ 0 & \text{for } i \neq j. \end{cases} \tag{2.3.12}$$

Higher moments can be calculated in a similar way.

If a lattice would be considered, the impurity potentials would have the form $\alpha_i \delta_{\bar{r},\bar{r}_i}$. When dealing with lattices, it is custom to set the number of impurity potentials equal to the number of lattice sites, which means that the impurity density is a function of the lattice constant

$$n = \frac{1}{a^d}. \tag{2.3.13}$$

A difference with the continuous case is that in the continuous case the units of α_i are energy times volume, while in the discrete case the units of α_i are energy. Adding all the individual impurity potentials gives the total potential

$$U_{dis}(\bar{r}) = \sum_{i=1}^{N(a)} \alpha_i \delta_{\bar{r},\bar{r}_i}. \tag{2.3.14}$$

A discrete Fourier transform is introduced

$$\mathcal{F}\left\{f(\bar{r})\right\} = F(\bar{q}) = \sum_{\{\bar{r}\}} e^{-i\bar{q}\cdot\bar{r}} f(\bar{r}), \tag{2.3.15a}$$

$$\mathcal{F}^{-1}\left\{F(\bar{q})\right\} = f(\bar{r}) = \frac{1}{(2\pi)^3} \int d^3\bar{q} e^{i\bar{q}\cdot\bar{r}} F(\bar{q}). \tag{2.3.15b}$$

Applying the discrete Fourier transform to the potential leads to

$$U_{dis}(\bar{q}) = \mathcal{F}\left\{U_{dis}(\bar{r})\right\} = \sum_{\{\bar{r}\}} e^{-i\bar{q}\cdot\bar{r}} \sum_{i=1}^{N} \alpha_i \delta_{\bar{r},\bar{r}_i} = \sum_{i=1}^{N} \alpha_i e^{-i\bar{q}\cdot\bar{r}_i},$$

$$U_{dis}(\bar{q}) = \sum_{i=1}^{N} \alpha_i e^{-i\bar{q}\cdot\bar{r}_i}. \tag{2.3.16}$$

The average over the amplitudes for the first and second moment is taken

$$\mathbb{E}\left[U_{dis}(\bar{q})\right] = \sum_{i=1}^{N} \mathbb{E}\left[\alpha_i\right] e^{-i\bar{q}\cdot\bar{r}_i} = 0, \tag{2.3.17}$$

$$\mathbb{E}\left[U_{dis}(\bar{q})U_{dis}(\bar{q}')\right] = \sum_{i,j=1}^{N} \mathbb{E}\left[\alpha_i\alpha_j\right] e^{-i(\bar{q}\cdot\bar{r}_i + \bar{q}'\cdot\bar{r}_j)} = \begin{cases} \tilde{U}_2' \sum_{i=1}^{N} e^{-i\left(\bar{q}+\bar{q}'\right)\cdot\bar{r}_i} & \text{for } i = j \\ 0 & \text{for } i \neq j. \end{cases} \tag{2.3.18}$$

In this section $\tilde{U}_2$ and $\tilde{U}_2'$ occur. Both are equal in value, but the former has units energy squared times volume to the power $2d$, where d is the dimension, while the latter has units energy squared.

2.3.2 Diagrammatic perturbation theory for equal impurities

The quantity that has to be calculated is the Green's function, because this will eventually give information on how the impurities impact the energies of the system. The diagrammatic perturbation theory is first discussed for the assumptions that all the impurity potentials are the same and that the positions of the impurities are independently generated from a uniform distribution (see section 2.3.1). The shape of the impurity potential can still have any form, it is just the same for every impurity.

The full time-independent Green's function can be written as the Born series (see section 2.1.4 Born series and Dyson's equation)

$$\hat{G}^+(E) = \hat{G}_0^+(E) + \hat{G}_0^+(E)\hat{V}\hat{G}_0^+(E) + \hat{G}_0^+(E)\hat{V}\hat{G}_0^+(E)\hat{V}\hat{G}_0^+(E) + \dots . \tag{2.3.19}$$

The series is also called the perturbation series. It is decided to work in the momentum basis: $\langle\hat{p}|\,\hat{V}\,|\hat{p}\rangle' = V(\bar{p},\bar{p}')$. The Hamiltonian in momentum space is equal to

$$H_c(\bar{p},\bar{p}') = H_0(\bar{p},\bar{p}')\delta_{\bar{p},\bar{p}'} + V(\bar{p},\bar{p}'). \tag{2.3.20}$$

The time-independent free Green's function (see equation (2.1.18a)) is

$$G_0^+(\bar{p};\bar{p}',E) = \delta_{\bar{p},\bar{p}'} \frac{\hat{I}}{E + i\epsilon - H_0(\bar{p},\bar{p}')} = \frac{\hat{I}}{E + i\epsilon - H_0(\bar{p})} = G_0(\bar{p},E). \tag{2.3.21}$$

The perturbation series of equation (2.3.19) is now written in momentum space

$$G^+(\bar{p};\bar{p}',E) = G_0^+(\bar{p},E) + G_0^+(\bar{p},E)V(\bar{p},\bar{p}')G_0^+(\bar{p}',E) + G_0^+(\bar{p},E)V(\bar{p},\bar{p}'')G_0^+(\bar{p}'',E)V(\bar{p}'',\bar{p}')G_0^+(\bar{p}',E) + \dots . \tag{2.3.22}$$

The full Green's function consists of a sum of possible processes. The zeroth order term corresponds to zero impurity interactions (free propagation), while the first order term involves one interaction with an impurity, the second order term has two interactions etc. A summation over all the intermediate momentum values (for example $\bar{p}''$ in the second order term) is implied, because only the incoming and outgoing momenta are fixed while the intermediate momenta can take on any value and it necessary to sum over all the possible processes. The implied summations are only relevant for the second order term and higher. The perturbation series in equation (2.3.22) has an intuitive diagrammatic representation.

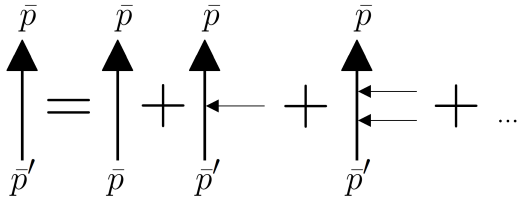

Figure 2.3.1: Diagrammatic presentation of the perturbation series (Born series). The total propagator (Green's function) consists of a sum of possible processes. The first diagram of the sum corresponds to free propagation, there is no interaction with the impurity potentials, for the second diagram there is one interaction with an impurity, in the third there are two interactions etc.

The scattering potential only depends on the difference between the incoming and outgoing momenta. Therefore it is convenient to introduce a new notation: $V(\bar{p},\bar{p}') = V(\bar{p}-\bar{p}')$. From equation (2.3.5), using $\bar{p} = \hbar\bar{k}$

$$V(\bar{p}-\bar{p}') = V_{imp}(\bar{p}-\bar{p}')\sum_{i=1}^{N} e^{-\frac{i}{\hbar}(\bar{p}-\bar{p}')\cdot\bar{r}_i}. \tag{2.3.23}$$

Different samples put between the leads correspond to different Green's functions since the impurity configuration is different. Ensemble averages can be calculated by averaging over an ensemble of conductors with impurity configurations that were generated from the same position distribution. It is assumed that the distribution is the independent and random distribution introduced in the beginning of subsection 2.3.1. In this case expectation values of observables can be calculated with equation (2.3.7). This averaging over all the realisations of the impurity configuration is now done for the potential

$$\langle V(\bar{p}-\bar{p}')\rangle = \frac{1}{V^N}V_{imp}(\bar{p}-\bar{p}')V^{N-1}\int_V e^{-\frac{i}{\hbar}(\bar{p}-\bar{p}')\cdot\bar{r}_1}d^3\bar{r}_1 + \frac{1}{V^N}V_{imp}(\bar{p}-\bar{p}')V^{N-1}\int_V e^{-\frac{i}{\hbar}(\bar{p}-\bar{p}')\cdot\bar{r}_2}d^3\bar{r}_2 + ... =$$
$$\frac{1}{V}V_{imp}(\bar{p}-\bar{p}')\sum_{i=1}^{N}\int_V e^{-\frac{i}{\hbar}(\bar{p}-\bar{p}')\cdot\bar{r}_i}d^3\bar{r}_i.$$

The integral will average out to zero unless $\bar{p} = \bar{p}'$ and therefore

$$\langle V(\bar{p}-\bar{p}')\rangle = \frac{1}{V}V_{imp}(\bar{p}-\bar{p}')\delta(\bar{p}-\bar{p}')\cdot N,$$
$$\langle V(\bar{p}-\bar{p}')\rangle = nV_{imp}(\bar{p}=0). \tag{2.3.24}$$

The calculated expectation value of the potential is used to find the first order term of the ensemble averaged Green's function

$$\begin{aligned}\left\langle G^+(\bar{p};\bar{p}',E)\right\rangle = \left\langle G_0^+(\bar{p},E)\right\rangle + \left\langle G_0^+(\bar{p},E)V(\bar{p}-\bar{p}')G_0^+(\bar{p}',E)\right\rangle + \\ \left\langle G_0^+(\bar{p},E)V(\bar{p}-\bar{p}'')G_0^+(\bar{p}'',E)V(\bar{p}''-\bar{p}')G_0^+(\bar{p}',E)\right\rangle + ... \ .\end{aligned} \tag{2.3.25}$$

The zeroth order term of the perturbation series will not be modified by taking the expectation value, because it obviously does not depend on the configuration of the impurities. For completeness the diagrammatic representation before and after averaging is included.

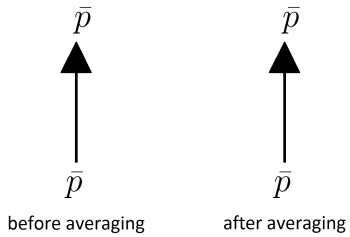

Figure 2.3.2: Two diagrammatic representations of the zeroth order of the Born series. The left diagram corresponds with the situation where the averaging has not taken place yet, while the right one is after averaging over all the disorder configurations. Because the zeroth order term represents no electron-impurity interaction, the averaging has no effect and the two diagrams are the same.

The first order term of the perturbation series is $\left\langle G_0^+(\bar{p},E)V(\bar{p}-\bar{p}')G_0^+(\bar{p}',E)\right\rangle$ and this is equal to $nV_{imp}(\bar{p}=0)\left[G_0^+(\bar{p},E)\right]^2$ by equation (2.3.24). However it is set to zero because it represents a constant in the Hamiltonian.

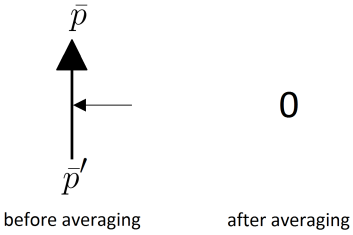

Figure 2.3.3: Two diagrammatic representations of the first order term of the perturbation series (Born series) before and after averaging. The left diagram represents the situation before the impurity averaging has occurred. The horizontal arrow indicates that the electron interacts once with an impurity. The incoming electron has an arbitrary momentum of $\bar{p}'$ and the outgoing electron has a momentum of $\bar{p}$. The right image shows the situation after the averaging.

If a constant $-nV_{imp}(\bar{p}=0)$ would be added to the Hamiltonian then the single terms

$$-nV_{imp}(\bar{p}=0)\left[G_0^+(\bar{p},E)\right]^2,\ \ (-nV_{imp}(\bar{p}=0))^2\left[G_0^+(\bar{p},E)\right]^3,\ \ (-nV_{imp}(\bar{p}=0))^3\left[G_0^+(\bar{p},E)\right]^4,\ \ldots, \quad (2.3.26)$$

would appear in the perturbation series. Further cross terms would appear of which the first is equal to $2\cdot -nV_{imp}(\bar{p}=0)\cdot\langle V(\bar{p}-\bar{p}')\rangle\left[G_0^+(\bar{p},E)\right]^3 = -2n^2\left(V_{imp}(\bar{p}=0)\right)^2\left[G_0^+(\bar{p},E)\right]^3$. The first of the single terms in equation (2.3.26) cancels the original first order term $nV_{imp}(\bar{p}=0)\left[G_0^+(\bar{p},E)\right]^2$. Higher order terms will be cancelled by parts of the higher order terms in the perturbation series. It appears that the contributions of the terms in the perturbation series which correspond to a diagrammatic representation which contains one or more isolated impurity interactions can be set to zero because they can be worked away by adding a constant to the Hamiltonian. This is intuitive, because when there is an isolated perturbation and the varying strength of the perturbation is averaged, it corresponds to a constant value and can be modelled by adding a constant to the potential of the Hamiltonian. It was seen that this indeed happened to the first order term; the diagrammatic representation contained an isolated impurity perturbation and the contribution in the perturbation series disappeared after averaging by cancelling with the added constant.

The second order term in the perturbation series is $\left\langle G_0^+(\bar{p},E)V(\bar{p}-\bar{p}'')G_0^+(\bar{p}'',E)V(\bar{p}''-\bar{p}')G_0^+(\bar{p}',E)\right\rangle$. Substituting equation 2.3.23 in this expression gives

$$G_0^+(\bar{p},E)\sum_{\bar{p}''}V_{imp}(\bar{p}-\bar{p}'')G_0^+(\bar{p}'',E)V_{imp}(\bar{p}''-\bar{p}')G_0^+(\bar{p}',E)\left\langle\sum_{i,j=1}^{N}e^{-\frac{i}{\hbar}(\bar{p}-\bar{p}'')\cdot\bar{r}_i}e^{-\frac{i}{\hbar}(\bar{p}''-\bar{p}')\cdot\bar{r}_j}\right\rangle.$$

Two cases are considered: $i \neq j$ and $i = j$. When $i \neq j$, then $\left\langle \sum_{\substack{i,j=1 \\ i\neq j}}^{N} e^{-\frac{i}{\hbar}(\bar{p}-\bar{p}'')\cdot\bar{r}_i} e^{-\frac{i}{\hbar}(\bar{p}''-\bar{p}')\cdot\bar{r}_j} \right\rangle = \frac{N(N-1)}{V^2}\delta(\bar{p}-\bar{p}'')\delta(\bar{p}''-\bar{p}')$. Equation (2.3.7) was used to apply the averaging operation. In the thermodynamic limit N and V go to infinity while keeping their ratio fixed. This means that $N(N-1)/V^2$ approaches n^2 in this limit, which gives

$$\left\langle G_0^+(\bar{p},E)V(\bar{p}-\bar{p}'')G_0^+(\bar{p}'',E)V(\bar{p}''-\bar{p}')G_0^+(\bar{p}',E)\right\rangle^{i\neq j} = n^2\left(V_{imp}(\bar{p}=0)\right)^2\left[G_0^+(\bar{p},E)\right]^3. \tag{2.3.27}$$

This contribution adds to the second term of equation (2.3.26) and then they cancel together with the first cross term which is $-2n^2\left(V_{imp}(\bar{p}=0)\right)^2\left[G_0^+(\bar{p},E)\right]^3$. Indeed the diagrammatic representation of the second order term for $i \neq j$ contains two isolated impurity perturbations.

When $i = j$, then $\left\langle \sum_{i=1}^{N} e^{-\frac{i}{\hbar}(\bar{p}-\bar{p}'')\cdot\bar{r}_i} e^{-\frac{i}{\hbar}(\bar{p}''-\bar{p}')\cdot\bar{r}_i} \right\rangle = \frac{N}{V^2}\delta(\bar{p}-\bar{p}') = \frac{n}{V}\delta(\bar{p}-\bar{p}')$. The equal summation indices mean that two impurities are located at the same position and the electrons scatters off both of them. The second order term of the impurity averaged Born series is

$$\left\langle G_0^+(\bar{p},E)V(\bar{p}-\bar{p}'')G_0^+(\bar{p}'',E)V(\bar{p}''-\bar{p}')G_0^+(\bar{p}',E)\right\rangle^{i=j} =$$
$$\frac{n}{V}\delta(\bar{p}-\bar{p}')G_0^+(\bar{p},E)\sum_{\bar{p}''}V_{imp}(\bar{p}-\bar{p}'')G_0^+(\bar{p}'',E)V_{imp}(\bar{p}''-\bar{p}')G_0^+(\bar{p}',E),$$

$$\left\langle G_0^+(\bar{p},E)V(\bar{p}-\bar{p}'')G_0^+(\bar{p}'',E)V(\bar{p}''-\bar{p}')G_0^+(\bar{p}',E)\right\rangle^{i=j} = \frac{n}{V}\left[G_0^+(\bar{p},E)\right]^2\sum_{\bar{p}'}\left|V_{imp}(\bar{p}-\bar{p}')\right|^2 G_0^+(\bar{p}',E). \tag{2.3.28}$$

In the continuum limit the summation becomes an integral

$$\left\langle G_0^+(\bar{p},E)V(\bar{p}-\bar{p}'')G_0^+(\bar{p}'',E)V(\bar{p}''-\bar{p}')G_0^+(\bar{p}',E)\right\rangle^{i=j} = n\left[G_0^+(\bar{p},E)\right]^2\int\frac{d^3\bar{p}'}{(2\pi\hbar)^3}\left|V_{imp}(\bar{p}-\bar{p}')\right|^2 G_0^+(\bar{p}',E). \tag{2.3.29}$$

Figure 2.3.4 shows the diagrammatic representation of the second order term before and after averaging. The second order term corresponds with two impurity interactions, giving two possibilities: the electron interacts once with two impurities at different positions or the electron interacts with two impurities at the same position. It was seen that the first scenario can be normalized away while the second one gives a contribution. The arc in figure 2.3.4 means that there are two impurities with the same position on which the electron scattered. In general: the number of arcs corresponds to the number of sites involved in the scattering process and the number of connections to the main line tells the number of interactions the electron experienced.

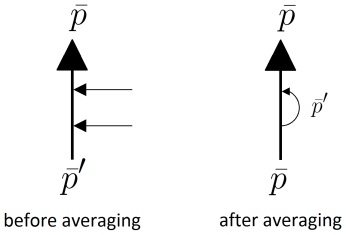

Figure 2.3.4: Diagrammatic representations of the second order term of the Born series before and after averaging. The left diagram corresponds with the situation before averaging over all the impurity configurations has taken place. The two horizontal arrows indicate that an electron interacts twice with an impurity. The meaning of the diagram on the right is that the electron comes in with a certain momentum, it interacts with an impurity after which it moves to a different value in momentum space and then moves back to its original momentum by interacting again with an impurity at the same position.

The momentum at the beginning and end of the right diagram of figure 2.3.4 is the same. All diagrams that contribute to the impurity averaged Green's function have this momentum conservation, because the other diagrams average out.

The third order term in the perturbation series is $\langle G_0^+(\bar{p},E)V(\bar{p}-\bar{p}''')G_0^+(\bar{p}''',E)V(\bar{p}'''-\bar{p}'')G_0^+(\bar{p}'',E)V(\bar{p}''-\bar{p}')G_0^+(\bar{p}',E)\rangle$. Equation (2.3.23) is substituted in this expression, giving

$$G_0^+(\bar{p},E)\sum_{\bar{p}'''.\bar{p}''}V_{imp}(\bar{p}-\bar{p}''')G_0^+(\bar{p}''',E)V_{imp}(\bar{p}'''-\bar{p}'')G_0^+(\bar{p}'',E)V_{imp}(\bar{p}''-\bar{p}')G_0^+(\bar{p}',E)\cdot$$
$$\left\langle\sum_{i,j,k=1}^{N}e^{-\frac{i}{\hbar}(\bar{p}-\bar{p}''')\cdot\bar{r}_i}e^{-\frac{i}{\hbar}(\bar{p}'''-\bar{p}'')\cdot\bar{r}_j}e^{-\frac{i}{\hbar}(\bar{p}''-\bar{p}')\cdot\bar{r}_k}\right\rangle.$$

There are three different cases: $i\neq j\neq k$, $i=j\neq k$ (or $i\neq j=k$ or $i=k\neq j$) and $i=j=k$. When $i\neq j\neq k$, then

$$\left\langle\sum_{\substack{i,j,k=1\\ i\neq j\neq k}}^{N}e^{-\frac{i}{\hbar}(\bar{p}-\bar{p}''')\cdot\bar{r}_i}e^{-\frac{i}{\hbar}(\bar{p}'''-\bar{p}'')\cdot\bar{r}_j}e^{-\frac{i}{\hbar}(\bar{p}''-\bar{p}')\cdot\bar{r}_k}\right\rangle=\frac{N(N-1)(N-2)}{V^3}\delta(\bar{p}-\bar{p}''')\delta(\bar{p}'''-\bar{p}'')\delta(\bar{p}''-\bar{p}')\simeq$$

$n^3\delta(\bar{p}-\bar{p}''')\delta(\bar{p}'''-\bar{p}'')\delta(\bar{p}''-\bar{p}')$. Therefore:

$$\begin{gathered}\left\langle G_0^+(\bar{p},E)V(\bar{p}-\bar{p}''')G_0^+(\bar{p}''',E)V(\bar{p}'''-\bar{p}'')G_0^+(\bar{p}'',E)V(\bar{p}''-\bar{p}')G_0^+(\bar{p}',E)\right\rangle^{i\neq j\neq k}=\\ n^3\left(V_{imp}(\bar{p}=0)\right)^3\left[G_0^+(\bar{p},E)\right]^4.\end{gathered}\tag{2.3.30}$$

This exactly cancels with the third term of equation (2.3.26). Indeed the diagrammatic representation for $i\neq j\neq k$ has three 'dangling' arrows. When two summation indices are equal but the third is not, then $\left\langle\sum_{\substack{i,j,k=1\\ i=j\neq k}}^{N}e^{-\frac{i}{\hbar}(\bar{p}-\bar{p}''')\cdot\bar{r}_i}e^{-\frac{i}{\hbar}(\bar{p}'''-\bar{p}'')\cdot\bar{r}_j}e^{-\frac{i}{\hbar}(\bar{p}''-\bar{p}')\cdot\bar{r}_k}\right\rangle=\frac{N(N-1)}{V^3}\delta(\bar{p}-\bar{p}'')\delta(\bar{p}''-\bar{p}')\simeq\frac{n^2}{V}\delta(\bar{p}-\bar{p}'')\delta(\bar{p}''-\bar{p}')$. Thus:

$$\left\langle G_0^+(\bar{p},E)V(\bar{p}-\bar{p}''')G_0^+(\bar{p}''',E)V(\bar{p}'''-\bar{p}'')G_0^+(\bar{p}'',E)V(\bar{p}''-\bar{p}')G_0^+(\bar{p}',E)\right\rangle^{i=j\neq k}=$$
$$\frac{n^2}{V}\delta(\bar{p}-\bar{p}'')\delta(\bar{p}''-\bar{p}')G_0^+(\bar{p},E)\sum_{\bar{p}'''.\bar{p}''}V_{imp}(\bar{p}-\bar{p}''')G_0^+(\bar{p}''',E)V_{imp}(\bar{p}'''-\bar{p}'')G_0^+(\bar{p}'',E)V_{imp}(\bar{p}''-\bar{p}')G_0^+(\bar{p}',E),$$

$$\begin{gathered}\left\langle G_0^+(\bar{p},E)V(\bar{p}-\bar{p}''')G_0^+(\bar{p}''',E)V(\bar{p}'''-\bar{p}'')G_0^+(\bar{p}'',E)V(\bar{p}''-\bar{p}')G_0^+(\bar{p}',E)\right\rangle^{i=j\neq k}=\\ nV_{imp}(\bar{p}=0)\cdot\frac{n}{V}\left[G_0^+(\bar{p},E)\right]^3\sum_{\bar{p}'}\left|V_{imp}(\bar{p}-\bar{p}')\right|^2G_0^+(\bar{p}',E).\end{gathered}\tag{2.3.31}$$

This term cancels with a cross term that was acquired by adding the constant $-nV_{imp}(\bar{p}=0)$ to the Hamiltonian. It consists of the constant $-nV_{imp}(\bar{p}=0)$ with a different sign times the expectation value of $(V(\bar{p}-\bar{p}'))^2$ (see equation (2.3.28)) with an additional $G_0^+(\bar{p},E)$. For the last case the summation indices are all equal, giving $\left\langle\sum_{\substack{i,j,k=1\\ i=j=k}}^{N}e^{-\frac{i}{\hbar}(\bar{p}-\bar{p}''')\cdot\bar{r}_i}e^{-\frac{i}{\hbar}(\bar{p}'''-\bar{p}'')\cdot\bar{r}_j}e^{-\frac{i}{\hbar}(\bar{p}''-\bar{p}')\cdot\bar{r}_k}\right\rangle=\frac{N}{V^3}\delta(\bar{p}-\bar{p}')\simeq\frac{n}{V^2}\delta(\bar{p}-\bar{p}')$. This leads to

$$\left\langle G_0^+(\bar{p},E)V(\bar{p}-\bar{p}''')G_0^+(\bar{p}''',E)V(\bar{p}'''-\bar{p}'')G_0^+(\bar{p}'',E)V(\bar{p}''-\bar{p}')G_0^+(\bar{p}',E)\right\rangle^{i=j=k}=$$
$$\frac{n}{V^2}\delta(\bar{p}-\bar{p}')G_0^+(\bar{p},E)\sum_{\bar{p}'''.\bar{p}''}V_{imp}(\bar{p}-\bar{p}''')G_0^+(\bar{p}''',E)V_{imp}(\bar{p}'''-\bar{p}'')G_0^+(\bar{p}'',E)V_{imp}(\bar{p}''-\bar{p}')G_0^+(\bar{p}',E),$$

$$\begin{gathered}\left\langle G_0^+(\bar{p},E)V(\bar{p}-\bar{p}''')G_0^+(\bar{p}''',E)V(\bar{p}'''-\bar{p}'')G_0^+(\bar{p}'',E)V(\bar{p}''-\bar{p}')G_0^+(\bar{p}',E)\right\rangle^{i=j=k}=\\ \frac{n}{V^2}\left[G_0^+(\bar{p},E)\right]^2\sum_{\bar{p}''.\bar{p}'}V_{imp}(\bar{p}-\bar{p}'')G_0^+(\bar{p}'',E)V_{imp}(\bar{p}''-\bar{p}')G_0^+(\bar{p}',E)V_{imp}(\bar{p}'-\bar{p}).\end{gathered}\tag{2.3.32}$$

In the continuum limit the summations become integrals

$$\begin{aligned}&\left\langle G_0^+(\bar{p},E)V(\bar{p}-\bar{p}''')G_0^+(\bar{p}''',E)V(\bar{p}'''-\bar{p}'')G_0^+(\bar{p}'',E)V(\bar{p}''-\bar{p}')G_0^+(\bar{p}',E)\right\rangle^{i=j=k}=\\ &n\left[G_0^+(\bar{p},E)\right]^2\int\frac{d^3\bar{p}''}{(2\pi\hbar)^3}\int\frac{d^3\bar{p}'}{(2\pi\hbar)^3}V_{imp}(\bar{p}-\bar{p}'')G_0^+(\bar{p}'',E)V_{imp}(\bar{p}''-\bar{p}')G_0^+(\bar{p}',E)V_{imp}(\bar{p}'-\bar{p}).\end{aligned}\tag{2.3.33}$$

Figure 2.3.5 shows the diagrammatic representation of the third order term before and after averaging. The third order term corresponds to three interactions. There are three possibilities here: the electron interacts three times with impurities at different positions, the electron interacts twice with the impurities at the same position and once with an impurity at a different position or the electron interacts three times with impurities at the same position. It was shown that the first two can be normalized away while the last scenario gives a contribution. There is one arc in the right diagram of figure 2.3.5 meaning there is only scattering at one position in the scattering process. There are three connections to the main line meaning there were three interactions. The contribution of diagrams that involve more than scattering twice off the same impurity site is small and therefore these diagrams are often disregarded. The approximation, where contributions that involve scattering more than twice off the same impurity site are neglected, is called the Born approximation. Apart from the fact that the diagrams, which are neglected in the Born approximation, give a small contribution, there is another reason to make this approximation. As will later become clear, application of the Born approximation allows for the development of the self-consistent Born approximation in section 2.3.4.

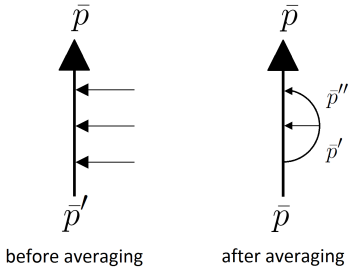

Figure 2.3.5: Diagrammatic representations of the third order term of the Born series before and after averaging. The left diagram corresponds with the situation before averaging. The horizontal lines in the left diagram indicate that an electron interacts three times with an impurity. Further, the momentum of the incoming electron is $\bar{p}'$ and the outgoing momentum is $\bar{p}$. The diagram on the right corresponds with the situation after averaging. In the diagram it is shown that the incoming and outgoing momentum of the electron are equal to each other. All the other cases did not give a contribution. The connection between the arrows signify that the impurities with which the electron interacts are all at the same position. The type of diagram, where the electron interacts more than twice with impurities at the same position is often neglected.

The fourth order term in the perturbation series is $\left\langle G_0^+(\bar{p},E)V(\bar{p}-\bar{p}'''')G_0^+(\bar{p}'''',E)V(\bar{p}''''-\bar{p}''')G_0^+(\bar{p}''',E)V(\bar{p}'''-\bar{p}'')G_0^+(\bar{p}'',E)V(\bar{p}''-\bar{p}')G_0^+(\bar{p}',E)\right\rangle$. Substituting equation (2.3.23) in this expression gives

$$G_0^+(\bar{p},E)\sum_{\bar{p}'''',\bar{p}''',\bar{p}''}V_{imp}(\bar{p}-\bar{p}'''')G_0^+(\bar{p}'''',E)V_{imp}(\bar{p}''''-\bar{p}''')G_0^+(\bar{p}''',E)V_{imp}(\bar{p}'''-\bar{p}'')G_0^+(\bar{p}'',E)V_{imp}(\bar{p}''-\bar{p}')G_0^+(\bar{p}',E)\cdot$$
$$\left\langle\sum_{i,j,k,l=1}^{N}e^{-\frac{i}{\hbar}(\bar{p}-\bar{p}'''')\cdot\bar{r}_i}e^{-\frac{i}{\hbar}(\bar{p}''''-\bar{p}''')\cdot\bar{r}_j}e^{-\frac{i}{\hbar}(\bar{p}'''-\bar{p}'')\cdot\bar{r}_k}e^{-\frac{i}{\hbar}(\bar{p}''-\bar{p}')\cdot\bar{r}_l}\right\rangle.$$

There are four different cases: all summation indices are equal, three are equal and one is different, two equal pairs or none are equal. Only the cases where all summation indices are equal or when there are two equal pairs give a contribution that is not cancelled by the effect of adding a constant to the Hamiltonian. These two cases do not contain any 'dangling' arrows in the diagrammatic representation. When there are

two pairs of equal summation indices for example $i = j \neq k = l$

$$\left\langle \sum_{\substack{i,j,k,l=1 \\ i=j\neq k=l}}^{N} e^{-\frac{i}{\hbar}(\bar{p}-\bar{p}'''')\cdot\bar{r}_i} e^{-\frac{i}{\hbar}(\bar{p}''''-\bar{p}''')\cdot\bar{r}_j} e^{-\frac{i}{\hbar}(\bar{p}'''-\bar{p}'')\cdot\bar{r}_k} e^{-\frac{i}{\hbar}(\bar{p}''-\bar{p}')\cdot\bar{r}_l} \right\rangle = \frac{N(N-1)}{V^4}\delta(\bar{p}-\bar{p}''')\delta(\bar{p}'''-\bar{p}') \simeq$$

$$\frac{n^2}{V^2}\delta(\bar{p}-\bar{p}''')\delta(\bar{p}'''-\bar{p}').$$

This gives

$$\left\langle G_0^+(\bar{p},E)V(\bar{p}-\bar{p}'''')G_0^+(\bar{p}'''',E)V(\bar{p}''''-\bar{p}''')G_0^+(\bar{p}''',E)V(\bar{p}'''-\bar{p}'')G_0^+(\bar{p}'',E)V(\bar{p}''-\bar{p}')G_0^+(\bar{p}',E)\right\rangle^{i=j\neq k=l} =$$

$$\frac{n^2}{V^2}\left[G_0^+(\bar{p},E)\right]^3 \sum_{\bar{p}'',\bar{p}'} \left|V_{imp}(\bar{p}-\bar{p}'')\right|^2 G_0^+(\bar{p}'',E)\left|V_{imp}(\bar{p}-\bar{p}')\right|^2 G_0^+(\bar{p}',E).$$

Also the cases $i = k \neq j = l$ and $i = l \neq j = k$ should be added. They can be calculated in a similar way. In the case all the summation indices are equal

$$\left\langle \sum_{\substack{i,j,k,l=1 \\ i=j=k=l}}^{N} e^{-\frac{i}{\hbar}(\bar{p}-\bar{p}'''')\cdot\bar{r}_i} e^{-\frac{i}{\hbar}(\bar{p}''''-\bar{p}''')\cdot\bar{r}_j} e^{-\frac{i}{\hbar}(\bar{p}'''-\bar{p}'')\cdot\bar{r}_k} e^{-\frac{i}{\hbar}(\bar{p}''-\bar{p}')\cdot\bar{r}_l} \right\rangle = \frac{N}{V^4}\delta(\bar{p}-\bar{p}') = \frac{n}{V^3}\delta(\bar{p}-\bar{p}').$$

The fourth order contribution for equal summation indices is equal to

$$\frac{n}{V^3}\left[G_0^+(\bar{p},E)\right]^2 \sum_{\bar{p}''',\bar{p}'',\bar{p}'} V_{imp}(\bar{p}-\bar{p}''')G_0^+(\bar{p}''',E)V_{imp}(\bar{p}'''-\bar{p}'')G_0^+(\bar{p}'',E)\cdot \\ V_{imp}(\bar{p}''-\bar{p}')G_0^+(\bar{p}',E)V_{imp}(\bar{p}'-\bar{p}). \tag{2.3.34}$$

Figure 2.3.6 shows the diagrammatic representation of the fourth order term before and after averaging. The fourth order term corresponds to four interactions. There are four possibilities: the electrons interacts four times with impurities at different positions, the electrons interacts twice with one impurity site and twice with a different impurity site, the electron interacts with three impurities at the same position and once with an impurity at another position or the electron interacts four times with impurities at the same position. The first and third scenario were normalized away by adding a constant to the Hamiltonian while the second and fourth scenario gave a contribution. The second scenario could be realised in three different ways and the fourth scenario in only one way, resulting in four contributing diagrams.

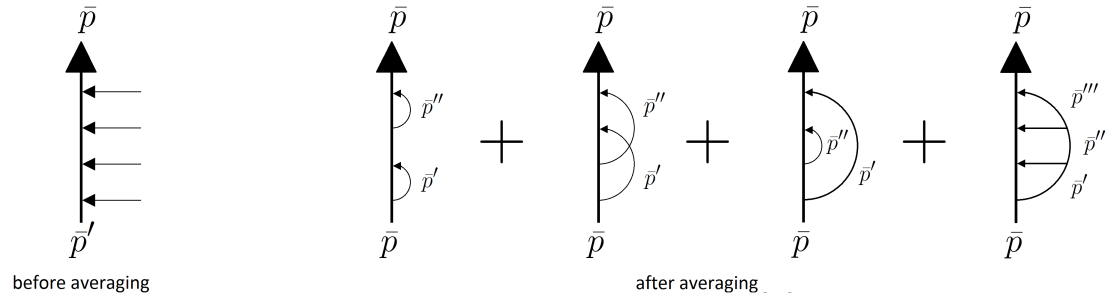

Figure 2.3.6: Diagrammatic representations of the fourth order term of the Born series before and after averaging. The leftmost diagram corresponds with the situation before averaging. The incoming momentum of the electron is the arbitrary $\bar{p}'$ and the outgoing momentum is $\bar{p}$. The horizontal lines indicate that the electron interacts four times with an impurity before leaving the studied sample. The four diagrams on the right correspond with the situation after the impurity averaging has been applied. They each display one of four different scenarios, that did not average to zero. In the four diagrams on the right it is further shown that the incoming and outgoing momentum of the electron are equal to each other.

The terms that involve more than two interactions at one impurity position give a much smaller contribution to the Green's function than the ones that involve only two. In the Born approximation the diagrams that correspond to scattering more than twice off the same impurity site are neglected.

It is useful to stress here that all the diagrams that contribute to the impurity averaged Green's function do not contain any 'dangling' impurity lines, because these diagrams can be normalized away. Also all the contributing diagrams have the same ingoing as outgoing momentum, because the diagrams, that do not have this momentum conservation, average out.

Some of the possible non-normalisable and momentum conserving processes are gathered in the self-energy. Using the self-energy, the ensemble averaged Green's function can be expressed in a compact implicit expression

$$G^+(\bar{p},E) = G_0^+(\bar{p},E) + G_0^+(\bar{p},E)\Sigma^+(\bar{p},E)G^+(\bar{p},E) = G_0^+(\bar{p},E) + G^+(\bar{p},E)\Sigma^+(\bar{p},E)G_0^+(\bar{p},E). \quad (2.3.35)$$

See section 2.3.4 for a discussion about the self-energy in the context of diagrammatic perturbation theory (see also section 2.1.4). A new notation is introduced in equation (2.3.35), namely: $G^+(\bar{p},E) = \langle G^+(\bar{p};\bar{p}',E)\rangle$. It is clear that $G^+(\bar{p},E)$ is the impurity averaged Green's function, because it only depends on $\bar{p}$ and not on $\bar{p}'$ (contributing diagrams have the same ingoing as outgoing momentum). In contrast, the non-ensemble averaged Green's function, $G^+(\bar{p};\bar{p}',E)$, depends on both $\bar{p}$ and $\bar{p}'$.

2.3.3 Diagrammatic perturbation theory for non-equal delta impurities

The diagrammatic perturbation theory is discussed for the case that the impurities have a delta shape of which the amplitudes are independently generated from a zero mean distribution. Just as in section 2.3.2 the full time-independent Green's function is averaged over an ensemble of conductors. For every realisation of a disordered conductor in the ensemble not only the positions of the impurities but also the amplitudes of the impurities vary. Ensemble averaging corresponds to taking the average over all the possible configurations of the impurity positions and amplitudes. The derivation will be very similar to that of the previous section because while the impurities are not equal now, they all have the same shape.

It is decided to work in the wavevector basis. The Born series and its diagrammatic representation in this basis are equal to

$$\begin{aligned} G^+(\bar{k};\bar{k}',E) = G_0^+(\bar{k},E) + G_0^+(\bar{k},E)U(\bar{k}-\bar{k}')G_0^+(\bar{k}',E) + \\ G_0^+(\bar{k},E)U(\bar{k}-\bar{k}'')G_0^+(\bar{k}'',E)U(\bar{k}''-\bar{k}')G_0^+(\bar{k}',E) + \dots \ . \end{aligned} \quad (2.3.36)$$

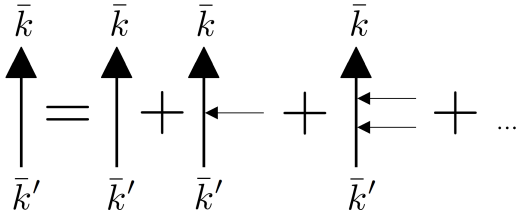

Figure 2.3.7: Diagrammatic representation of the Born series in the wavevector basis. The horizontal arrows denote perturbations. The leftmost diagram corresponds the full (non-averaged) Green's function. The first diagram to the right of the equal sign corresponds with free propagation, the second diagram with one perturbation, the third diagram with two perturbations etc. The wave vector of the incoming electron is equal $\bar{k}'$, while $\bar{k}$ is the wave vector at the end of the process.

The average over all the realisations of the impurity configurations is taken on both sides of equation (2.3.36) giving

$$\begin{aligned} \left\langle G^+(\bar{k};\bar{k}',E)\right\rangle = \left\langle G_0^+(\bar{k},E)\right\rangle + \left\langle G_0^+(\bar{k},E)U(\bar{k}-\bar{k}')G_0^+(\bar{k}',E)\right\rangle + \\ \left\langle G_0^+(\bar{k},E)U(\bar{k}-\bar{k}'')G_0^+(\bar{k}'',E)U(\bar{k}''-\bar{k}')G_0^+(\bar{k}',E)\right\rangle + \dots \ . \end{aligned} \quad (2.3.37)$$

A summation over all the intermediate wavevectors (for example $\bar{k}''$ in the second order term) is implied, because only the incoming and outgoing wavevectors are fixed while the intermediate wavevectors can take on any value and it necessary to sum over all the possible processes.

The equations for the first and second moment in the Fourier domain that resulted from the assumptions regarding the impurities are repeated (see section 2.3.1), namely

$$\mathbb{E}\left[U(\bar{q})\right] = 0 \tag{2.3.38}$$

and

$$\mathbb{E}\left[U(\bar{q})U(\bar{q}')\right] = \sum_{i,j=1}^{N} \mathbb{E}\left[\alpha_i \alpha_j\right] e^{-i\left(\bar{q}\cdot\bar{r}_i + \bar{q}'\cdot\bar{r}_j\right)} = \begin{cases} \tilde{U}_2 \sum\limits_{\tilde{i}=1}^{N} e^{-i\left(\bar{q}+\bar{q}'\right)\cdot\bar{r}_{\tilde{i}}} & \text{for } i = j \\ 0 & \text{for } i \neq j. \end{cases} \tag{2.3.39}$$

Because the positions of the impurities are random and independently generated, equation (2.3.7) can be used to calculate expectation values.

The zeroth order term of equation (2.3.37) is not modified by averaging over the conductor ensemble, because it does not depend on the impurity configuration and therefore

$$\left\langle G_0^+(\bar{k}, E)\right\rangle = G_0^+(\bar{k}, E). \tag{2.3.40}$$

The diagrammatic representation of the zeroth order term is included for completeness.

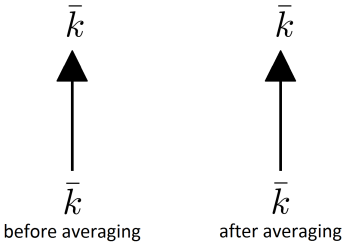

Figure 2.3.8: Diagrammatic representations of the zeroth order term of the Born series before and after ensemble averaging. The left diagram corresponds with the situation before impurity averaging has taken place, while the right one with the situation after the averaging. Because there is no impurity interaction at all, the averaging process does not change anything and the two diagrams are the same.

Because $\mathbb{E}\left[U(\bar{q})\right] = 0$ the value of $\langle U(\bar{q})\rangle$ is equal to zero. It does not matter that the positions change during the averaging because the amplitudes already average to zero and thus

$$\left\langle G_0^+(\bar{k}, E) U_{imp}(\bar{k} - \bar{k}') G_0^+(\bar{k}', E)\right\rangle = 0. \tag{2.3.41}$$

This is true for the continuous case as well as the discrete one. Figure 2.3.9 shows the diagrams for the first order term.

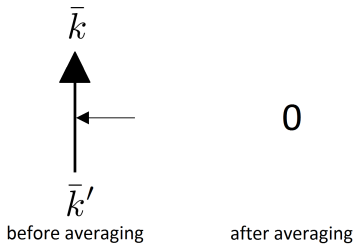

Figure 2.3.9: Diagrammatic representations of the first order term of the Born series before and after ensemble averaging. The left diagram is without averaging. The incoming electron has an arbitrary wave vector $\bar{k}'$. The horizontal arrow indicates that there is one impurity interaction after which the electrons wave vector changes to $\bar{k}$. The right image shows the situation after averaging. The first order term of the impurity averaged Born series is equal to zero.

For the second order term the expression for $\mathbb{E}\left[U(\bar{q})U(\bar{q}')\right]$ (see equation (2.3.39)) is needed. Using this equation and equation (2.3.7) gives $\left\langle U(\bar{k}-\bar{k}'')U(\bar{k}''-\bar{k}')\right\rangle = \frac{\tilde{U}_2}{V^2}\left\langle \sum_{i=1}^{N} e^{-i\left(\bar{q}+\bar{q}'\right)\cdot\bar{r}_i}\right\rangle = \tilde{U}_2\frac{N}{V^2}\delta(\bar{q}+\bar{q}') = \tilde{U}_2\frac{n}{V}\delta((\bar{k}-\bar{k}'')+(\bar{k}''-\bar{k}')) = \tilde{U}_2\frac{n}{V}\delta(\bar{k}-\bar{k}')$. If a tight-binding approach would be used, the expression for $\mathbb{E}\left[U_{dis}(\bar{q})U_{dis}(\bar{q}')\right]$ is given by equation (2.3.18) and the averaging in done with equation (2.3.8), this gives $\frac{a^{3N}}{V^N}\cdot\left(\frac{V}{a^3}\right)^{N-2}\cdot\tilde{U}_2'\cdot\delta_{\bar{k},\bar{k}'}\cdot N = \frac{a^6 n\tilde{U}_2'}{V}\delta_{\bar{k},\bar{k}'}$. Note that there is an apostrophe on the $\tilde{U}_2$, because it has different units than $\tilde{U}_2$. The second order term for the continuous system is

$$\left\langle G_0^+(\bar{k},E)U(\bar{k}-\bar{k}'')G_0^+(\bar{k}'',E)U(\bar{k}''-\bar{k}')G_0^+(\bar{k}',E)\right\rangle = \tilde{U}_2\frac{n}{V}\left[G_0^+(\bar{k},E)\right]^2\sum_{\bar{k}''}G_0^+(\bar{k}'',E).$$

After renaming this is rewritten to

$$\left\langle G_0^+(\bar{k},E)U(\bar{k}-\bar{k}'')G_0^+(\bar{k}'',E)U(\bar{k}''-\bar{k}')G_0^+(\bar{k}',E)\right\rangle = \frac{n}{V}\tilde{U}_2\left[G_0^+(\bar{k},E)\right]^2\sum_{\bar{k}'}G_0^+(\bar{k}',E). \tag{2.3.42}$$

The summation can be written as an integral, giving

$$\left\langle G_0^+(\bar{k},E)U(\bar{k}-\bar{k}'')G_0^+(\bar{k}'',E)U(\bar{k}''-\bar{k}')G_0^+(\bar{k}',E)\right\rangle = n\tilde{U}_2\left[G_0^+(\bar{k},E)\right]^2\int\frac{d^3\bar{k}'}{(2\pi)^3}G_0^+(\bar{k}',E). \tag{2.3.43}$$

For completeness the second order term is also given for the discrete case

$$\left\langle G_0^+(\bar{k},E)U(\bar{k}-\bar{k}'')G_0^+(\bar{k}'',E)U(\bar{k}''-\bar{k}')G_0^+(\bar{k}',E)\right\rangle = a^6 n\tilde{U}_2'\left[G_0^+(\bar{k},E)\right]^2\int\frac{d^3\bar{k}'}{(2\pi)^3}G_0^+(\bar{k}',E), \tag{2.3.44}$$

where a is the lattice constant. Figure 2.3.10 shows the diagrams for the second order term.

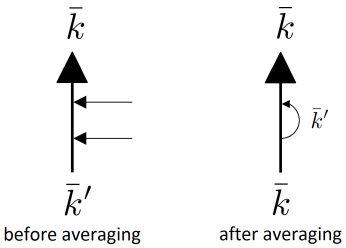

Figure 2.3.10: Diagrammatic representation of the second order term of the perturbation series before and after ensemble averaging. The left diagram corresponds with the second order term of the Born series before impurity averaging has been applied. The incoming wave vector of the electrons is $\bar{k}'$ and $\bar{k}$ is the outgoing wave vector. The two horizontal arrows imply that there is interaction with two impurities. The right diagram corresponds with the second order term of the Born series after impurity averaging has been applied. The meaning of the diagram on the right is that the electron comes in with a certain wave vector, it interacts with an impurity after which it moves to a different k-value and then moves back to its original wave vector by interacting again with an impurity at the same position.

In order to evaluate the third order term, the third moment,

$$\mathbb{E}\left[U(\bar{q})U(\bar{q}')U(\bar{q}'')\right] = \sum_{i,j,k=1}^{N} \mathbb{E}\left[\alpha_i\alpha_j\alpha_k\right] e^{-i\left(\bar{q}\cdot\bar{r}_i+\bar{q}'\cdot\bar{r}_j+\bar{q}''\cdot\bar{r}_k\right)},$$

needs to be calculated. Because the amplitudes are generated independently and $\mathbb{E}\left[\alpha_i\right] = 0$, the only way $\mathbb{E}\left[\alpha_i\alpha_j\alpha_k\right]$ is non-zero, is when $i = j = k$ and therefore

$$\mathbb{E}\left[U(\bar{q})U(\bar{q}')U(\bar{q}'')\right] = \sum_{i,j,k=1}^{N} \mathbb{E}\left[\alpha_i\alpha_j\alpha_k\right] e^{-i\left(\bar{q}\cdot\bar{r}_i+\bar{q}'\cdot\bar{r}_j+\bar{q}''\cdot\bar{r}_k\right)} = \begin{cases} \tilde{U}_3 \sum_{i=1}^{N} e^{-i\left(\bar{q}+\bar{q}'+\bar{q}''\right)\cdot\bar{r}_i} & \text{for } i=j=k \\ 0 & \text{otherwise.} \end{cases} \tag{2.3.45}$$

Using equation (2.3.45) and equation (2.3.7) gives $\left\langle U(\bar{k}-\bar{k}''')U(\bar{k}'''-\bar{k}'')U(\bar{k}''-\bar{k}')\right\rangle =$
$\frac{\tilde{U}_3}{V^3}\left\langle \sum_{i=1}^{N} e^{-i\left(\bar{q}+\bar{q}'+\bar{q}''\right)\cdot\bar{r}_i}\right\rangle = \tilde{U}_3\frac{n}{V^2}\delta(\bar{k}-\bar{k}')$. The result would be $\frac{a^9 n\tilde{U}_3'}{V^2}\delta_{\bar{k},\bar{k}'}$ for a discrete space. For the continuous limit the third order term is

$$\left\langle G_0^+(\bar{k},E)U(\bar{k}-\bar{k}''')G_0^+(\bar{k}''',E)U(\bar{k}'''-\bar{k}'')G_0^+(\bar{k}'',E)U(\bar{k}''-\bar{k}')G_0^+(\bar{k}',E)\right\rangle = \frac{n}{V^2}\tilde{U}_3\left[G_0(\bar{k},E)\right]^2\left(\sum_{\bar{k}'} G_0^+(\bar{k}',E)\right)^2. \tag{2.3.46}$$

The summation can be written as an integral

$$n\tilde{U}_3\left[G_0(\bar{k},E)\right]^2\left(\int \frac{d^3\bar{k}'}{(2\pi)^3} G_0^+(\bar{k}',E)\right)^2. \tag{2.3.47}$$

The third order term involves more than scattering twice at one impurity position, such contributions are relatively small and are therefore often neglected (Born approximation). Figure 2.3.11 shows the diagrammatic representation of the third order term.

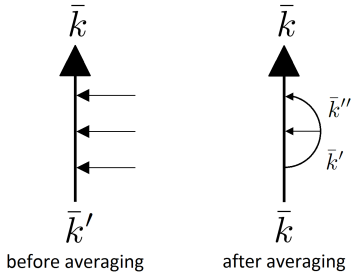

Figure 2.3.11: Diagrammatic representation of the third order term of the perturbation series before and after ensemble averaging. The left diagram corresponds with the situation before the impurity averaging has occurred. The horizontal arrows indicate that the electron interacts three times with an impurity. The right diagram corresponds with the situation after the impurity averaging has been applied. The connection between the arrows signify that the impurities with which the electron interacts are all at the same position.

For the fourth order term, the fourth moment,

$$\mathbb{E}\left[U(\bar{q})U(\bar{q}')U(\bar{q}'')U(\bar{q}''')\right] = \sum_{i,j,k,l=1}^{N} \mathbb{E}\left[\alpha_i\alpha_j\alpha_k\alpha_l\right] e^{-i\left(\bar{q}\cdot\bar{r}_i+\bar{q}'\cdot\bar{r}_j+\bar{q}''\cdot\bar{r}_k+\bar{q}'''\cdot\bar{r}_l\right)},$$

needs to be calculated. There are now four different ways to get a non-zero value expectation value: $i=j\neq k=l$, $i=k\neq j=l$, $i=l\neq j=k$ or $i=j=k=l$. Evaluation for the different cases gives

$$\mathbb{E}\left[U(\bar{q})U(\bar{q}')U(\bar{q}'')U(\bar{q}''')\right] = \sum_{i,j,k,l=1}^{N} \mathbb{E}\left[\alpha_i\alpha_j\alpha_k\alpha_l\right] e^{-i\left(\bar{q}\cdot\bar{r}_i+\bar{q}'\cdot\bar{r}_j+\bar{q}''\cdot\bar{r}_k+\bar{q}'''\cdot\bar{r}_l\right)} =$$

$$\begin{cases} \left(\tilde{U}_2\right)^2 \sum\limits_{\substack{\tilde{i},\tilde{j}=1 \\ \tilde{i}\neq\tilde{j}}}^{N} e^{-i\left[\left(\bar{q}+\bar{q}'\right)\cdot\bar{r}_{\tilde{i}}+\left(\bar{q}''+\bar{q}'''\right)\cdot\bar{r}_{\tilde{j}}\right]} & \text{for } i=j\neq k=l \\ \left(\tilde{U}_2\right)^2 \sum\limits_{\substack{\tilde{i},\tilde{j}=1 \\ \tilde{i}\neq\tilde{j}}}^{N} e^{-i\left[\left(\bar{q}+\bar{q}''\right)\cdot\bar{r}_{\tilde{i}}+\left(\bar{q}'+\bar{q}'''\right)\cdot\bar{r}_{\tilde{j}}\right]} & \text{for } i=k\neq j=l \\ \left(\tilde{U}_2\right)^2 \sum\limits_{\substack{\tilde{i},\tilde{j}=1 \\ \tilde{i}\neq\tilde{j}}}^{N} e^{-i\left[\left(\bar{q}+\bar{q}'''\right)\cdot\bar{r}_{\tilde{i}}+\left(\bar{q}'+\bar{q}''\right)\cdot\bar{r}_{\tilde{j}}\right]} & \text{for } i=l\neq j=k \\ \tilde{U}_4 \sum\limits_{\tilde{i}=1}^{N} e^{-i\left(\bar{q}+\bar{q}'+\bar{q}''+\bar{q}'''\right)\cdot\bar{r}_{\tilde{i}}} & \text{for } i=j=k=l \\ 0 & \text{otherwise.} \end{cases} \tag{2.3.48}$$

The case where $i=j=k=l$ involves more than scattering twice off the same impurity site and is neglected

in the Born approximation. Equation (2.3.7) is used to calculate the ensemble averages

$$\left\langle U_{imp}(\bar{k}-\bar{k}'''')U_{imp}(\bar{k}''''-\bar{k}''')U_{imp}(\bar{k}'''-\bar{k}'')U_{imp}(\bar{k}''-\bar{k}')\right\rangle = \left(\tilde{U}_2\right)^2\frac{N(N-1)}{V^4}\delta(\bar{q}+\bar{q}')\delta(\bar{q}''+\bar{q}''')+$$
$$\left(\tilde{U}_2\right)^2\frac{N(N-1)}{V^4}\delta(\bar{q}+\bar{q}'')\delta(\bar{q}'+\bar{q}''')+\left(\tilde{U}_2\right)^2\frac{N(N-1)}{V^4}\delta(\bar{q}+\bar{q}''')\delta(\bar{q}'+\bar{q}'')+\tilde{U}_4\frac{N}{V^4}\delta(\bar{q}+\bar{q}'+\bar{q}''+\bar{q}''')=$$
$$\frac{n^2}{V^2}\left(\tilde{U}_2\right)^2\delta(\bar{k}-\bar{k}''')\delta(\bar{k}'''-\bar{k}')+\frac{n^2}{V^2}\left(\tilde{U}_2\right)^2\delta(\bar{k}-\bar{k}''''+\bar{k}'''-\bar{k}'')\delta(\bar{k}''''-\bar{k}'''+\bar{k}''-\bar{k}')+$$
$$\frac{n^2}{V^2}\left(\tilde{U}_2\right)^2\delta(\bar{k}-\bar{k}''''+\bar{k}''-\bar{k}')\delta(\bar{k}''''-\bar{k}'')+\frac{n}{V^3}\tilde{U}_4\delta(\bar{k}-\bar{k}').$$

The fourth order term is then equal to

$$\left\langle G_0^+(\bar{k},E)U_{imp}(\bar{k}-\bar{k}'''')G_0^+(\bar{k}'''',E)U_{imp}(\bar{k}''''-\bar{k}''')G_0^+(\bar{k}''',E)U_{imp}(\bar{k}'''-\bar{k}'')G_0^+(\bar{k}'',E)U_{imp}(\bar{k}''-\bar{k}')G_0^+(\bar{k}',E)\right\rangle =$$
$$\frac{n^2}{V^2}\left(\tilde{U}_2\right)^2\left[G_0^+(\bar{k},E)\right]^3\sum_{\bar{k}',\bar{k}''}G_0^+(\bar{k}',E)G_0^+(\bar{k}'',E)+\frac{n^2}{V^2}\left(\tilde{U}_2\right)^2\left[G_0^+(\bar{k},E)\right]^2\sum_{\bar{k}',\bar{k}''}G_0^+(\bar{k}''-\bar{k}'+\bar{k},E)G_0^+(\bar{k}'',E)G_0^+(\bar{k}',E)+$$
$$\frac{n^2}{V^2}\left(\tilde{U}_2\right)^2\left[G_0^+(\bar{k},E)\right]^2\sum_{\bar{k}',\bar{k}''}G_0^+(\bar{k}'',E)\left[G_0^+(\bar{k}',E)\right]^2+\frac{n}{V^3}\tilde{U}_4\left[G_0^+(\bar{k},E)\right]^2\left(\sum_{\bar{k}'}G_0^+(\bar{k}',E)\right)^3. \tag{2.3.49}$$

The summations can be written as integrals, giving

$$\left\langle G_0^+(\bar{k},E)U_{imp}(\bar{k}-\bar{k}'''')G_0^+(\bar{k}'''',E)U_{imp}(\bar{k}''''-\bar{k}''')G_0^+(\bar{k}''',E)U_{imp}(\bar{k}'''-\bar{k}'')G_0^+(\bar{k}'',E)U_{imp}(\bar{k}''-\bar{k}')G_0^+(\bar{k}',E)\right\rangle =$$
$$n^2\left(\tilde{U}_2\right)^2\left[G_0^+(\bar{k},E)\right]^3\left(\int\frac{d^3\bar{k}'}{(2\pi)^3}G_0^+(\bar{k}',E)\right)^2+$$
$$n^2\left(\tilde{U}_2\right)^2\left[G_0^+(\bar{k},E)\right]^2\int\frac{d^3\bar{k}''}{(2\pi)^3}\int\frac{d^3\bar{k}'}{(2\pi)^3}G_0^+(\bar{k}''-\bar{k}'+\bar{k},E)G_0^+(\bar{k}'',E)G_0^+(\bar{k}',E)+$$
$$n^2\left(\tilde{U}_2\right)^2\left[G_0^+(\bar{k},E)\right]^2\int\frac{d^3\bar{k}''}{(2\pi)^3}\int\frac{d^3\bar{k}'}{(2\pi)^3}G_0^+(\bar{k}'',E)\left[G_0^+(\bar{k}',E)\right]^2+$$
$$n\tilde{U}_4\left[G_0^+(\bar{k},E)\right]^2\left(\int\frac{d^3\bar{k}'}{(2\pi)^3}G_0^+(\bar{k}',E)\right)^3. \tag{2.3.50}$$

Figure 2.3.12 shows the diagrammatic representation of the fourth order term.

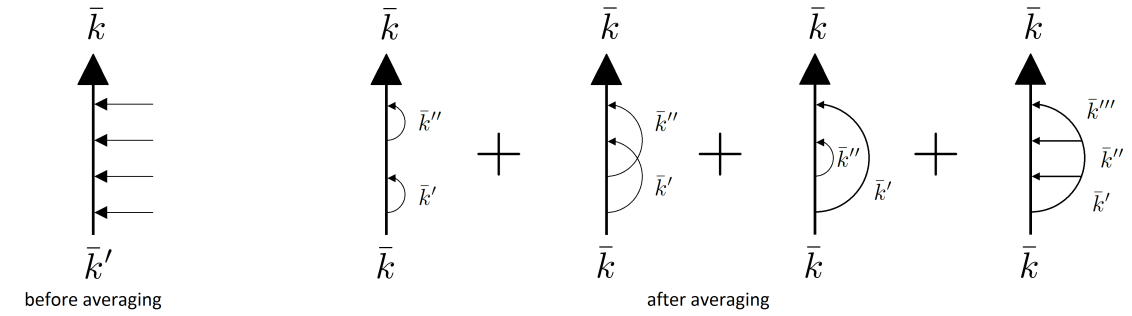

Figure 2.3.12: Diagrammatic representation of the fourth order term of the Born series before and after ensemble averaging. The leftmost diagram corresponds with the situation before the impurity averaging over all the disorder configurations has been implemented. After the averaging, there are four types of diagrams that survive. The last one of these diagrams involves scattering off the same impurity site more than twice. It gives a very small contribution and is therefore often neglected.

It is good to notice that in the Born approximation besides the first moment, which was assumed to be zero, only the second moment of the impurity amplitude distribution is needed. Higher moments only appear

in terms which involve scattering off an impurity site more than twice. Further the Born approximation becomes better when the amplitude distribution involves a lot of moments which are equal to zero. A normal distribution for example has uneven moments equal to zero.

In the Born approximation higher order diagrams are straight-forward to draw. All the the impurity perturbations need to form pairs in order to give a relevant contribution. This means that the diagrams can be generated by connecting all the horizontal arrows, in the diagrams before the averaging, with a partner. It is then also possible to directly write down the formula corresponding with a given diagram. The formula's have a pre-factor of $\left(n\tilde{U}_2\right)^{m/2}$, where m is the number of impurity perturbations (number of horizontal arrows in the diagrams before the averaging) and the structure of the free Green's functions can be seen from the flow of the diagrams. For example: the diagram where the first and second, third and fourth and fifth and sixth arrow form pairs, gives a contribution

$$\left(n\tilde{U}_2\right)^3 \left[G_0^+(\bar{k},E)\right]^4 \left(\int \frac{d^3\bar{k}}{(2\pi)^3} G_0^+(\bar{k}',E)\right)^3 .$$

When the number of impurity perturbations increases, the contribution of each diagram decreases, while the number of possibilities to form pairs increases. In certain cases it can happen that the series diverges, because the contribution per diagram does not go down fast enough when the number of perturbations increases.

Further it is repeated here that all the contributing diagrams do not contain any 'dangling' impurity lines. Also all the contributing diagrams have the same ingoing as outgoing momentum, because the diagrams, that have 'dangling' impurity lines or do not have momentum conservation, average out.

2.3.4 Self-Energy and 1SBA

The self-energy is introduced in order to write the ensemble averaged Green's function in a more compact expression. The principle is the same for the cases of equal impurities (section 2.3.2) and non-equal delta impurities (section 2.3.3). It is chosen to draw the diagrams in the wavevector basis.

The diagrams can be classified by their topology; they are put into different groups based on how many times the diagram can be cut into pieces without cutting a curved line. For example: figure 2.3.13 shows three diagrams; two from the sixth order term term and one from the fourth order term. The left diagram can be cut twice resulting in three diagrams, the middle diagram can be cut once, while the right diagram can not be cut. The left and middle diagram belong to the second and first reducible group respectively, while the right one belongs to the irreducible group.

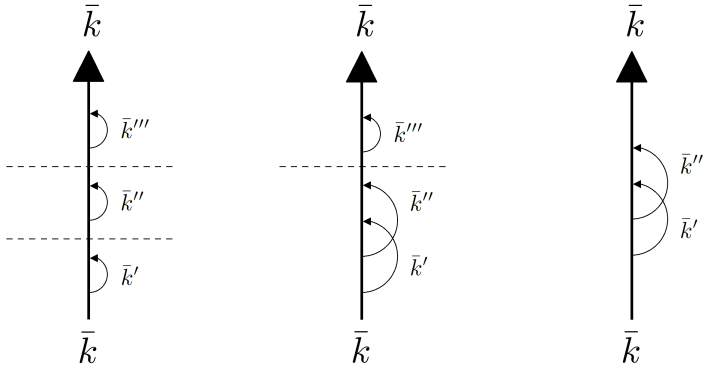

Figure 2.3.13: Three examples of diagrams that belong into different groups based on their topology. The left diagram can be cut into three other diagrams, the middle one can be cut into two, while the right diagram can not be cut into other diagrams.

The self-energy is defined as the sum of all the formula's corresponding to the diagrams that belong in the irreducible group but with the free propagating parts at the end cut off. The first couple of diagrams that

the sum consists of are presented in figure 2.3.14.

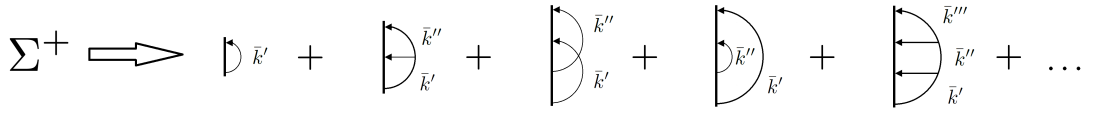

Figure 2.3.14: The self-energy is equal to the sum of all the terms that correspond to diagrams of the irreducible group, but with the end parts cut off.

The ensemble averaged Green's function can be written as

$$G^+(\bar{k},E) = G_0^+(\bar{k},E) + G_0^+(\bar{k},E)\Sigma^+(E)G_0^+(\bar{k},E) + G_0^+(\bar{k},E)\Sigma^+(E)G_0^+(\bar{k},E)\Sigma^+(E)G_0^+(\bar{k},E) + \dots . \quad (2.3.51)$$

By construction all the possible diagrams are taken into account without double counting. The zeroth order term, $G_0^+(\bar{k},E)$, corresponds with free propagation, the first order term consists of the contribution of all the irreducible diagrams, the term $G_0^+(\bar{k},E)\Sigma^+(E)G_0^+(\bar{k},E)\Sigma^+(E)G_0^+(\bar{k},E)$ only contains the diagrams of the first reducible group, etc.

The diagrams that involve more than scattering twice off the same impurity site are neglected in the Born approximation. Figure 2.3.15 shows the first couple of diagrams for the self-energy that are included in this approximation.

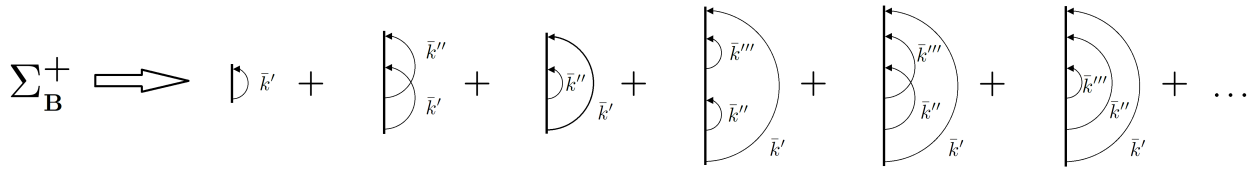

Figure 2.3.15: The self-energy in the Born approximation is equal to the sum of all the terms that correspond to diagrams of the irreducible group, but with the end parts cut off and that do not involve more than scattering twice off the same impurity position.

Rewriting equation (2.3.51) to

$$G^+(\bar{k},E) = G_0^+(\bar{k},E) + G_0^+(\bar{k},E)\Sigma^+(E)\left[G_0^+(\bar{k},E) + G_0^+(\bar{k},E)\Sigma^+(E)G_0^+(\bar{k},E) + ...\right].$$

The part in brackets is equal to $G^+(\bar{k},E)$, giving

$$G^+(\bar{k},E) = G_0^+(\bar{k},E) + G_0^+(\bar{k},E)\Sigma^+(E)G^+(\bar{k},E). \quad (2.3.52)$$

Solving for $G^+(\bar{k},E)$ gives

$$G^+(\bar{k},E) = \frac{1}{\left[G_0(\bar{k},E)\right]^{-1} - \Sigma^+(E)}. \quad (2.3.53)$$

Also, by putting in the value for $\left[G_0^+(\bar{k},E)\right]^{-1}$ (see equation (2.1.18a)) yields

$$G^+(\bar{k},E) = \frac{1}{E + i\epsilon - H_0(\bar{k}) - \Sigma^+(E)}. \quad (2.3.54)$$

When the self-energy is a number, it can be split in a real and imaginary part

$$\Sigma^+(E) = \sigma(E) - i\eta(E). \quad (2.3.55)$$

When the self-energy is a matrix, it can be split in a Hermitian and anti-Hermitian matrix

$$\hat{\Sigma}^+(E) = \hat{\Sigma}^+_H(E) + \hat{\Sigma}^+_{AH}(E). \tag{2.3.56}$$

The split self-energy is inserted in the expression for the impurity averaged Green's function (see equation (2.3.54))

$$G^+(\bar{k}, E) = \frac{1}{E - H_0(\bar{k}) - \sigma(E) + i(\epsilon + \eta(E))} \tag{2.3.57}$$

or in matrix form

$$\hat{G}^+(E) = \frac{\hat{I}}{E + i\epsilon - \hat{H}_0 - \hat{\Sigma}^+_H(E) - \hat{\Sigma}^+_{AH}(E))}. \tag{2.3.58}$$

The physical meaning of the real/Hermitian and imaginary/anti-Hermitian part of the self-energy becomes clear by going to the time domain through the application of the inverse Fourier transform. Comparison of equations (2.3.57) and (2.3.58) with equation (2.1.14a) directly gives

$$G^+(t; t', k) = -\frac{i}{\hbar} e^{-i(H_0(k)+\sigma)(t-t')/\hbar} \cdot e^{-\eta(t-t')/\hbar}, \tag{2.3.59a}$$

$$\hat{G}^+(t; t') = -\frac{i}{\hbar} e^{-i(\hat{H}_0+\hat{\Sigma}^+_H+\hat{\Sigma}^+_{AH})(t-t')/\hbar}. \tag{2.3.59b}$$

In equation (2.3.59a) it can be seen that the real part of the self-energy shifts the energies of the electrons, while the imaginary part of the self-energy causes the ensemble averaged Green's function to decay with time. Note that the shift of the energy levels, caused by the real part of the self-energy, depends on the energy and therefore is not a trivial shift from a physical point of view. When the self-energy is a matrix, the hermitian part of the self-energy causes the energy levels to shift.

So far we have an expansion of the self-energy, besides this series it is useful to derive a selfconsistent relation for the Born approximation where the self-energy is expressed in terms of the impurity averaged Green's function (which in turn depends on the self-energy). The diagrammatic representation of the self-consistent relation in the Born approximation is presented in figure 2.3.16. The straight lines between the arcs in this figure correspond to the full propagator, while they represented free propagation in the previous figures.

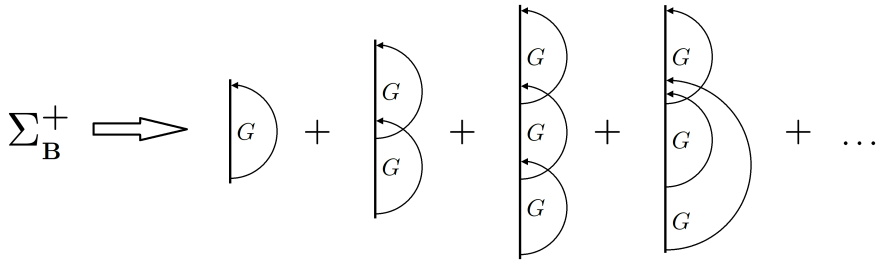

Figure 2.3.16: Diagrammatic representation of the self-energy under the Born approximation in terms of the full Green's function.

It can be visualised that the all the diagrams are included and not double counted in this construction, use equation (2.3.51) and figure 2.3.15 to see this. A self-consistent relation as presented in figure 2.3.16 is only possible for the Born approximation and not for the general self-energy.

The first diagram gives the largest contribution. When the higher order diagrams are neglected, the self-consistent relation for the self-energy is given by equation (2.3.60a) for equal impurities and by equation (2.3.60b) for non-equal delta impurities. These equations can be found by using equation (2.3.29) for equal impurities and equation (2.3.43) for non-equal delta impurities. In equation (2.3.29) and equation (2.3.43) the

free Green's function in the integral is replaced by the full Green's function and the pre-factor $\left[G_0^+(\bar{k},E)\right]^2$ is removed because the free propagating ends are cut off

$$\Sigma^+(E) = n\int \frac{d^3\bar{p}'}{(2\pi\hbar)^3}\left|V_{imp}(\bar{p}-\bar{p}')\right|^2 G^+(\bar{p}',E), \tag{2.3.60a}$$

$$\Sigma^+(E) = n\tilde{U}_2\int \frac{d^3\bar{k}}{(2\pi)^3}G^+(\bar{k},E). \tag{2.3.60b}$$

The expression for the full Green's function, equation (2.3.54), is subsituted in equations (2.3.60a) and (2.3.60b)

$$\Sigma^+(E) = n\lim_{\epsilon\to 0}\int \frac{d^3\bar{p}'}{(2\pi\hbar)^3}\cdot\frac{\left|V_{imp}(\bar{p}-\bar{p}')\right|^2}{E+i\epsilon-H_0(\bar{p}')-\Sigma^+(E)}, \tag{2.3.61a}$$

$$\Sigma^+(E) = n\tilde{U}_2\lim_{\epsilon\to 0}\int \frac{d^3\bar{k}}{(2\pi)^3}\cdot\frac{1}{E+i\epsilon-H_0(\bar{k})-\Sigma^+(E)}. \tag{2.3.61b}$$

The discrete version of equation (2.3.61b) is obtained by removing the pre-factor $\left[G_0^+(\bar{k},E)\right]^2$ in equation (2.3.44) and replacing $G_0^+(\bar{k},E)$ in the integrand by the full Green's function

$$\Sigma^+(E) = a^6 n\tilde{U}_2'\lim_{\epsilon\to 0}\int \frac{d^3\bar{k}}{(2\pi)^3}\cdot\frac{1}{E+i\epsilon-H_0(\bar{k})-\Sigma^+(E)}. \tag{2.3.62}$$

For clarity the limit $\epsilon\to 0$ is added in equation (2.3.62); this limit was left out for brevity in many other equations, but should be added to any equation that has an $i\epsilon$ in it.

Equations (2.3.61a), (2.3.61b), (2.3.62) and also (2.3.65) and (2.3.67) are called the first order self-consistent Born approximation, for which the abbreviation 1SBA will be used. The term first order, refers to the fact that the equations are based only on the first diagram of figure 2.3.16. The equations are self-consistent, because the outcome of the integral is also present in the denominator of the integrand. Lastly, the Born approximation refers to the fact that diagrams, which involved more than scattering twice off the same impurity location, were neglected in the construction of figure 2.3.16.

It is useful to relate the self-energy to the real space Green's function. Wavevector space and real space are related to each other by the Fourier transform,

$$f(\bar{k}) = \int d^3\bar{r} f(\bar{r})e^{-i\bar{k}\cdot\bar{r}}, \tag{2.3.63a}$$

$$f(\bar{r}) = \frac{1}{(2\pi)^3}\int d^3\bar{k} f(\bar{k})e^{i\bar{k}\cdot\bar{r}}, \tag{2.3.63b}$$

where f is a test function. Entering $\bar{r}=0$ in equation (2.3.63b) gives

$$f(0) = \int \frac{d^3\bar{k}}{(2\pi)^3} f(\bar{k}). \tag{2.3.64}$$

Applying this relation to equation (2.3.60b) yields the relation between the real space Green's function and the self-energy for non-equal delta impurities

$$\Sigma^+(E) = n\tilde{U}_2\int \frac{d^3\bar{k}}{(2\pi)^3}G^+(\bar{k},E) = n\tilde{U}_2\cdot G^+(\bar{r}=0,E),$$

$$\Sigma^+(E) = n\tilde{U}_2 G^+(\bar{r}=0,E). \tag{2.3.65}$$

If the space would be a lattice, the Fourier transform is

$$f(\bar{k}) = \sum_{\{\bar{r}\}} f(\bar{r}) e^{-i\bar{k}\cdot\bar{r}}, \tag{2.3.66a}$$

$$f(\bar{r}) = \frac{1}{(2\pi)^3} \int_{BZ} d^3\bar{k} f(\bar{k}) e^{i\bar{k}\cdot\bar{r}}, \tag{2.3.66b}$$

where BZ stands for the first Brillouin zone. By taking $\bar{r} = 0$ in equation (2.3.66b) and subsequently combining the result with equation (2.3.62) gives

$$\Sigma^+(E) = a^6 n \tilde{U}_2' G^+(\bar{r} = 0, E). \tag{2.3.67}$$

2.3.5 Scaling of the disorder strength

Hamiltonians are often discretized in order to study systems through computer simulations. Such a tight-binding approach (see section 2.2) involves one or more lattice constants.

It is possible to add all kinds of disorder to such systems by for example modifying the on-site energy of the lattice sites. As was seen in section 2.3.4 the effect of average disorder can be incorporated by adding the real or hermitian part of the self-energy to the Hamiltonian. Formula's for the first order Born approximation of the self-energy in the case of a lattice and non-equal delta impurities were derived in section 2.3.4, namely equations 2.3.62 and 2.3.67. In the aforementioned equations the impurity density, n, depends on the lattice constant, see equation (2.3.13). When the lattice constant becomes smaller the fluctuations in the on-site energies increase and therefore a smaller lattice constant corresponds to stronger disorder. A scaling factor needs to be added to make sure that while varying a, the disorder strength does not change allowing for fair comparison between systems with different values of the lattice constant. Fermi's golden rule can be used to estimate the mean free path length. This length should not depend on the lattice constant and therefore with this approach it will become clear how to scale $\tilde{U}_2'$.

The calculation for the mean free path length with delta impurities for the continuous case can be found in Appendix C. Fermi's golden rule is equal to

$$\Gamma_{i\to f} = \frac{2\pi}{\hbar} \sum_f \left| \langle f | \hat{H}_{int} | i \rangle \right|^2 \delta(E_i - E_f). \tag{2.3.68}$$

The initial and final state are defined on a lattice and thus have the form $|\psi\rangle_i = \sum_l \psi_l |l\rangle$ and $|\psi\rangle_f = \sum_m \psi_m |m\rangle$ (see section 2.2). Without the disorder the wave function would be a plane wave and thus $|\psi\rangle_i$ and $|\psi\rangle_f$ are set to plane waves. Wavelengths are restricted to $\lambda_n = \frac{2(N-1)a}{n}$, which gives $k_n = \frac{2\pi n}{2(N-1)a}$. Therefore the coefficients of the initial and final state are $\psi_l = \frac{1}{\sqrt{N}} e^{\frac{i2\pi n_k}{2(N-1)a} \cdot la}$ and $\psi_m = \frac{1}{\sqrt{N}} e^{\frac{i2\pi n_{k'}}{2(N-1)a} \cdot ma}$.

The matrix element is now calculated with $|\psi\rangle_i = \sum_l \frac{1}{\sqrt{N}} e^{\frac{i\pi n_k l}{(N-1)}} |l\rangle$, $|\psi\rangle_f = \sum_m \frac{1}{\sqrt{N}} e^{\frac{i\pi n_{k'} m}{(N-1)}} |m\rangle$ and $\hat{H}_{imp} = \sum_p \alpha_p |p\rangle \langle p|$ giving

$$\left| \langle f | \hat{H}_{int} | i \rangle \right|^2 = \langle f | \hat{H}_{int} | i \rangle \langle i | \hat{H}_{int} | f \rangle = \frac{1}{N^2} \left[\sum_m e^{\frac{-i\pi n_{k'} m}{(N-1)}} \langle m | \left(\sum_p \alpha_p |p\rangle \langle p| \right) \sum_l e^{\frac{i\pi n_k l}{(N-1)}} |l\rangle \right] \cdot$$

$$\left[\sum_l e^{-\frac{i\pi n_k l}{(N-1)}} \langle l | \left(\sum_q \alpha_q |q\rangle \langle q| \right) \sum_m e^{\frac{i\pi n_{k'} m}{(N-1)}} |m\rangle \right] = \frac{1}{N^2} \sum_{p,q} \alpha_p \alpha_q e^{\frac{i\pi p}{(N-1)}(n_k - n_k')} e^{\frac{-i\pi q}{(N-1)}(n_k - n_k')}.$$

The impurity average of the matrix element is taken. Use that $\mathbb{E}[\alpha_p \alpha_q] = 0$ if $p \neq q$ and $\mathbb{E}\left[\alpha_p^2\right] = \tilde{U}_2'$. Notice that when $p = q$ the complex exponentials cancel each other and therefore

$$\left\langle \left| \langle f | \hat{H}_{int} | i \rangle \right|^2 \right\rangle_{imp} = \frac{\tilde{U}_2'}{N^2} \cdot N = \frac{\tilde{U}_2'}{N} = \tilde{U}_2' \left(\frac{a}{L} \right)^d,$$

$$\left\langle \left| \langle f | \hat{H}_{int} | i \rangle \right|^2 \right\rangle_{imp} = \tilde{U}_2' \left(\frac{a}{L} \right)^d. \tag{2.3.69}$$

The parameter d is the dimension of the studied system. The calculated matrix element is put into equation (2.3.68) giving

$$\Gamma = \frac{2\pi a^d \tilde{U}_2'}{\hbar L^d} \sum_{k'} \delta(E_k - E_{k'}). \tag{2.3.70}$$

The density of states is defined as

$$D(E_k) = \frac{1}{L^d} \sum_{k'} \delta(E_k - E_{k'}). \tag{2.3.71}$$

Therefore:

$$\Gamma = \frac{2\pi a^d \tilde{U}_2'}{\hbar} D(E_k). \tag{2.3.72}$$

The mean free path length can be calculated with equation:

$$l_{free} = v_F \cdot \tau_{free} = \frac{v_F}{\Gamma} = \frac{v_F \hbar}{2\pi a^d \tilde{U}_2'} \frac{1}{D(E_k)}.$$

Rewriting, by using that $v_F = \sqrt{\frac{2E_F}{m}}$, yields

$$l_{free} = \frac{\hbar}{2\pi a^d \tilde{U}_2'} \sqrt{\frac{2E_F}{m}} \frac{1}{D(E_k)}. \tag{2.3.73}$$

The mean free path length can be made independent of the lattice constant by replacing $\tilde{U}_2'$ by $\tilde{U}_2'/a^d$. Therefore is

$$\tilde{U}_{2,s}' = \frac{\tilde{U}_2'}{a^d}, \tag{2.3.74}$$

the sought after scaling formula. The scaling of $\tilde{U}_2'$ allows to vary the lattice constant while maintaining a constant effective disorder strength.

This result is not surprising considering equations (2.3.61b) and (2.3.62). Equation (2.3.61b) gives the self-consistent Born approximation for a continuous 3D space with a fixed impurity concentration, while equation (2.3.62) gives the self-consistent Born approximation for a 3D lattice with an impurity concentration $n = 1/a^3$. If $\tilde{U}_2'$ in equation (2.3.62) is replaced by its scaled version and the limit $a \to 0$ is taken, the result is equation 2.3.61b. This reasoning can mathematically be displayed as

$$\lim_{a\to 0} a^6 n \tilde{U}_{2,s}' \lim_{\epsilon \to 0} \int \frac{d^3\bar{k}}{(2\pi)^3} \cdot \frac{1}{E + i\epsilon - H_0(\bar{k}) - \Sigma^+(E)} =$$

$$\lim_{a\to 0} \tilde{U}_2' \lim_{\epsilon \to 0} \int_{-\pi/a}^{\pi/a} \frac{d^3\bar{k}}{(2\pi)^3} \cdot \frac{1}{E + i\epsilon - H_0(a\bar{k}) - \Sigma^+(E)} \to n\tilde{U}_2 \lim_{\epsilon \to 0} \int_{-\infty}^{\infty} \frac{d^3\bar{k}}{(2\pi)^3} \cdot \frac{1}{E + i\epsilon - H_0(\bar{k}) - \Sigma^+(E)}.$$

Thus by scaling $\tilde{U}_2'$ with the lattice constant is, as if having a constant impurity concentration and thus having the same disorder strength for different lattice constants.

3 Simulation

3.1 Simple models

3.1.1 Free particle in a 1D infinite space

In order to get more intuition what the effect of disorder is on a system, it is decided to first investigate its effect on relatively simple systems.

Consider a one dimensional infinite space, with a constant potential, which can be set to zero. The Hamiltonian for such a system is

$$\hat{H} = -\frac{\hbar^2}{2m}\frac{d^2}{dx^2}. \tag{3.1.1}$$

The dispersion relation for this Hamiltonian is

$$E(k_x) = \frac{\hbar^2 k_x^2}{2m} \tag{3.1.2}$$

and the eigenfunctions are plane waves.

The Hamiltonian of equation (3.1.1) is discretized on a 1D lattice with N sites, periodic boundary conditions and lattice constant a. The number of sites N is very large in order to approximate the infinite space. The matrix elements of the Hamiltonian are given by equation (2.2.7) with $V(ia) = 0$ and $t = \hbar^2/2ma^2$, which results in

$$\hat{H} = 2t\sum_i |i\rangle\langle i| - t\sum_{\langle i,j\rangle} |i\rangle\langle j|. \tag{3.1.3}$$

The summation indices i and j run over all the lattice points and $\langle\ \rangle$ means nearest neighbours. In the Hamiltonian it can be seen that the on-site energy is $2t$ and the hopping energy is $-t$.

The Fourier and inverse Fourier transform are respectively defined as

$$|\bar{k}\rangle = \frac{1}{\sqrt{N}}\sum_i e^{-i\bar{k}\cdot\bar{r}_i}|i\rangle, \tag{3.1.4a}$$

$$|i\rangle = \frac{1}{\sqrt{N}}\sum_{\bar{k}} e^{i\bar{k}\cdot\bar{r}_i}|\bar{k}\rangle. \tag{3.1.4b}$$

Applying the Fourier transform to the on-site part of the Hamiltonian gives

$$\frac{2t}{N}\sum_i\sum_{\bar{k},\bar{k}'} e^{i(\bar{k}-\bar{k}')\cdot\bar{r}_i}|\bar{k}\rangle\langle\bar{k}'|.$$

Interchanging the summations and realizing that $\sum_{i=1}^{N} e^{i(\bar{k}-\bar{k}')\cdot\bar{r}_i} = N\delta_{\bar{k},\bar{k}'}$, gives

$$\hat{H}_{on} = 2t\sum_{\bar{k}}|\bar{k}\rangle\langle\bar{k}|. \tag{3.1.5}$$

Before applying the Fourier transform to the hopping part of the Hamiltonian, the hopping term is rewritten as

$$-t\left(\sum_i |i\rangle\langle i+1| + |i+1\rangle\langle i|\right). \tag{3.1.6}$$

Equation (3.1.6) takes every hopping possibility into account without double counting.

Now applying the Fourier transform, the hopping part of the Hamiltonian becomes

$$-\frac{t}{N}\left(\sum_i\sum_{\bar{k},\bar{k}'} e^{i(\bar{k}\cdot\bar{r}_i-\bar{k}'\cdot(\bar{r}_i+a\hat{x}))}|\bar{k}\rangle\langle\bar{k}'| + e^{i(\bar{k}\cdot(\bar{r}_i+a\hat{x})-\bar{k}'\cdot\bar{r}_i)}|\bar{k}\rangle\langle\bar{k}'|\right) = -\frac{t}{N}\sum_{\bar{k},\bar{k}'}\left(e^{-i\bar{k}'\cdot a\hat{x}} + e^{i\bar{k}\cdot a\hat{x}}\right)\sum_i e^{i(\bar{k}-\bar{k}')\cdot\bar{r}_i}|\bar{k}\rangle\langle\bar{k}'|.$$

Again using that $\sum_{i=1}^{N} e^{i(\bar{k}-\bar{k}')\cdot\bar{r}_i} = N\delta_{\bar{k},\bar{k}'}$ gives

$$\hat{H}_{hop} = -t\sum_{\bar{k}}\left(e^{i\bar{k}\cdot a\hat{x}} + e^{-i\bar{k}\cdot a\hat{x}}\right)\left|\bar{k}\right\rangle\left\langle\bar{k}\right|. \tag{3.1.7}$$

The complete Hamiltonian in Fourier space is thus

$$\hat{H} = 2t\sum_{\bar{k}}\left|\bar{k}\right\rangle\left\langle\bar{k}\right| - t\sum_{\bar{k}}\left(e^{i\bar{k}\cdot a\hat{x}} + e^{-i\bar{k}\cdot a\hat{x}}\right)\left|\bar{k}\right\rangle\left\langle\bar{k}\right|. \tag{3.1.8}$$

Equation (3.1.8) can be written in the form $\hat{H} = \sum_{\bar{k}}\left|\bar{k}\right\rangle H(\bar{k})\left\langle\bar{k}\right|$, where $H(\bar{k}) = 2t - t\left(e^{i\bar{k}\cdot a\hat{x}} + e^{-i\bar{k}\cdot a\hat{x}}\right) = 2t - t\left(e^{iak_x} + e^{-iak_x}\right) = 2t - 2t\cos(ak_x) = 2t\left(1-\cos(ak_x)\right) \equiv H(k_x)$. The dispersion relation is

$$H(k_x) = 2t\left(1-\cos(ak_x)\right). \tag{3.1.9}$$

Figure 3.1.1 shows plots of the band structure of the discretized and exact system around $k = 0$. In order to visualize the effect of the chosen lattice constant, the discretized dispersion relation is plotted for three different values of a.

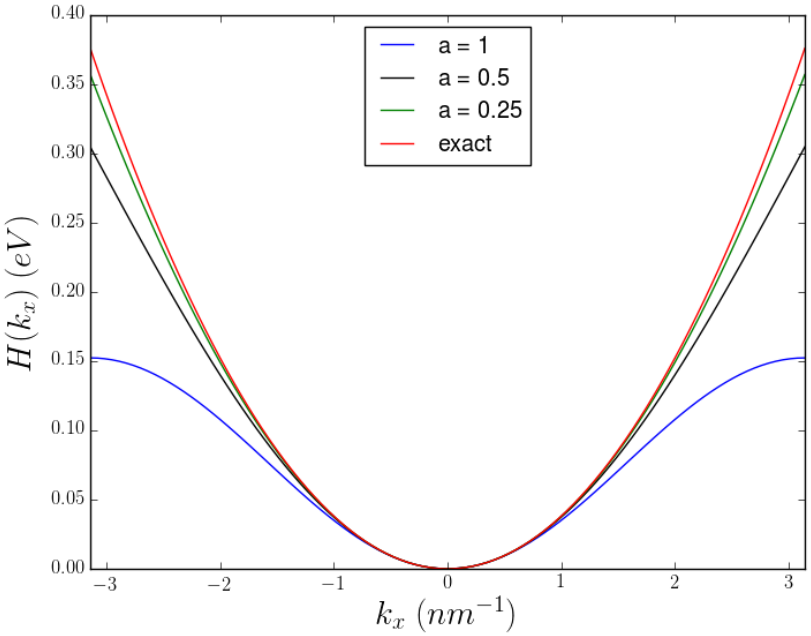

Figure 3.1.1: Three plots of the discretized Hamiltonian (see equation (3.1.9)) of a free particle in an one dimensional infinite space. Each of the three curves corresponds with a different lattice constant (1, 0.5 and 0.25 nm). The exact dispersion, a parabola, is plotted in red (see equation (3.1.2)). The wavevector k_x runs from $-\pi$ to π.

A Taylor expansion of $H(k_x)$ around $k_x = 0$ can be made

$$H(k_x) = 2t\left(1 - \left(1 - \frac{a^2k_x^2}{2} + \frac{a^4k_x^4}{24} - \ldots\right)\right) = ta^2k_x^2 - \frac{ta^4k_x^4}{12} + \ldots.$$

Using that $t = \hbar^2/2ma^2$ gives

$$H(k_x) = \frac{\hbar^2k_x^2}{2m} - \frac{\hbar^2a^2k_x^4}{24m} + \ldots. \tag{3.1.10}$$

When the limit $a \to 0$ is taken, only the first term survives and the dispersion relation is

$$E(k_x) = \frac{\hbar^2 k_x^2}{2m}. \tag{3.1.11}$$

Looking back at equation (3.1.2), this is indeed the result that should be obtained when $a \to 0$. Indeed it can be seen in figure 3.1.1 that the bands have a parabolic shape around $k_x = 0$ and the dispersion relation approaches more and more a perfect parabola when a becomes smaller.

It is interesting to see what will happen to the band structure if average disorder is added to the system. The band structure corresponding to the system with average disorder could be calculated by generating realisations of the system where independent and identically distributed disorder potentials are added to the on-site energies and by consequently averaging over all the calculated band structures. In this case the system is infinite and therefore only the analytical approach, as discussed in section 2.3, is applied and not the 'brute force' method outlined in the previous sentence.

It is imagined that the amplitudes are generated independently from a uniform distribution in the interval $[-U_0/2, U_0/2]$. The first moment of this distribution is zero and the second moment is $U_0^2/12$. Further the impurity concentration is equal to $1/a$.

In order to take the effect of the disorder into account the self-consistency relation of equation (2.3.62) could be solved, which for the presented situation takes the form

$$\Sigma^+(E) = a^2 n \tilde{U}_2' \lim_{\epsilon \to 0} \int_{-\pi/a}^{\pi/a} \frac{dk_x}{2\pi} \cdot \frac{1}{E + i\epsilon - 2t(1 - \cos(ak_x)) - \Sigma^+(E)}. \tag{3.1.12}$$

One might think that the limit $\epsilon \to 0$ in equation (3.1.12) can be carried out before calculating the integral. This is not allowed; the infinitesimal small ϵ has to remain in the integrand and the limit $\epsilon \to 0$ is carried out after evaluating the integral. The ϵ guarantees that no poles are located on the integration path. In appendix B.1 the integral self-consistency relation is solved numerically, however a different procedure is presented here. Instead of solving equation (3.1.12), the self-energy is obtained by making use of equation (2.3.67), which for the system of this section is

$$\Sigma^+(E) = a^2 n \tilde{U}_2' G^+(x = 0, E).$$

In order to fairly compare self-energies evaluated for different lattice constants, the second moment of the uniform distribution, $U_0^2/12$, is scaled according to equation (2.3.74): $\tilde{U}_{2,s}' = \tilde{U}_2'/a = U_0^2/12a$. The scaling with a however does not effect the units of the equation. Further applying $n = 1/a$ (equation (2.3.13)) gives

$$\Sigma^+(E) = \frac{U_0^2}{12} G^+(x = 0, E). \tag{3.1.13}$$

The software package Kwant[8] is used to apply the tight-binding approach. An infinite chain is build and the on-site and hopping energies are set as described by the Hamiltonian (see equation (3.1.3)). Then Kwant is used to calculate the Green's function at the origin, subsequently equation (3.1.13) gives the self-energy. This result is then used to modify the on-site energies of all the lattice sites after which the Green's function at the origin is calculated again. The process is iterated until the change of the self-energy is below a threshold level. In practice an Anderson mixing scheme is used so that only a few iterations are required to obtain a solution for the self-energy.

Tables 3.1.1, 3.1.2 and 3.1.3 lists some of the self-energies attained from the simulation. The energy levels for which the self-energies are calculated are fixed at 0.05, 0.10 and 0.15 eV respectively. For each of the energies, the value of U_0 and the lattice constant are varied. The self-energies are solved with very high accuracy, 10^{-14}, but the values in the tables are rounded to two digits.

a (nm)	$U_0 = 0.001\ (eV)$	$U_0 = 0.01\ (eV)$	$U_0 = 0.1\ (eV)$	$U_0 = 1\ (eV)$
1	$-6.9 \cdot 10^{-12} + 1.2 \cdot 10^{-6}j$	$-6.9 \cdot 10^{-8} + 1.2 \cdot 10^{-4}j$	$-6.3 \cdot 10^{-4} + 1.1 \cdot 10^{-2}j$	$-0.013 + 0.28j$
0.5	$-9.0 \cdot 10^{-12} + 10.0 \cdot 10^{-7}j$	$-9.0 \cdot 10^{-8} + 10.0 \cdot 10^{-5}j$	$-8.4 \cdot 10^{-4} + 9.8 \cdot 10^{-3}j$	$-0.095 + 0.35j$
0.25	$-9.1 \cdot 10^{-12} + 9.6 \cdot 10^{-7}j$	$-9.1 \cdot 10^{-8} + 9.6 \cdot 10^{-5}j$	$-8.5 \cdot 10^{-4} + 9.4 \cdot 10^{-3}j$	$-0.15 + 0.33j$

Table 3.1.1: The table shows the calculated self-energies for the Hamiltonian of a free particle in an one dimensional infinite space. The results are obtained from a simulation using Kwant. The energy level was set at $E = 0.05\ eV$ and the lattice constants and disorder strength are varied.

a (nm)	$U_0 = 0.001\ (eV)$	$U_0 = 0.01\ (eV)$	$U_0 = 0.1\ (eV)$	$U_0 = 1\ (eV)$
1	$6.0 \cdot 10^{-12} + 1.2 \cdot 10^{-6}j$	$6.0 \cdot 10^{-8} + 1.2 \cdot 10^{-4}j$	$5.5 \cdot 10^{-4} + 1.1 \cdot 10^{-2}j$	$0.011 + 0.28j$
0.5	$-2.2 \cdot 10^{-12} + 7.4 \cdot 10^{-7}j$	$-2.2 \cdot 10^{-8} + 7.4 \cdot 10^{-5}j$	$-2.2 \cdot 10^{-4} + 7.4 \cdot 10^{-3}j$	$-0.076 + 0.35j$
0.25	$-2.3 \cdot 10^{-12} + 6.9 \cdot 10^{-7}j$	$-2.3 \cdot 10^{-8} + 6.9 \cdot 10^{-5}j$	$-2.3 \cdot 10^{-4} + 6.9 \cdot 10^{-3}j$	$-0.14 + 0.32j$

Table 3.1.2: The self-energies correspond to the Hamiltonian of a free particle in an one dimensional infinite space. The results obtained from the simulation are shown for an energy level of 0.10 eV and for different lattice constants and disorder strengths.

a (nm)	$U_0 = 0.001\ (eV)$	$U_0 = 0.01\ (eV)$	$U_0 = 0.1\ (eV)$	$U_0 = 1\ (eV)$
1	$4.0 \cdot 10^{-9} + 4.4 \cdot 10^{-6}j$	$3.7 \cdot 10^{-5} + 4.3 \cdot 10^{-4}j$	$7.2 \cdot 10^{-3} + 1.5 \cdot 10^{-2}j$	$0.036 + 0.28j$
0.5	$-9.0 \cdot 10^{-13} + 6.3 \cdot 10^{-7}j$	$-9.0 \cdot 10^{-9} + 6.3 \cdot 10^{-5}j$	$-9.0 \cdot 10^{-5} + 6.3 \cdot 10^{-3}j$	$-0.057 + 0.35j$
0.25	$-1.0 \cdot 10^{-12} + 5.7 \cdot 10^{-7}j$	$-1.0 \cdot 10^{-8} + 5.7 \cdot 10^{-5}j$	$-1.0 \cdot 10^{-4} + 5.7 \cdot 10^{-3}j$	$-0.12 + 0.32j$

Table 3.1.3: The table gives the self-energies with an energy level set to 0.15 eV for various lattice constants and disorder strengths. The Hamiltonian is that of a free particle in a one dimensional infinite space.

In figure 3.1.2 the real and imaginary part of the self-energy are plotted as a function of the lattice constant. The energy level and disorder strength are set to 0.05 and 0.1 eV respectively.

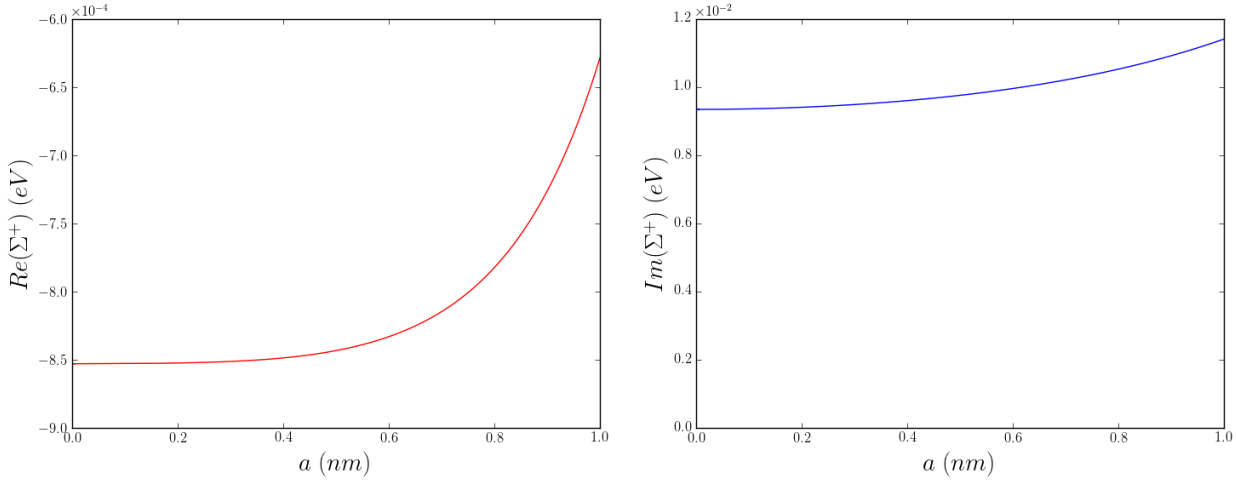

Figure 3.1.2: Plots of the real and imaginary part of the self-energy as a function of the lattice constant. The Hamiltonian is that of a free particle in an one dimensional infinite space. The energy level is fixed at 0.05 eV and the disorder strength is set to 0.1 eV.

The real and imaginary part of the self-energy converge asymptotically towards certain values when the lattice constant is decreased.

Because the impurity density is $1/a$, the on-site energy fluctuates more rapidly over a certain distance for smaller lattice constants and therefore a smaller lattice constant corresponds to stronger disorder. By scaling the formula for the self-energy with a, the effective disorder remains constant and self-energies evaluated for different lattice constants can be fairly compared. The red and blue curve in figure 3.1.2 have a shape that agrees with this reasoning. At large lattice constants Σ^+ is changing at a relatively fast pace due to the tight-binding Hamiltonian, but for lattice constants smaller than roughly 0.4 nm the tight-binding Hamiltonians become more or less equal for $E = 0.05\ eV$ and thus the red and blue curve become flat, eventually reaching a continuous limit. If figure 3.1.2 is plotted for a lower energy than 0.05 eV the real and imaginary part already become roughly flat at a lattice constant higher than 0.4 nm and for energies higher than 0.05 eV the curves become roughly flat at a smaller lattice constant than 0.4 nm.

Now the lattice constant is fixed at 0.25 nm, the energy level is 0.05 eV and the disorder strength is varied.

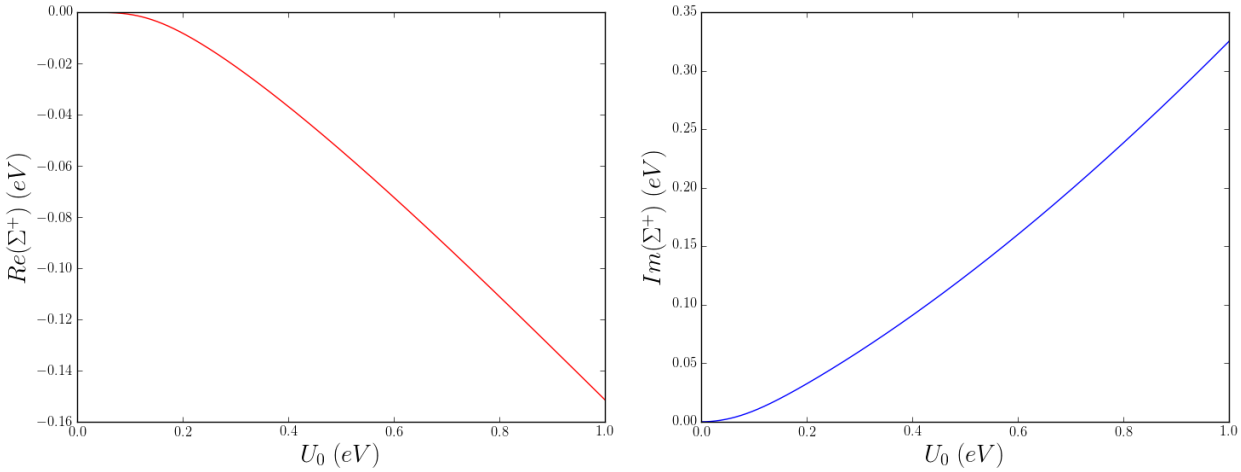

Figure 3.1.3: Plots of the real and imaginary part of the self-energy as a function of the disorder strength. The Hamiltonian is that of a free particle in an one dimensional infinite space. The energy level is fixed at 0.05 eV and the lattice constant is set to 0.25 nm.

Clearly from figure 3.1.3 the real part as well as the imaginary part of the self-energy go further away from zero as the disorder strength increases. The parabolic shape agrees with formula (3.1.13): $\Sigma^+ \propto U_0^2$.

Lastly the lattice constant and disorder strength are fixed while the energy is varied.

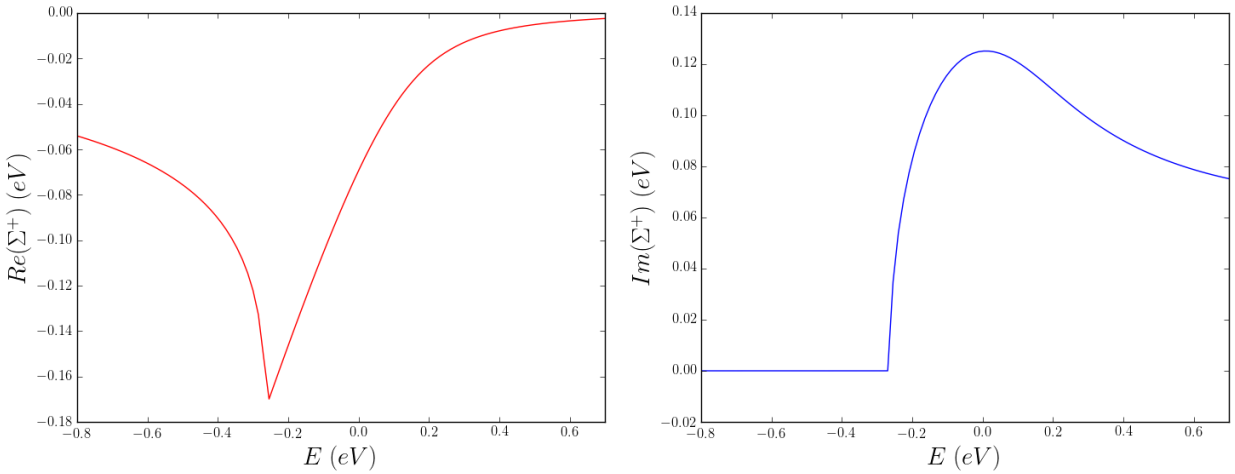

Figure 3.1.4: Plots of the real and imaginary part of the self-energy as a function of energy with $a = 0.25\ nm$ and $U_0 = 0.5\ eV$. The Hamiltonian is that of a free particle in an one dimensional infinite space.

In figure 3.1.4 it is seen that the real part of the self-energy goes asymptotically to zero for high energies. Starting from a high energy moving downwards, the real part of the self-energy becomes smaller and smaller, but then, at some energy, there is a discontinuity in the derivative and the real part of the self-energy goes up again. The imaginary part of the self-energy has a maximum at $E = 0\ eV$ and becomes zero at the same energy where the real part has a discontinuity in the derivative.

The real part of the self-energy shifts the bands up or down (see equation (2.3.59a)). In order to get the first Born approximation of the tight-binding average disorder band structure, the real part of the self-energy at a certain energy, E_0, is added to the Hamiltonian and the band structure is calculated. However, this calculated band structure is only valid at the energy E_0 and therefore only the states at E_0 are kept. In formula form

$$E(k_{dis}) - E_0 = 0, \tag{3.1.14}$$

where $E(k_{dis})$ is the band structure calculated for a Hamiltonian with a self-energy evaluated at E_0. The solutions (E_0, k_{dis}) are the disordered states. The process is carried out for a wide range of E_0-values, consequently all the average disordered states are found and the band structure is constructed. An example of the effect of the disorder on the band structure is shown in figure 3.1.5 for $U_0 = 0.2\ eV$ and $U_0 = 0.5\ eV$.

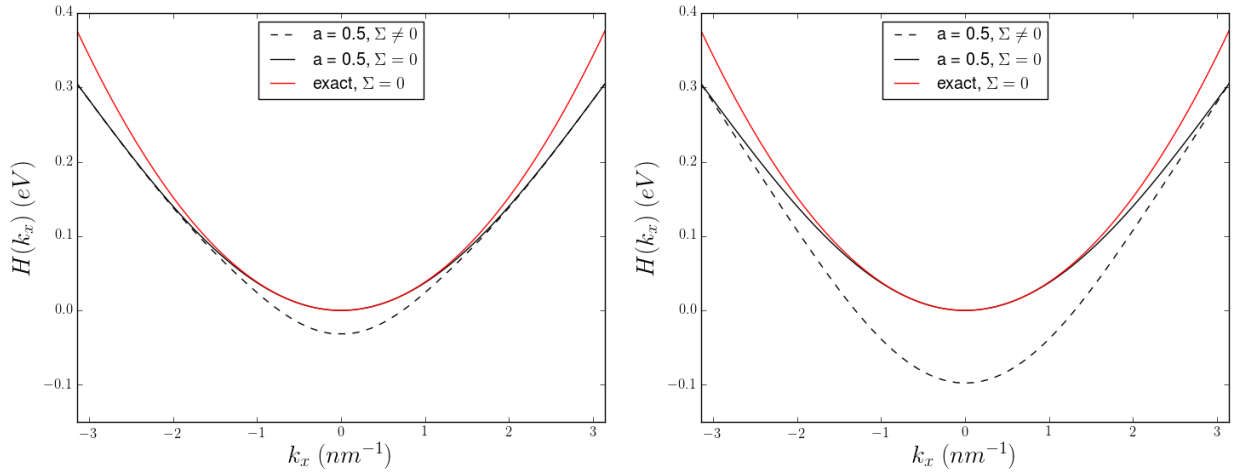

Figure 3.1.5: In each figure there are two plots of the band structure for the lattice constant 0.5 nm: one with the correction for the added disorder (dashed line) and without the disorder (non-dashed line). The exact dispersion relation is also added in red. The Hamiltonian is that of a free particle in an one dimensional infinite space. The left figure corresponds with a disorder strength of 0.2 eV and the right figure with a disorder strength of 0.5 eV.

In the two figures it can be seen that the effect of the disorder is that the bands shift downwards. For wave vectors around the Γ-point the downward shift is stronger than for larger k-values.

During the construction of the bands in the two plots in figure 3.1.5, only values on the right side of the derivative-discontinuity point were used in the corresponding real part of the self-energy versus energy plots (see the left plot in figure 3.1.4 with $a = 0.25\ nm$ and $U_0 = 0.5\ eV$). A question that might arise is, if for all values of U_0 only values on the right side of the derivative-discontinuity point are used. If this would not be the case the disordered band would get flatter[3] around the Γ-point; fortunately this distortion does not happen. The derivative-discontinuity point in the real part of the self-energy versus energy plot, $(E^*, Re(\Sigma^+)^*)$, is for every U_0 such that $E^* < Re(\Sigma^+)^*$. It is therefore only necessary to discuss the right side of the $Re(\Sigma^+)$ versus energy plot. At high energies the electrons are not bothered by the impurities, the difference between the disordered and non-disordered states disappear and therefore the real part of the self-energy goes asymptotically to zero for high energies. Lower energy electrons are more strongly influenced by the impurities and $Re(\Sigma^+)$ becomes more negative when the energy is decreased. The difference between the disordered and non-disordered states increases for lower energies and has its maximum at the Γ-point. It can be said that disorder creates states below the band.

Throughout the work the focus was mainly on the real or Hermitian part of the self-energy. The imaginary or anti-Hermitian part causes the ensemble averaged Green's function to decay with time (see equations (2.3.59a) and (2.3.59b)). The retarded Green's function propagates the wave function (see equation (2.1.11)) and thus the imaginary/anti-Hermitian part of the self-energy gives a decaying component to the wave function. A question that might arise is, if the shape of the right plot in figure 3.1.4, which shows the imaginary part of the self-energy versus the energy, makes sense. The aforementioned plot has parameters $a = 0.25\ nm$ and $U_0 = 0.5\ eV$ and therefore matches with the green dashed band in the right image of figure

[3]If only the right side of the derivative-discontinuity point would be used, the process of seeking disordered states would go as follows: pick a relative high energy E_0, the self-energy at that energy is evaluated, the real part is added to the Hamiltonian, the disordered band is plotted and it is checked if the disordered band and horizontal line at energy E_0 cross. Because a relatively high E_0 was picked there will be two crossings. Consequently E_0 is lowered and new disordered states are found. During the lowering of E_0, the disordered band of E_0 and the horizontal line E_0 both move down, but the horizontal line goes down faster than the parabola so that at a certain E_0 no more states are found. If the real part of the self-energy versus energy plot would be such, that also the left side of the derivative-discontinuity point would be used, the situation would occur that while lowering E_0 the disordered band of E_0 is moving upwards. Because they are now moving towards each other, the crossings (disordered states) move faster inwards towards $k = 0$ and the constructed disordered band would appear flatter around the Γ-point.

3.1.5. From the green dashed band it can be seen that there are not disordered states for energies below roughly $-0.11\ eV$ and therefore the values of $Im(\Sigma^+)$ have no meaning for energies below $-0.11\ eV$. At energies higher than roughly $0.7\ eV$ the tight binding approximation with $a = 0.25\ nm$ does no approximate the real band well any more and it therefore make no sense to investigate $Im(\Sigma^+)$ (or $Re(\Sigma^+)$) for energies higher than $0.7\ eV$. In the relevant energy-interval, $[-0.11\ eV, 0.7\ eV]$, $Im(\Sigma^+)$ has a maximum at $E = 0\ eV$. This makes sense, because the electron is bothered mostly by the impurities when its energy is low compared to the impurity potential amplitudes. When the energy of the electron is increased, it feels relatively less of the impurities and therefore $Im(\Sigma^+)$ decreases and the wave function decays slower.

3.1.2 Particle in a 1D quantum well

Consider a 1D quantum well with

$$\hat{H} = -\frac{\hbar^2}{2m}\frac{d^2}{dx^2} + V(x), \quad \text{where} \quad V(x) = \begin{cases} 0 & \text{for } 0 < x < L \\ \infty & \text{otherwise.} \end{cases} \tag{3.1.15}$$

There is no potential gradient for $0 < x < L$ and an infinite potential otherwise. The energy levels for this Hamiltonian are

$$E_n = \frac{n^2\hbar^2\pi^2}{2mL^2} \tag{3.1.16}$$

and the eigenfunctions are

$$\psi_n(x) = \sqrt{\frac{2}{L}}\,\sin\Big(\frac{n\pi x}{L}\Big) \tag{3.1.17}$$

with $n = 1, 2, 3, \ldots$.

The Hamiltonian of equation (3.1.15) is discretized between $0 < x < L$ on a 1D lattice with $N + 1$ sites and lattice constant a. The matrix elements of the Hamiltonian are given by equation (2.2.7)

$$\hat{H} = 2t\sum_i |i\rangle\langle i| - t\sum_{\langle i,j\rangle} |i\rangle\langle j|\,, \tag{3.1.18}$$

where$t = \hbar^2/2ma^2$. The summation indices i and j run over all the lattice points and $\langle\ \rangle$ means nearest neighbours. In equation (3.1.18) it can be seen that the on-site energy is $2t$ and the hopping energy is $-t$. The on-site and hopping energies are given as input to Kwant[8]. The calculation is done with a well length of $L = 100\ nm$ and lattice constants of 1, 0.5 and 0.25 nm. The resulting energies and the wave function corresponding to the lowest energy are plotted in figure 3.1.6 and 3.1.7 respectively.

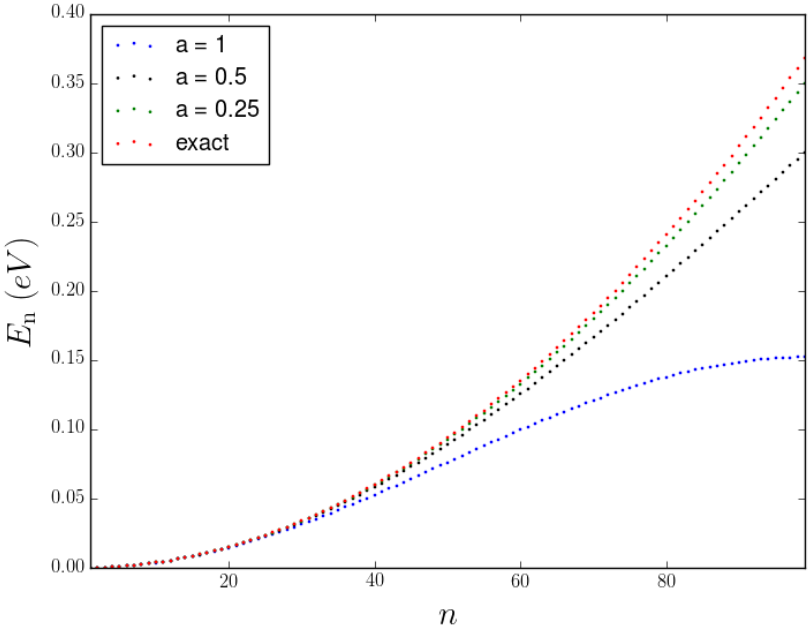

Figure 3.1.6: Three plots of the eigenvalues of the discretized Hamiltonian (see equation (3.1.18)) for different lattice constants and a plot of the exact energies (see equation (3.1.16)). The Hamiltonian corresponds to a 1D infinite well with length $L = 100\ nm$.

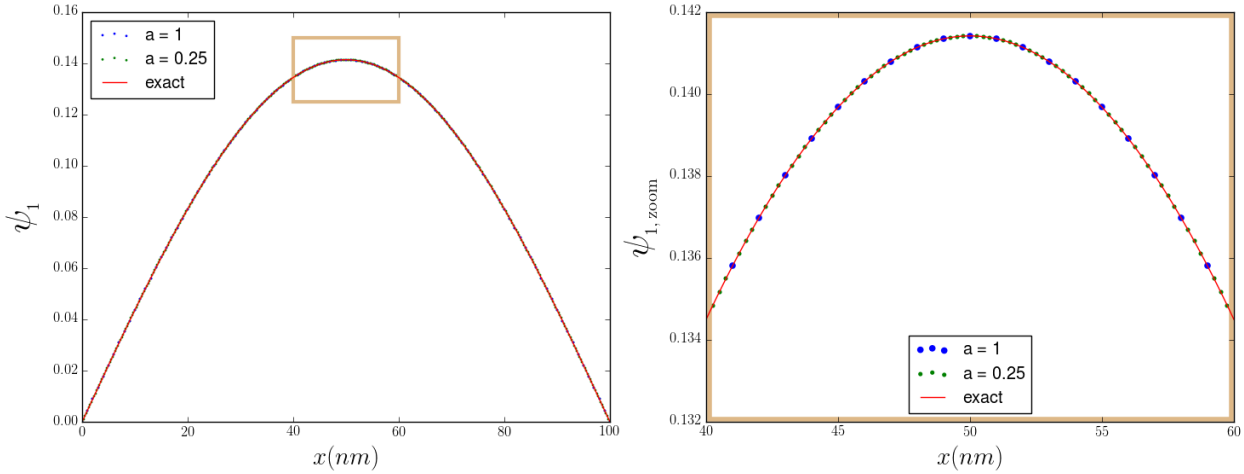

Figure 3.1.7: Left: Plots of the wave function corresponding with the lowest energy eigenvalue of a 1D quantum well with length 100 nm. The exact wave function is approximated using a tight binding approach with lattice constants $a = 1$ and $a = 0.25\ nm$. The red curve corresponds to the exact solution. Right: A zoom-in of the top part of the left figure.

In figure 3.1.6 it can be seen that when a becomes smaller the calculated energies come closer to the exact ones for ever higher values of n.

Figure 3.1.7 shows that the calculated wave functions corresponding to the lowest energy eigenvalue

approximate the exact wave function very well. This result is in agreement with the plot of the energies (figure 3.1.6), because the energies are very close to eachother for $n = 1$. Based on figure 3.1.6 it can be expected that for higher values of n the deviations of the approximated wave functions from the exact ones become more pronounced. The wave function is also plotted for $n = 20$.

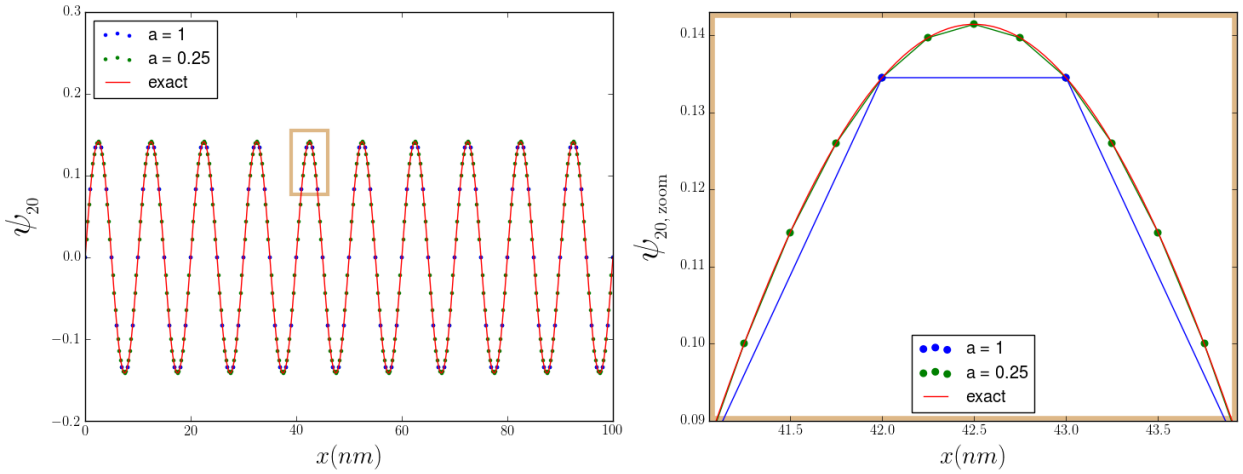

Figure 3.1.8: Left: Plots of the wave function corresponding with the twentieth eigenvalue of a 1D quantum well with length 100 nm. The red curve corresponds to the exact solution while the blue and green dots are the approximated points for different lattice constants. Right: A zoom-in of a top part of the left figure.

The zoomed-in plot of the 20-eigenfunction shows that for lattice constant $a = 1$ the approximation of the exact wave function becomes very crude, while for $a = 0.25$ the wave function is still approximated well by the calculated points.

Similar to section 3.1.1 it is interesting to see how average disorder will modify the energy levels of this system. In this example the system is finite and therefore the analytical approach as well as the 'brute force' method can be applied. The implementation of both approaches allows for comparison between them.

In case of the 'brute force' method, the disorder averaged energies are calculated by generating realisations of the system where independent and identically distributed disorder potentials are added to the on-site energies and by subsequently averaging over the energy levels of the realisations. In case of the analytical approach the first order self-consistent Born approximation (1SBA) is applied. The distribution where the disorder amplitudes are generated from is chosen to be the uniform distribution in the interval $[-U_0/2, U_0/2]$ and the impurity concentration, n, is equal to $1/a$. The self-energy is calculated by self-consistently solving equation (2.3.67), which for the described system is

$$\Sigma^+(E) = \frac{aU_0^2}{12} G^+(x = 0, E).$$

After scaling (see section 2.3.5) it obeys

$$\Sigma^+(E) = \frac{U_0^2}{12} G^+(x = 0, E). \tag{3.1.19}$$

Although the equations (3.1.13) and (3.1.19) are identical, the algorithm in this section, that is used to calculated the disordered states based on the first order self-consistent Born approximation, is different from the one described in section 3.1.1. In section 3.1.1 a range of energies were scanned, where for each energy, E_0, it was verified if there were any wave vectors, k_{dis}, for which equation (3.1.14) holds. In this section the calculation works in the other direction; the n-values are the input and the energy is the solution. For a

n-value an initial guess for the disordered energy is chosen, the self-energy can be calculated for this energy, consequently taking the real part of the self-energy and adding it to the Hamiltonian will give a new energy. The latter energy is used to replace the initial guess of the disordered energy. The process is repeated until the cange in energy is below a reasonable threshold value.

For the 'brute force' method as well as the 1SBA, the software package Kwant[8] is used. The length of the quantum well, the lattice constant and U_0 are set to 100 nm, 0.25 nm and 0.5 eV respectively. Figure 3.1.9 shows the result of the simulation, the purple dots correspond to the average disorder 'brute force' energies, the black dots are the energies with average disorder according to the analytical approach and the green ones give the tight-binding energy levels of the 'clean' quantum well.

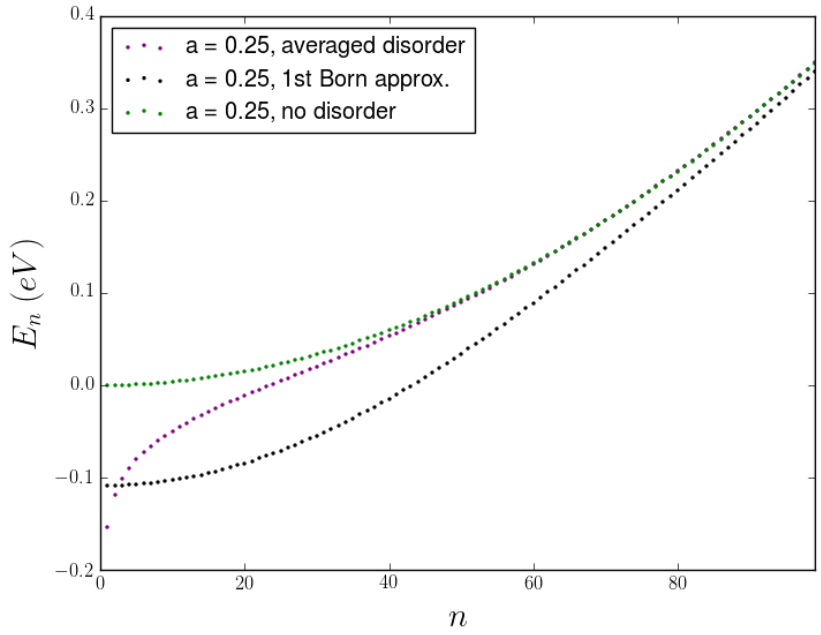

Figure 3.1.9: Three scatter plots of the energies of a 1D quantum well with a length of 100 nm. The purple dots are the energies calculated by averaging over disordered realisations of the system. Impurity amplitudes are generated from a uniform distribution in the interval $[-U_0/2, U_0/2]$ and added to the on-site energies. Next the eigenvalues are calculated and stored. By repeating the calculation many times and averaging over the stored eigenvalues the purple dots are the result. The black dots correspond to the energies according to the first order self-consistent Born approximation and the green ones are the energies of the quantum well without any disorder. The lattice constant is fixed at 0.25 nm and U_0 is 0.5 eV.

In figure 3.1.9 it can be seen that the 1SBA does not agree very well with the 'brute force' solution. At low energies the 'brute force' solution shows an exponential tail that is concave, while the analytical solution has a convex (distorted) parabolic shape. The two solutions cross and while the 'brute force' solution quickly approaches the zero disorder energies when n goes up, the analytical solution approaches it much slower.

It is possible to improve the analytical method by including the second diagram of figure 2.3.16 in the calculation. The equation for the second order self-consistent Born approximation (2SBA) is

$$\Sigma^+(\bar{k}, E) = a^6 n \tilde{U}_2' \int \frac{d^3\bar{k}'}{(2\pi)^3} G^+(\bar{k}', E) + a^{12} n^2 \left(\tilde{U}_2'\right)^2 \int \frac{d^3\bar{k}''}{(2\pi)^3} \int \frac{d^3\bar{k}'}{(2\pi)^3} G^+(\bar{k}'' - \bar{k}' + \bar{k}, E) G^+(\bar{k}'', E) G^+(\bar{k}', E), \tag{3.1.20}$$
$$\text{where } G^+(\bar{k}, E) = \frac{1}{E + i\epsilon - H_0(\bar{k}) - \Sigma^+(\bar{k}, E)}.$$

The result is a much more complicated self-consistent equation for the self-energy. Note that the self-energy also depends on the wave vector due to the second term. Not only solving for the self-energy becomes more

complicated, but also adjusting the band structure for the disorder is more cumbersome. Throughout this work only the 1SBA is applied, but for further research it could be worthwhile to investigate the 2SBA.

3.1.3 A 1D infinite space with a non-coupled matrix Hamiltonian

Consider a 1D infinite space with the Hamiltonian

$$\hat{H} = \hat{\sigma}_z \left(\frac{\Delta}{2} - \frac{\hbar^2}{2m} \frac{d^2}{dx^2} \right), \tag{3.1.21}$$

where $\hat{\sigma}_z$ is a Pauli spin matrix. The Hamiltonian is discretized and the on-site and hopping energies, which are matrices, are given as input to Kwant[8]. Figure 3.1.10 shows the tight-binding dispersion for different lattice constants as well as the exact dispersion. The wave vector runs from $-\pi$ to π and the value of Δ is 0.1 eV.

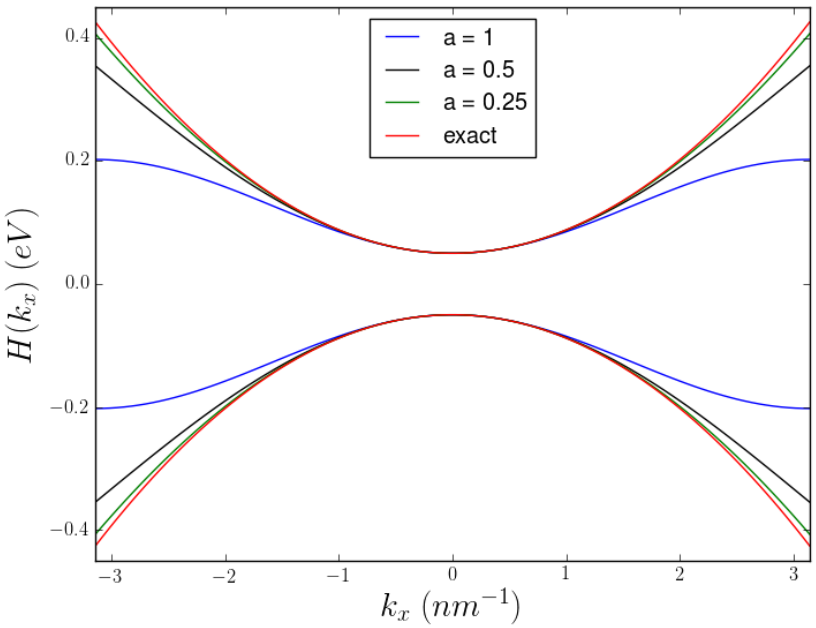

Figure 3.1.10: Three plots of the discretized Hamiltonian with different lattice constants and a plot of the exact energies. The Hamiltonian is that of a free electron and a free hole in an one dimensional infinite space. The wave vector k_x runs from $-\pi$ to π and $\Delta = 0.1$ eV.

It is investigated how average disorder will modify the band structure of this system. Because the system is infinite, application of the 'brute force' method as was done in section 3.1.2, is not possible. The effect of average disorder on the band structure will be calculated by applying the first order self-consistent Born approximation.

There is no coupling between the matrix elements of the Hamiltonian and therefore the self-energy is obtained by self-consistently solving equation (2.3.67) for the two matrix elements of the Hamiltonian separately.

The disorder amplitudes have the uniform distribution in the interval $[-U_0/2, U_0/2]$ and therefore $\tilde{U}_2' = U_0^2/12$. In order to fairly compare self-energies evaluated for different lattice constants, the second moment of the uniform distribution, $U_0^2/12$, is scaled according to equation (2.3.74): $\tilde{U}_{2,s}' = \tilde{U}_2'/a = U_0^2/12a$. The scaling with a however does not effect the units of the equation. Further the impurity density, n, is equal to

$1/a$. By taking the aforementioned comments into account, the equation for the self-energy is

$$\Sigma^+(E) = \frac{U_0^2}{12a} G^+(x = 0, E). \tag{3.1.22}$$

The real part of the self-energy is added to the Hamiltonian elements after which the disordered bands are plotted. However the self-energy is energy-dependent and therefore only states are kept at the energy for which the self-energy was calculated. In other words for every point on the disordered bands

$$E(k_{dis}) - E_0 = 0, \tag{3.1.23}$$

where E_0 is the energy at which Σ^+ was calculated and $E(k_{dis})$ the band structure that corresponds with $\hat{H} + Re(\Sigma^+)$. By scanning a range of energies, all the disordered states are found and the dispersion is constructed. Figure 3.1.11 shows the disordered as well as the 'clean' band structure for $\Delta = 0.1\ eV$, $a = 0.5\ nm$ and $U_0 = 0.2\ eV$. Also the exact no-disorder dispersion is plotted in red.

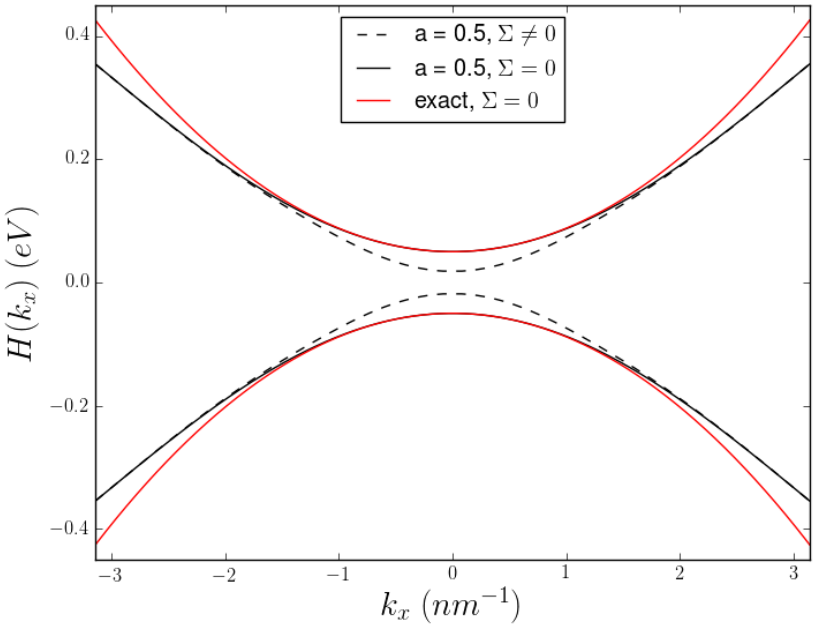

Figure 3.1.11: Plots of the dispersion with and without average disorder for $a = 0.5\ nm$ as well as the no-disorder exact dispersion (red parabolas). The Hamiltonian is that of a free electron and hole in an one dimensional infinite space and the disorder is taken into account through application of the first order self-consistent Born approximation. The wave vector k_x runs from $-\pi$ to π, $\Delta = 0.1\ eV$ and $U_0 = 0.2\ eV$.

In figure 3.1.11 it can be seen that the effect of the disorder is that the band gap becomes smaller, however a disorder strength of $U_0 = 0.2\ eV$ is not enough to close the gap completely. In figure 3.1.12 the disorder strength is increased to $U_0 = 0.4\ eV$ causing band inversion. Disorder can thus change the transport properties of a system dramatically.

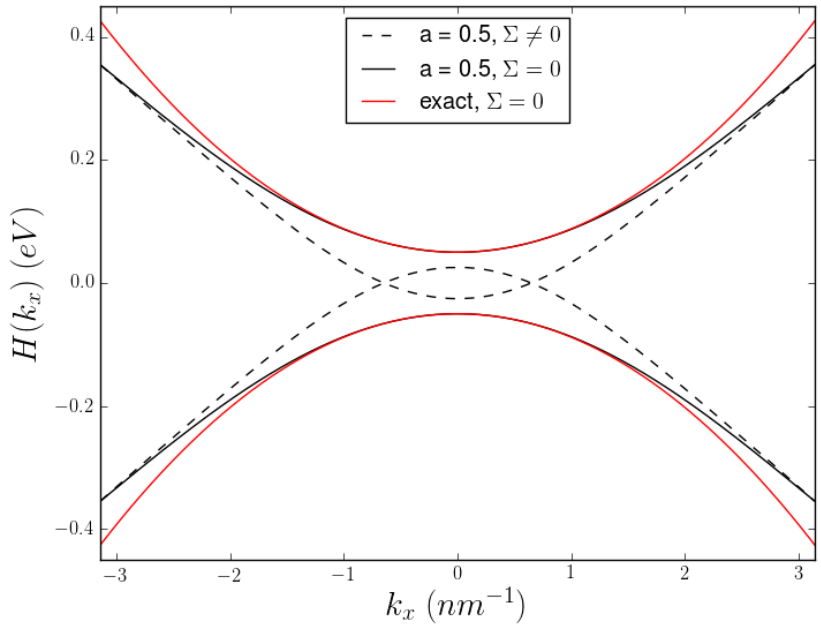

Figure 3.1.12: Band structure with and without average disorder for $a = 0.5\ nm$ as well as the no-disorder exact dispersion. The Hamiltonian is that for a free electron and hole in an infinite one dimensional space. The wave vector k_x runs from $-\pi$ to π, $\Delta = 0.1\ eV$ and $U_0 = 0.4\ eV$.

3.1.4 A 1D infinite space with a coupled matrix Hamiltonian

Consider a 1D infinite space with the Hamiltonian

$$\hat{H} = \hat{\sigma}_0 \left(-\frac{\hbar^2}{2m} \frac{d^2}{dx^2} \right) - \hat{\sigma}_y \left(\tilde{\alpha} i \hbar \frac{d}{dx} \right), \tag{3.1.24}$$

where $\hat{\sigma}_0$ is the identity matrix and $\hat{\sigma}_y$ is a Pauli spin matrix.

Defining a new parameter $\alpha = \tilde{\alpha}\hbar$ gives

$$\hat{H} = \hat{\sigma}_0 \left(-\frac{\hbar^2}{2m} \frac{d^2}{dx^2} \right) - \hat{\sigma}_y \left(\alpha i \frac{d}{dx} \right). \tag{3.1.25}$$

The value of α gives the strength of the Rashba spin-orbit coupling.

The Hamiltonian is discretized and the on-site and hopping energies, which are matrices, are given as input to Kwant[8]. Figure 3.1.14 shows the tight-binding dispersion for $a = 0.25\ nm$. The wave vector runs from $-\pi$ to π and the value of α is $0.05\ eVnm$.

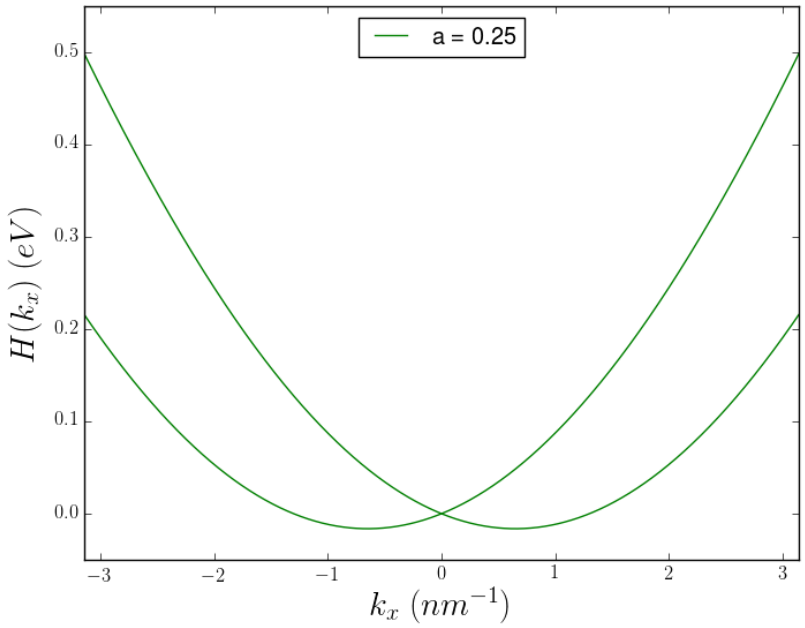

Figure 3.1.13: Plot of the discretized Hamiltonian with a lattice constant of 0.25 nm. The Hamiltonian is a non-diagonal two by two matrix and the space is one dimensional and infinite. The wave vector k_x runs from $-\pi$ to π and $\alpha = 0.05\ eVnm$.

It is interesting to see how average disorder will modify the band structure. The system is infinite and therefore it is not possible to average over generated realisations of disordered band structures (as was done in section 3.1.2). The effect of average disorder on the band structure is calculated by applying the first order self-consistent Born approximation. The disorder amplitudes have the uniform distribution in the interval $[-U_0/2, U_0/2]$ and therefore $\tilde{U}_2' = U_0^2/12$. In order to fairly compare self-energies evaluated for different lattice constants, the second moment of the uniform distribution, $U_0^2/12$, is scaled according to equation (2.3.74) and thus $\tilde{U}_{2,s}' = \tilde{U}_2'/a = U_0^2/12a$. The scaling with a however does not effect the units of the equation. Further the impurity density, n, is equal to $1/a$. With these parameters, equation (2.3.67) becomes

$$\Sigma^+(E) = \frac{U_0^2}{12a} G^+(x = 0, E). \tag{3.1.26}$$

There is coupling between the matrix elements of the Hamiltonian and it is therefore not possible to solve for each element separately. The self-energy evaluated at a certain energy is a non-diagonal 2×2 matrix. The Hermitian part of the self-energy matrix is added to the Hamiltonian after which the disordered bands are calculated. Only the disordered states that correspond to the energy at which the self-energy was evaluated are kept. By scanning a wide range of energies, the valid disordered states are found and the band structure is constructed.

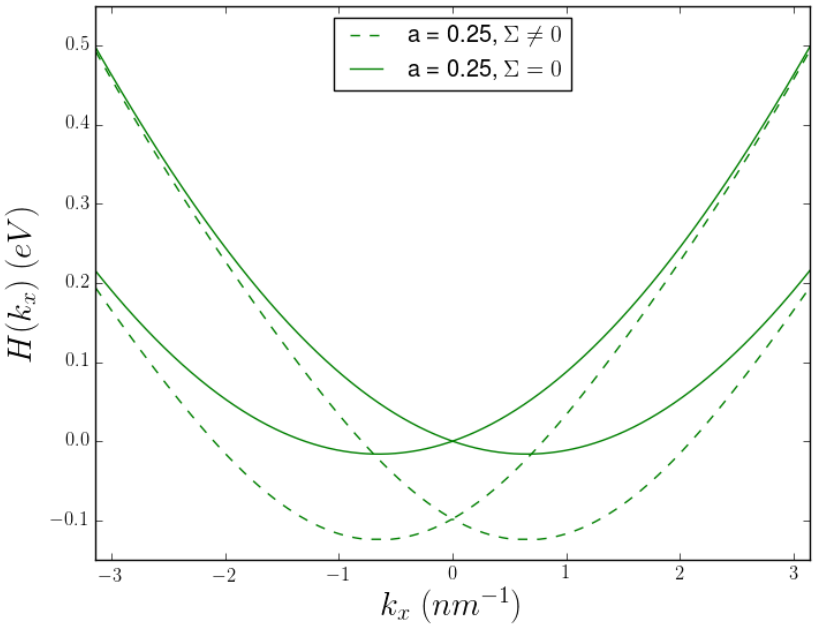

Figure 3.1.14: Band structure with and without disorder for a lattice constant of 0.25 nm. The Hamiltonian is a non-diagonal two by two matrix and the space is one dimensional and infinite. The disorder is taken into account through application of the first order self-consistent Born approximation. The wave vector k_x runs from $-\pi$ to π, $\alpha = 0.05\ eVnm$ and $U_0 = 0.5\ eV$.

3.1.5 Free particle in a 2D infinite space

Consider a two dimensional infinite space with a constant potential which can be set to zero. The Hamiltonian of such a system is

$$\hat{H} = -\frac{\hbar^2}{2m}\left(\frac{\partial^2}{\partial x^2} + \frac{\partial^2}{\partial y^2}\right). \tag{3.1.27}$$

The dispersion relation for this Hamiltonian is

$$E(k_x, k_y) = \frac{\hbar^2\left(k_x^2 + k_y^2\right)}{2m} \tag{3.1.28}$$

and the eigenfuntions are plane waves.

The Hamiltonian can be discretized,

$$\hat{H} = 4t\sum_{i,j}|i,j\rangle\langle i,j| - t\sum_{<i,j\ ;\ i',j'>}|i,j\rangle\langle i',j'|, \tag{3.1.29}$$

where the summation indices i, j run over all the lattice sites and $<\ >$ means nearest neighbours. The Hamiltonian is given as an input to Kwant[8] and the dispersion relation is calculated. Figures 3.1.15 and 3.1.16 show the result, where the tight-binding dispersion relation is plotted for three different lattice constants as well as the exact solution. In figure 3.1.15, k_y is set to zero and k_x runs from $-\pi$ to π, while in figure 3.1.16 both wavevectors run from $-\pi$ to π.

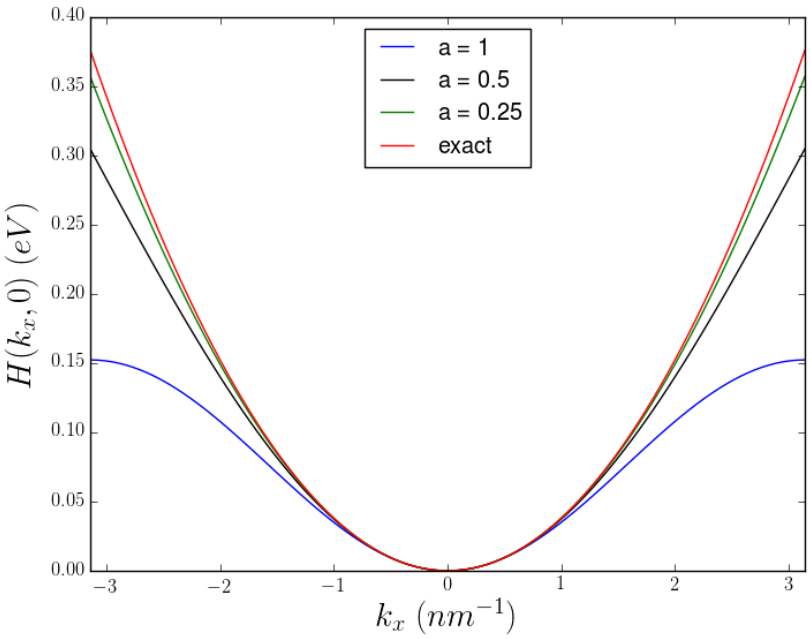

Figure 3.1.15: Three plots of the discretized Hamiltonian (see equation (3.1.29)) with different lattice constants and a plot of the exact dispersion (see equation (3.1.28)). The Hamiltonian corresponds to a free electron in a two dimensional infinite space. The wavevector k_x runs from $-\pi$ to π and k_y is set equal to 0.

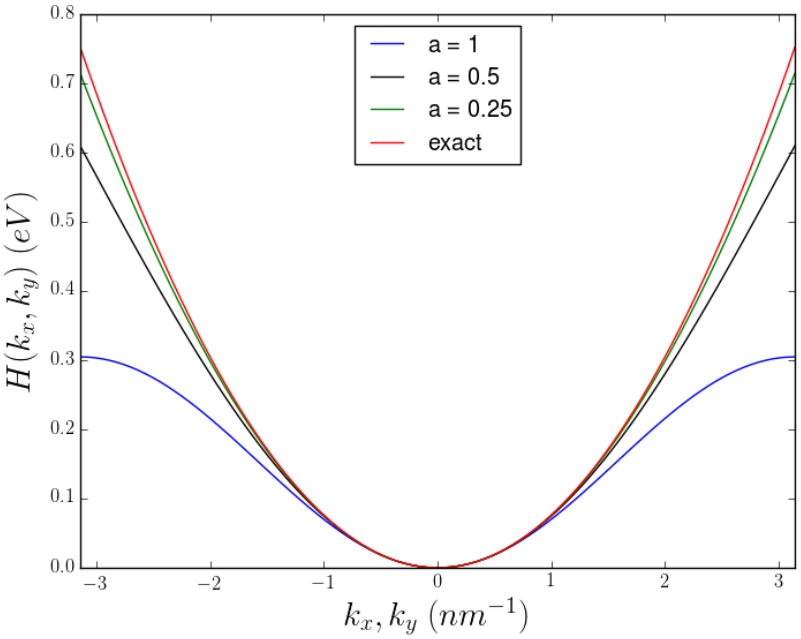

Figure 3.1.16: Plots of the discretized Hamiltonian for different lattice constants and a plot of the exact band structure (see equation (3.1.28)). The Hamiltonian corresponds to a free electron in a two dimensional infinite space. The wavevectors k_x and k_y run from $-\pi$ to π at an equal rate and thus the wavevector space is traversed diagonally.

Just as for the previous Hamiltonians the goal is to study the effect of average disorder on the dispersion. The problem is not one dimensional, making it more complicated. A separable wave function (e.g. $\psi(x,y) = \psi(x)\psi(y)$) does not necessarily correspond with a separable Green's function; this prevents treating each dimension separately when dealing with average disorder. The effect of average disorder is taken into account by applying the first order self-consistent Born approximation.

The distribution where the disorder amplitudes are generated from is chosen to be the uniform distribution in the interval $[-U_0/2, U_0/2]$. This distribution has first moment $\tilde{U}_1' = 0$ and second moment $\tilde{U}_2' = U_0^2/12$. The second moment, $U_0^2/12$, is scaled by dividing by a^2 (see equation (2.3.74)). Further the impurity concentration is equal to $1/a^2$. The first order approximation of the self-energy can be found by solving the self-consistent relation of equation (2.3.62), which for the presented situation is

$$\Sigma^+(E) = a^4 n \tilde{U}_2' \lim_{\epsilon\to 0} \int \frac{d^2\bar{k}}{(2\pi)^2} \cdot \frac{1}{E + i\epsilon - H_0(\bar{k}) - \Sigma^+(E)},$$

$$\Sigma^+(E) = \frac{U_0^2}{48\pi^2} \lim_{\epsilon\to 0} \int_{-\pi/a}^{\pi/a} dk_y \int_{-\pi/a}^{\pi/a} dk_x \cdot \frac{1}{E + i\epsilon - H_0(k_x, k_y) - \Sigma^+(E)}, \tag{3.1.30}$$

with $H_0(k_x, k_y) = 2t(1 - \cos(ak_x)) + 2t(1 - \cos(ak_y))$ in which $t = \hbar^2/2ma^2$. In appendix B.2 equation (3.1.30) is solved numerically, but a different procedure is outlined here.

For two dimensional problems the relation between the self-energy and Green's function for the first order self-consistent Born approximation is

$$\Sigma^+(E) = \frac{U_0^2}{24\pi} \int_{-\pi/a}^{\pi/a} dk_y \left[\frac{1}{2\pi} \int_{-\pi/a}^{\pi/a} dk_x G^+(k_x, k_y, E) \right]. \tag{3.1.31}$$

Using the Fourier transform (see equation (2.3.66b) and take $\bar{r} = 0$), equation (3.1.31) can be rewritten as

$$\Sigma^+(E) = \frac{U_0^2}{24\pi} \int_{-\pi/a}^{\pi/a} dk_y G^+(x = 0, k_y, E). \tag{3.1.32}$$

With the software package Kwant[8] an infinite one dimensional chain is build and the on-site and hopping energies are added, which are $2t+2t(1-\cos(ak_y))+\Sigma^+$ and $-t$ respectively, where $t = \hbar^2/2ma^2$. Subsequently a value for the lattice constant, the energy and an initial guess for Σ^+ are chosen. Then Kwant is used to calculate the Green's function at the origin for different values of k_y that lie in the interval $[-\pi/a, \pi/a]$. With these values the integral can be approximated and from there the self-energy. This result is then used to modify the on-site energies of all the lattice sites and the whole process is iterated until desired accuracy is obtained. By using an Anderson mixing scheme, the solution is typically found after just a few iterations.

Figure 3.1.17 shows the real and imaginary part of the self-energy plotted versus the lattice constant.

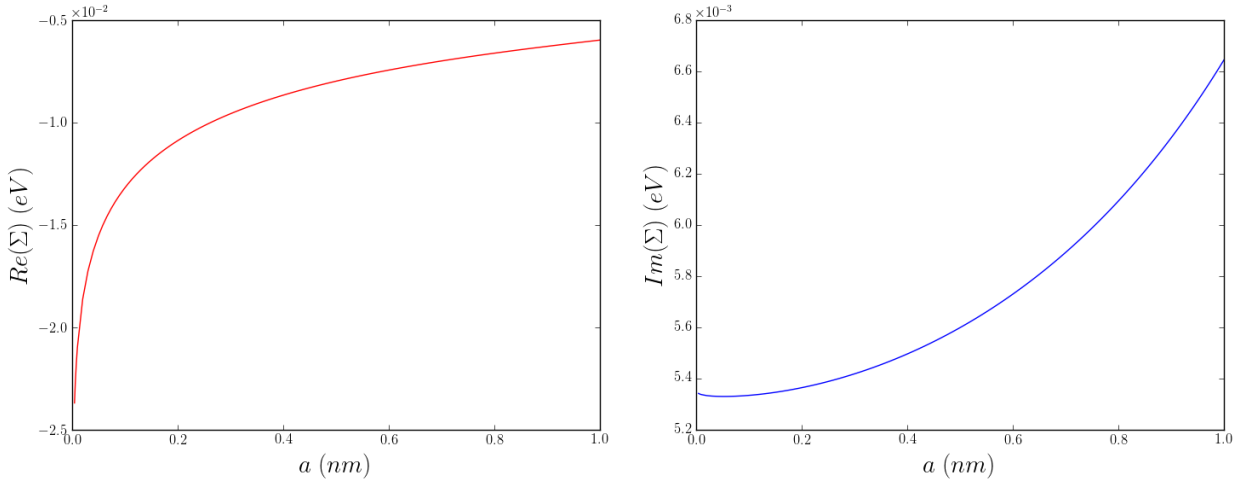

Figure 3.1.17: Plots of the real and imaginary part of the self-energy as a function of the lattice constant. The Hamiltonian is that of a free electron in a two dimensional infinite space. The energy level is fixed at 0.05 eV and the disorder strength is set to 0.1 eV. The self-energy is calculated using the first order self-consistent Born approximation and the impurity amplitudes have an uniform distribution in the interval $[-U_0/2, U_0/2]$.

The real and imaginary part of the self-energy do not converge towards a horizontal asymptote when the lattice constant is decreased. The real part curves downwards for small lattice constants instead of becoming horizontal and although the imaginary part seems to become 'flat', it curves upwards for different energy levels. This result is surprising, reflecting back on figure 3.1.2, which shows the same plots for the one dimensional case and reflecting on section 2.3.5, which discusses scaling of the disorder strength with the lattice constant. The argument why the curves were expected to look similar to figure 3.1.2 is repeated. The impurity density is $1/a^2$ and therefore the on-site energy fluctuates more rapidly over a certain distance for small lattice constants compared to large lattice constants and thus a small lattice constant corresponds with relatively strong disorder. By scaling the formula for the self-energy with a^2, the effective disorder remains constant and self-energies evaluated for different lattice constants can be fairly compared (see section 2.3.5). At large lattice constants Σ^+ is expected to change at a relatively fast pace due to the tight-binding Hamiltonian, but for small lattice constants there is hardly any difference between the tight-binding Hamiltonians for an energy of $E = 0.05$ eV (see figures 3.1.15 and 3.1.16). Unfortunately this is not reflected in the red line in figure 3.1.17, which shows a strong dependence on a for small values of a instead of being 'flat'. Fortunately however, both curves cross the y-axis and do not go to plus or minus infinity. It

is concluded that the shape of the plots in figure 3.1.17 do not make sense and the results are therefore expected to be wrong.

Figure 3.1.18 shows the real and imaginary part of the self-energy plotted versus the energy.

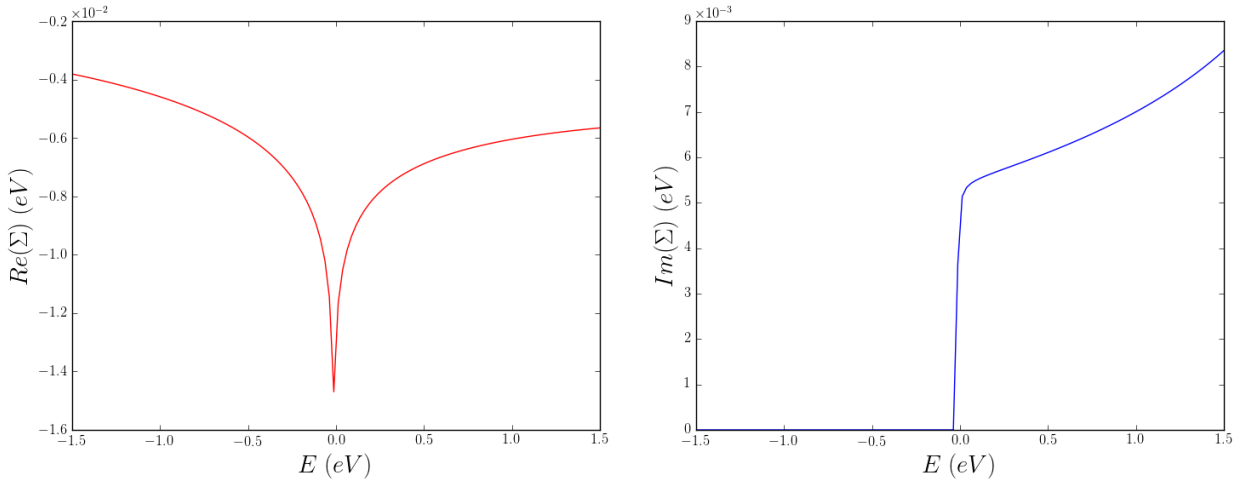

Figure 3.1.18: Plots of the real and imaginary part of the self-energy as a function of energy with $a = 0.25$ and $U_0 = 0.1\ eV$. The Hamiltonian is that of a free electron in a two dimensional infinite space. The self-energy is approximated using the first order self-consistent Born approximation.

At first sight the red curve in figure 3.1.18 looks similar to its one dimensional counterpart in figure 3.1.4; both plots have a derivative-discontinuity point. For the 1D case it was argued that at high energies the real part of the self-energy is expected to come close to zero, because at high energies the electrons barely notice the impurities. The red curve in figure 3.1.18 does not show this characteristic. The imaginary part is expected to have a maximum at $E = 0\ eV$ (see the 1D case for an explanation). Instead the blue plot in figure 3.1.18 moves upwards steeply before $E = 0\ eV$ but then keeps going upwards after $E = 0\ eV$. Just as figure 3.1.17, the plots in figure 3.1.18 do not make sense and the results are therefore expected to be wrong.

Figure 3.1.19 shows the dispersion relation for the disorder strength $0.2\ eV$ and lattice constant $0.25\ nm$. In the left plot the wave vector k_x runs from $-\pi$ to π and k_y is set equal to 0, while in the right plot both k_x and k_y run from $-\pi$ to π.

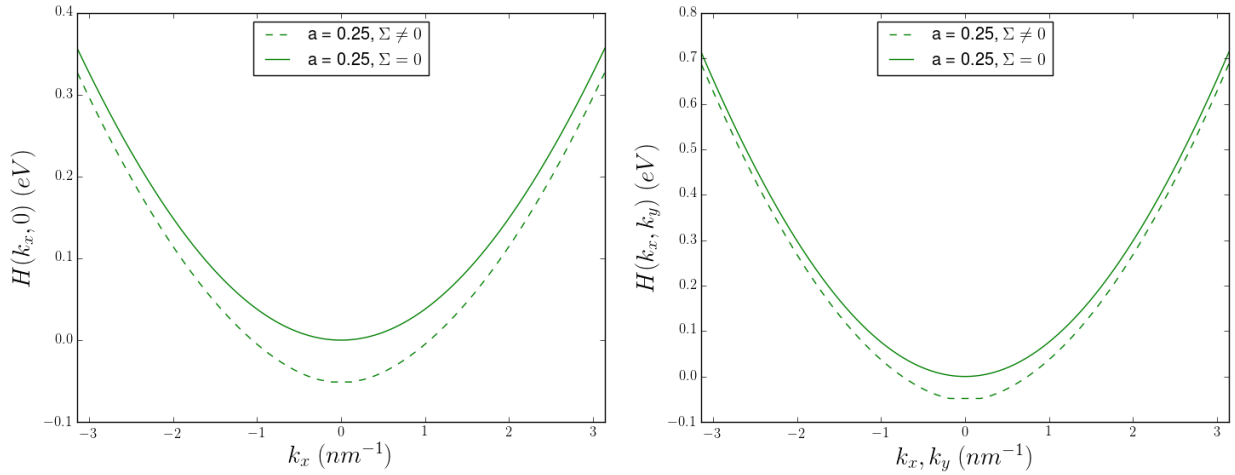

Figure 3.1.19: In each figure there are two plots of the band structure; one with the correction for added disorder (dashed line) and one without disorder (solid line). The lattice constant is 0.25 nm and $U_0 = 0.2\ eV$. In the left image the wave vector k_x runs from $-\pi$ to π with $k_y = 0$ and in the right image both k_x and k_y run from $-\pi$ to π. The Hamiltonian is that for a free particle in an one dimensional infinite space. The effect of disorder is taken into account through application of the first order self-consistent Born approximation and the impurity amplitudes have an uniform distribution in the interval $[-U_0/2, U_0/2]$.

Just as in figure 3.1.5 the energies corrected for average disorder are shifted downwards relative to the no-disorder energies and for wave vectors around the Γ point the downward shift is stronger than for larger k-values.

3.2 BHZ model

3.2.1 Original BHZ model

The theory in this section is based on [13], [14], [15] and [1]. A model, which can be used to describe quantum spin hall insulators, is the BHZ model. The BHZ Hamiltonian has the form

$$\hat{H}_{BHZ} = \begin{pmatrix} h(\bar{k}) & 0 \\ 0 & h^*(-\bar{k}) \end{pmatrix}, \text{ with}$$

$$\begin{aligned} h(\bar{k}) &= \epsilon(\bar{k}) + \bar{d}(\bar{k}) \cdot \bar{\sigma}, \\ \epsilon(\bar{k}) &= \left(C - D(k_x^2 + k_y^2)\right) \sigma_0, \\ \bar{d}(\bar{k}) &= \left[Ak_x, -Ak_y, M - B\left(k_x^2 + k_y^2\right)\right], \\ \bar{\sigma} &= [\sigma_x, \sigma_y, \sigma_z], \\ \bar{k} &= [k_x, k_y]. \end{aligned} \tag{3.2.1}$$

In an experiment, the values of the parameters A, B, C, D and M depend on the material and geometry. The values

$$\begin{aligned} A &= 364.5\ meVnm, \\ B &= -686\ meVnm^2, \\ C &= 0, \\ D &= -512\ meVnm^2, \end{aligned} \tag{3.2.2}$$

are realistic values from experiment (see [1]). The gap-parameter M determines if the system is in the insulating phase ($M > 0$), at the transition point ($M = 0$) or in the quantum spin hall phase ($M < 0$). Different values of M are used for the simulations in this section, while the parameters A, B, C and D are always equal to the values given by equation (3.2.2).

The two blocks in the Hamiltonian are not coupled and they can therefore be considered separately. The Hamiltonian corresponds to a time-reversal symmetric system with half-integer total spin and therefore has Kramers' degeneracy; the lower diagonal block, $h^*(-\bar{k})$, is the time-reversal counterpart of the upper diagonal block.

A lattice is build using the software package Kwant[8] and the on-site and hopping energies are obtained by using the Discretizer module. The three cases $M = 10$, $M = 0$ and $M = -10\ meV$ are considered and the lattice constant is set to 5 nm. Firstly, the system is made infinite in the x and y direction and the band structure is calculated. The result is four bulk bands of which only two are visible in a plot due the Kramers degeneracy. In figure 3.2.1, these bands are given a green color. Secondly, the system is made infinite in the x direction and finite in the y direction. Due to the confinement many bands appear, namely $L_y/a \cdot 4$ of which $L_y/a \cdot 2$ are visible in a plot due to Kramers degeneracy. In figure 3.2.1, these bands are grey colored, except for the outermost of these bands, which correspond to the edges of the system and are given a red color. The width of the well in the y direction, L_y, is set to 500 nm. For the infinite system the x-axis corresponds with the total wave vector, in which k_x and k_y have an equal weight and which runs from -0.03 to 0.03 nm^{-1}. For the finite system the x-axis corresponds to k_x, which in the plot is shown as k and which also runs from -0.03 to 0.03 nm^{-1}.

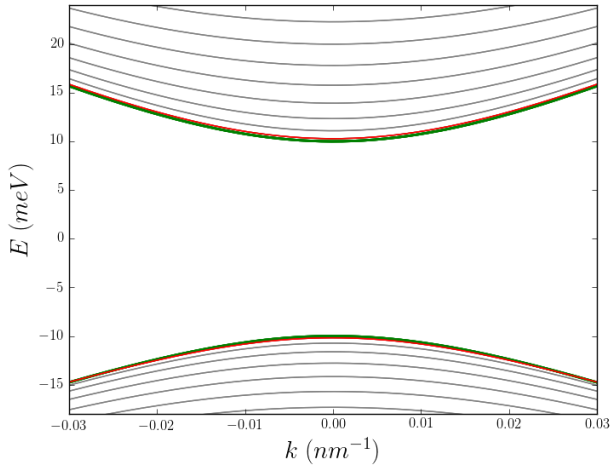

Figure **3.2.1.a:** $M = 10\ meV$, insulating phase

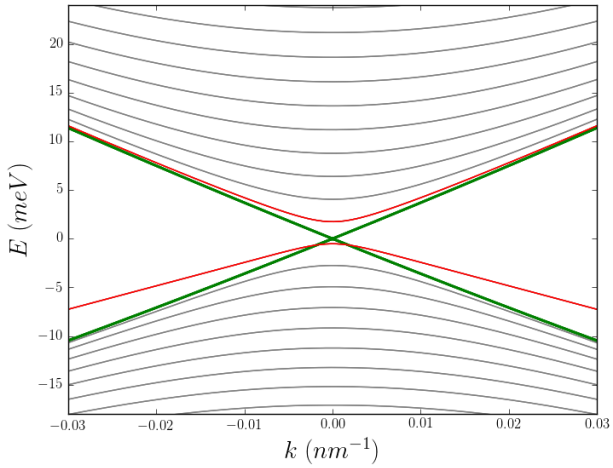

Figure **3.2.1.b:** $M = 0\ meV$, transition point

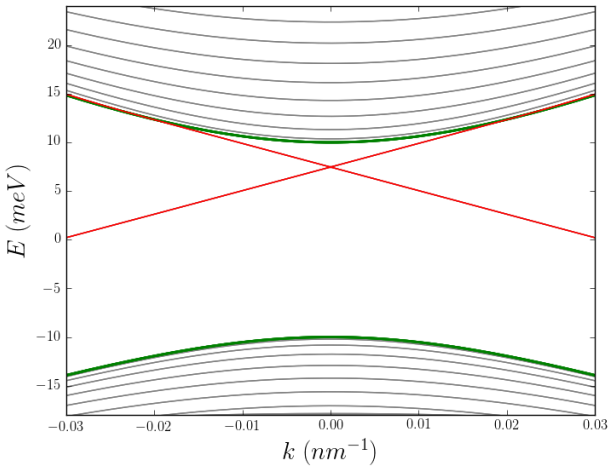

Figure **3.2.1.c:** $M = -10\ meV$, topological phase

Figure 3.2.1: Band structure for different values of the gap-parameter M. The Hamiltonian is the BHZ model. The lattice constant is set to 5 nm and for the calculation concerning the finite system, the width of the quantum well is set to 500 nm. The green bands mark the boundary of the bulk states. The rest of the bands have a grey color, except for the edge bands which are red colored.

In figure 3.2.1.a, the value of M is positive and the system is in the insulating phase; the bulk is gapped with a band gap of $2M = 20\ meV$ and there are no edge states in the gap. The band structure looks like that of a conventional insulator. When the value of M is decreased, the electron and hole bands come closer and touch for $M = 0$ at $k_x = k_y = 0$. A band inversion results when the value of M is lowered further and for these negative values of M, the system is in the topological phase. The topological phase (QSH insulator) has a gap in the two-dimensional bulk, but has topologically protected gapless edge states that lie inside the bulk insulating gap. The edge states have the property that two states with opposite spin-polarization counter-propagate at a given edge; for this reason, they are called helical edge states.

It is interesting to study transport as a function of disorder with the Fermi level placed in different regions of the band structure. In order to do a transport calculation, the system is changed to a finite size, namely a strip with $L_x = 5000\ nm$ and $L_y = 500\ nm$. The transport is in the x-direction, the lattice constant is

kept at 5 nm and the conductance is calculated using the Landauer-Büttiker formalism. The system is made disordered, by independently generating values from a uniform distribution in the interval $[-U_0/2, U_0/2]$ and adding them to the on-site energies. For every chosen interval, the conductance calculation is repeated 100 times and the average and variance of the outcomes are calculated. The average conductances are plotted and for some points errorbars are attached. The lengths of the errorbars are equal to the variances.

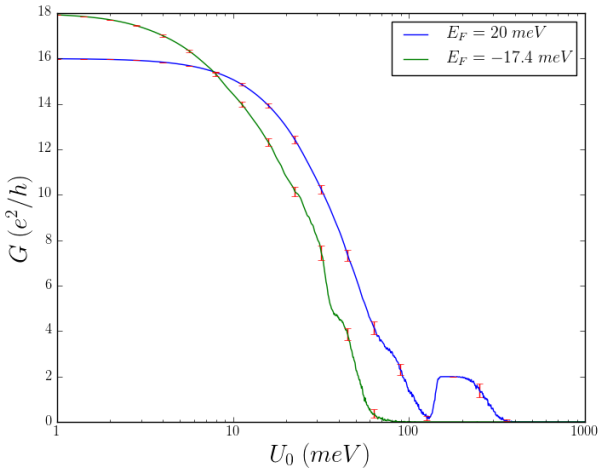

Figure **3.2.2.a:** Conductance, insulating phase

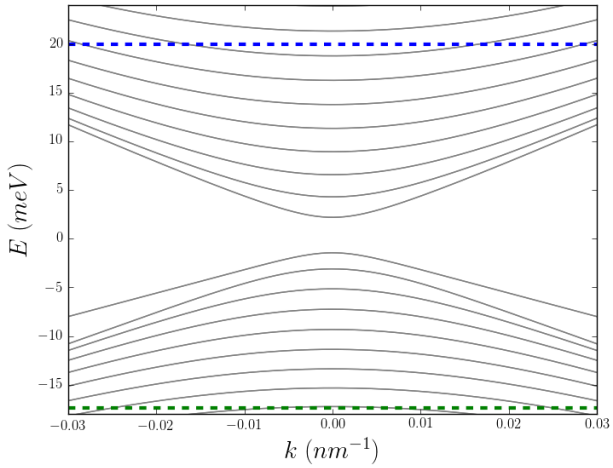

Figure **3.2.2.b:** Band structure, insulating phase

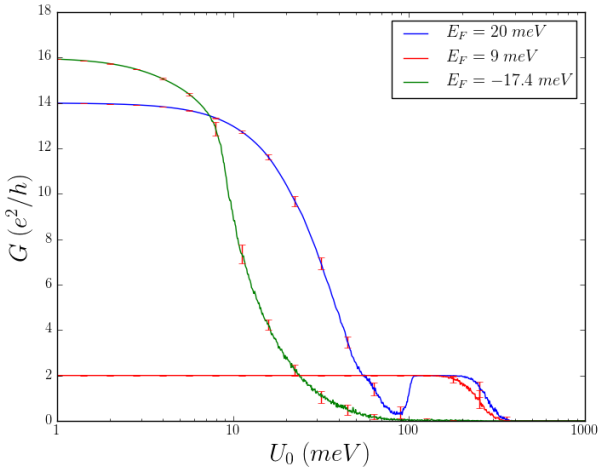

Figure **3.2.2.c:** Conductance, topological phase

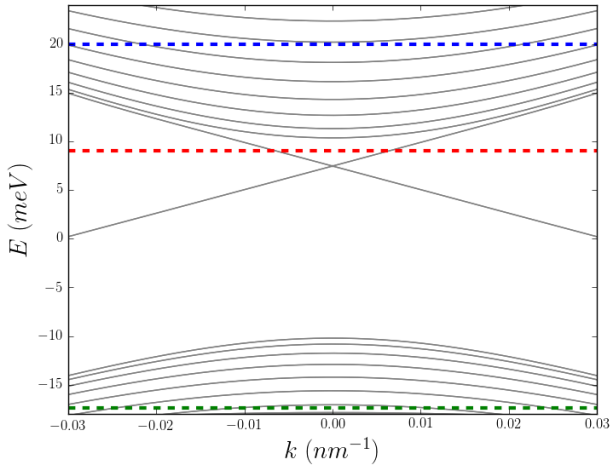

Figure **3.2.2.d:** Band structure, topological phase

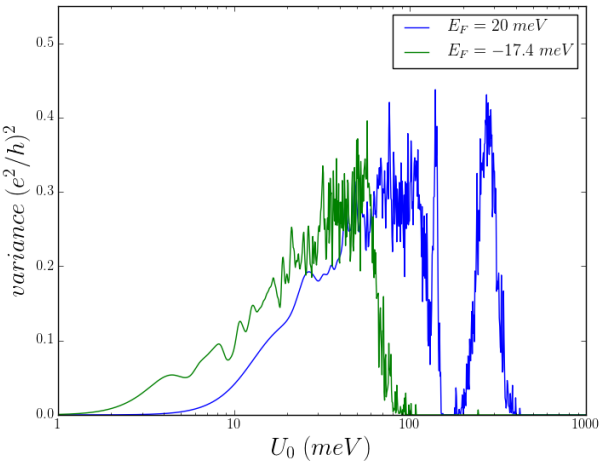

Figure **3.2.2.e:** Error, insulating phase

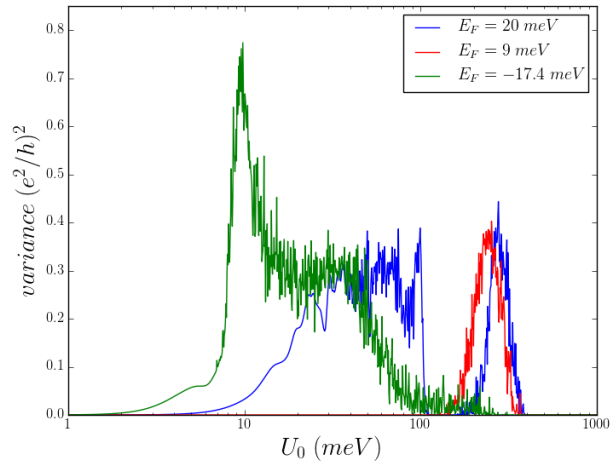

Figure **3.2.2.f:** Error, topological phase

Figure 3.2.2: The plots in figures 3.2.2.a and 3.2.2.c show the conductance as a function of disorder strength for the insulating ($M = 1\ meV$) and topological ($M = -10\ meV$) phase respectively. The Hamiltonian is the BHZ model. The system is a disordered strip with $L_x = 5000\ nm$ and $L_y = 500\ nm$. Transport is in x-direction and the lattice constant is set to 5 nm. The x-axis has a logarithmic scale with base 10. In order to illustrate how big the variances are, some points have errorbars attached to them. Figures 3.2.2.b and 3.2.2.d are the band structures (without disorder), in which the horizontal dashed lines show the positions of the Fermi levels. Lastly, figures 3.2.2.e and 3.2.2.f show the variance are as a function of U_0.

In figure 3.2.2.a the conductance is plotted as a function of U_0 for the insulating phase with $M = 1\ meV$, while figure 3.2.2.c shows the conductance for the topological phase with $M = -10\ meV$. The x-axis is plotted on a logarithmic scale in order to improve readability and for some points errorbars are added. The base of the logarithmic scale is 10 and the length of the errorbars corresponds to the variance. As is clear from figures 3.2.2.b and 3.2.2.d, the Fermi levels are chosen such that every region of the band structure is addressed. At last, figures 3.2.2.e and 3.2.2.f show the variance values for the insulating and topological phase respectively.

When the Fermi level is in the lower region of the band structure for both the insulating as well as the topological phase, the conductance starts at a certain number times the conductance quantum in the clean limit and decays to zero as U_0 is increased (green lines in figure 3.2.2). The disorder causes the clean-limit metal to transition into an Anderson insulator.

When the Fermi level is fixed such that it crosses the edge states in the topological phase, the conductance starts at two conductance quantum's and remains robust over a large range of U_0-values until it decays to zero at high disorder strengths (red line in figure 3.2.2.c). Figure 3.2.2.f shows that the variance is negligible up till the U_0-value at which the edge states start to break down. Thus, until a high disorder strength is reached, the electrons do not backscatter at all. The implemented impurities do not break time-reversal symmetry and therefore Kramers theorem holds. The edge states are time-reversed partners, they have the same energy and their wave functions are orthogonal. This way, the unit transmission of the helical edge states is protected. If the impurities would break time-reversal symmetry (e.g. magnetic impurities), the conductance should decay rapidly when the disorder strength is increased. The reason why the conductance decays at all, at high disorder strength, becomes clear later.

When the Fermi level is in the upper region of the band structure for both the insulating as well as the topological phase, the conductance is equal to a certain number times the conductance quantum in the clean limit, decays as U_0 is increased, goes up again, remains robust at two conductance quantum's during a certain U_0-interval and finally decays to zero (blue lines in figure 3.2.2). It is remarkable that the conductance after the usual metal-insulator transition goes up again and forms a plateau at two conductance quantum's. Note that the variances go to zero for the particular U_0-range. The conductance plateau is similar to what was described in the previous paragraph, where there were two transport modes that did not allow any back scattering. However, the quantized conductance can not be attributed to the relative robustness of edge states against disorder, because it occurs when there are no edge states in the clean limit (see figures 3.2.2.a and 3.2.2.b). The similarity between the conductance plateau and the edge states of the previous paragraph suggests that the disorder is responsible for the formation of edge states. In order to gain more insight if this is the case, the scaling of the conductance with the width of the strip is investigated. Figure 3.2.3 shows the average conductance plotted versus U_0 for five different widths. The Fermi level is fixed at 20 meV, the lattice constant is 5 nm, $L_x = 2000\ nm$ and $M = 2\ meV$. Per disorder strength 100 system realisations are used and for some points errorbars are included.

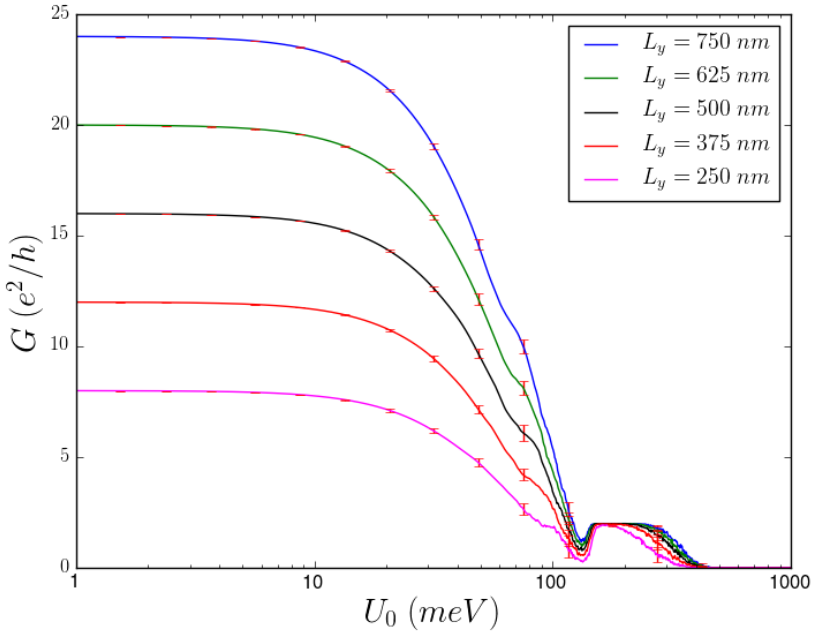

Figure 3.2.3: The conductance is plotted versus the disorder strength for widths: 750 nm, 625 nm, 500 nm, 375 nm and 250 nm. The Hamiltonian is the BHZ model and the sample has the shape of a rectangle. The length, which is also the direction of transport, is fixed at 2000 nm. The other parameters are: $a = 5\ nm$, $E_F = 20\ meV$ and $M = 2\ meV$.

For U_0-values below roughly 100 meV, the width of the strip has a clear effect on the conductance, namely a larger width gives a higher conductance. This relation is indicative that the bulk is contributing to the transport. When the value of U_0 is increased, the conductance becomes equal to two conductance quantum's for all the widths. In this U_0-interval the width of the strip does not influence the conductance and therefore the bulk is not contributing to the transport. Instead, it must be the edge states that allow electron flow.

The state of the system with the presence of disorder induced edge states and an insulating bulk, is called the topological Anderson insulator. One can not distinguish by the conductance alone whether the system is in the topological Anderson insulator state or in the state where the system is in the topological phase and the Fermi level is placed such that it crosses the edge states. It would have been interesting to add a 2D color plot with on one axis the disorder strength, on the other the Fermi level and the conductance as the color. The topological Anderson insulator regime would then appear as an island in the plot and one could easily see which conditions should be met for the system to be in this regime.

It is interesting to see what the effect of disorder is on the band structure of the BHZ Hamiltonian (see figure 3.2.1). To this end the first order self-consistent Born approximation is applied, which for two dimensions corresponds to

$$\Sigma^+(E) = a^4 n \tilde{U}_2' \lim_{\epsilon \to 0} \int \frac{d^2\bar{k}}{(2\pi)^2} \cdot \frac{1}{E + i\epsilon - H_0(\bar{k}) - \Sigma^+(E)}, \tag{3.2.3}$$

where a is the lattice constant, n the impurity density and $\tilde{U}_2'$ is the second moment of the amplitude impurity distribution. The impurities correspond to the addition of values, generated from a uniform distribution in the interval $[U_0/2, U_0/2]$, to the on-site energies of a tight-binding Hamiltonian. The second moment of the aforementioned uniform distribution is equal to $U_0^2/12$. In relation with previous sections it is mentioned that $\tilde{U}_2'$ is not scaled with the lattice constant. The objective is not to vary the lattice constant while maintaining

a constant effective disorder strength, instead the lattice constant is kept at 5 nm for all the simulations in this section. Further, the impurity density is equal to $1/a^2$ giving

$$\Sigma^+(E) = \frac{1}{12}\left(\frac{aU_0}{2\pi}\right)^2 \lim_{\epsilon\to 0}\int d^2\bar{k}\left[E + i\epsilon - H_0(\bar{k}) - \Sigma^+(E)\right]^{-1}. \tag{3.2.4}$$

Equation (3.2.4) is rewritten into

$$\Sigma^+(E) = \frac{(aU_0)^2}{24\pi}\int_{-\pi/a}^{\pi/a} dk_y \left[\frac{1}{2\pi}\int_{-\pi/a}^{\pi/a} dk_x G(k_x, k_y, E)\right]. \tag{3.2.5}$$

Subsequently using the Fourier transform (see equation (2.3.66b) with $\bar{r} = 0$) yields

$$\Sigma^+(E) = \frac{(aU_0)^2}{24\pi}\int_{-\pi/a}^{\pi/a} dk_y G(x = 0, k_y, E). \tag{3.2.6}$$

The Discretizer module for Kwant[8] is used to determine the on-site and hopping energies of the tight-binding version of the BHZ Hamiltonian. The next step is to use Kwant to build an infinite one dimensional chain for which the sites are spaced by the lattice constant and with the calculated on-site and hopping energies. Subsequently an initial guess for Σ^+ is chosen and added to the on-site energies of the sites. Next Kwant is used to calculate the Green's function at the origin for different values of k_y in the interval $[-\pi/a, \pi/a]$. With these values the integral can be approximated and from there the self-energy. The previous self-energy value is overwritten by the newly calculated one. By using an Anderson mixing scheme only a few iterations are required to obtain a high precision solution for the self-energy. The Hermitian part of the self-energy, which is evaluated at a certain energy, is added to the Hamiltonian. After diagonalisation disordered bands are obtained of which only the states are kept at the energy for which the self-energy was calculated. In other words for every point on the disordered bands

$$E(k_{dis}) - E_0 = 0, \tag{3.2.7}$$

where E_0 is the energy at which Σ^+ was calculated and $E(k_{dis})$ the band structure that corresponds with $\hat{H} + Re(\Sigma^+)$. By repeating the process for a wide range of energies, the disordered bulk and edge bands are constructed.

Figures 3.2.4 and 3.2.5 show the disordered band structures for the insulating and topological phase respectively. The value of U_0 is varied, while a is kept fixed.

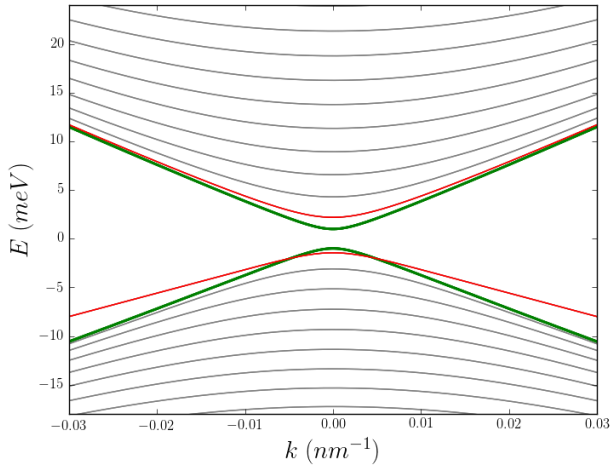

Figure **3.2.4.a:** $M = 1\ meV,\ \ U_0 = 0\ meV$

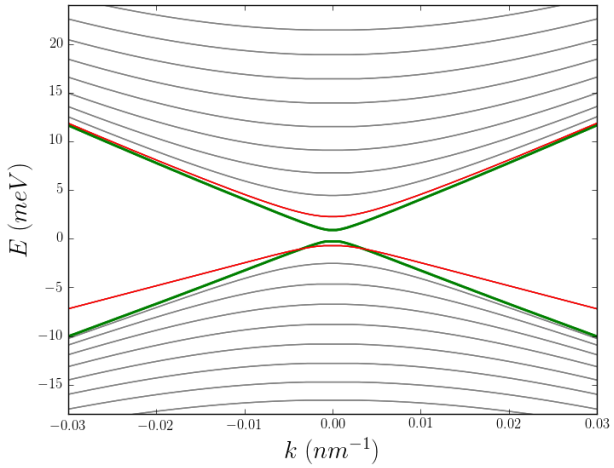

Figure **3.2.4.b:** $M = 1\ meV,\ \ U_0 = 30\ meV$

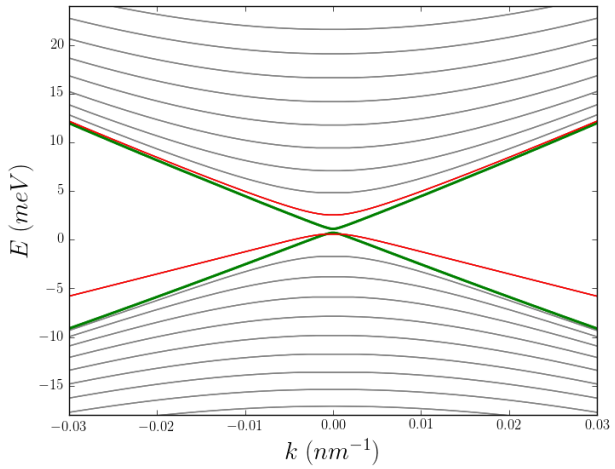

Figure **3.2.4.c:** $M = 1\ meV,\ \ U_0 = 50\ meV$

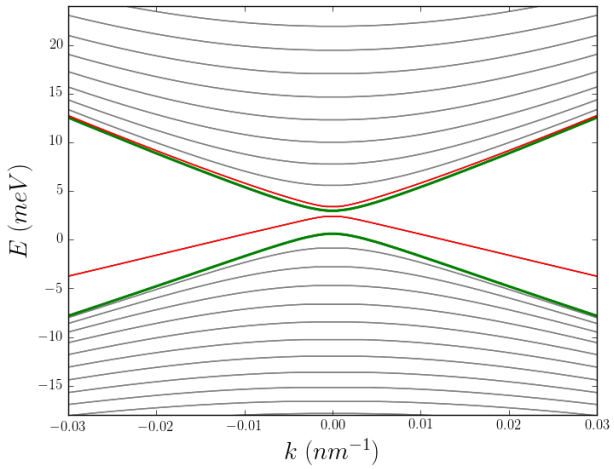

Figure **3.2.4.d:** $M = 1\ meV,\ \ U_0 = 70\ meV$

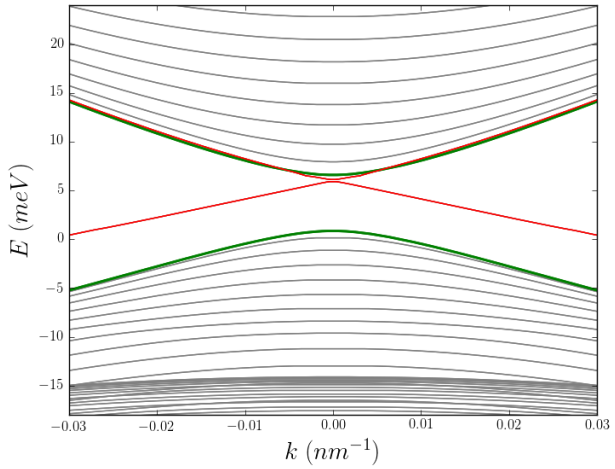

Figure **3.2.4.e:** $M = 1\ meV,\ \ U_0 = 100\ meV$

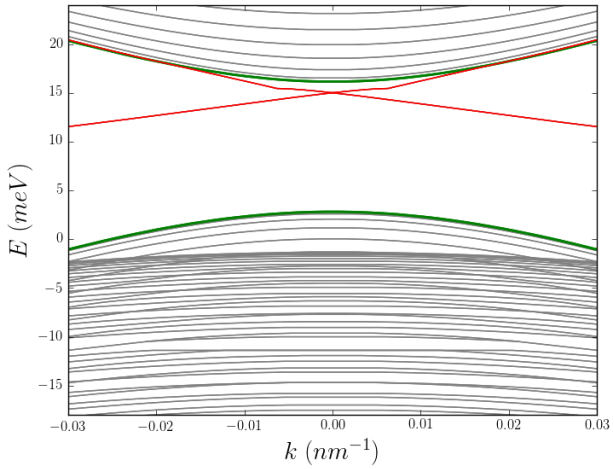

Figure **3.2.4.f:** $M = 1\ meV,\ \ U_0 = 160\ meV$

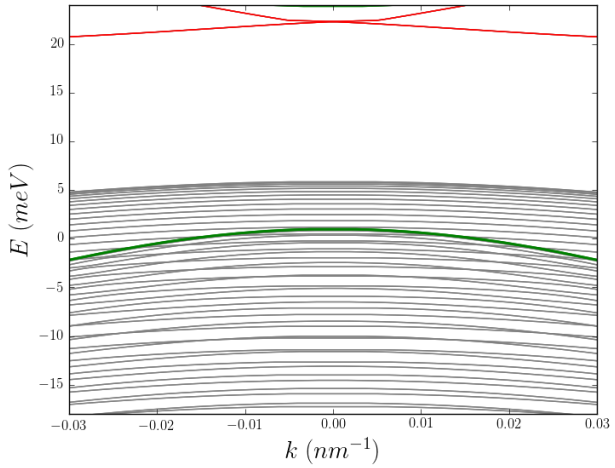

Figure **3.2.4.g:** $M = 1\ meV,\ \ U_0 = 200\ meV$

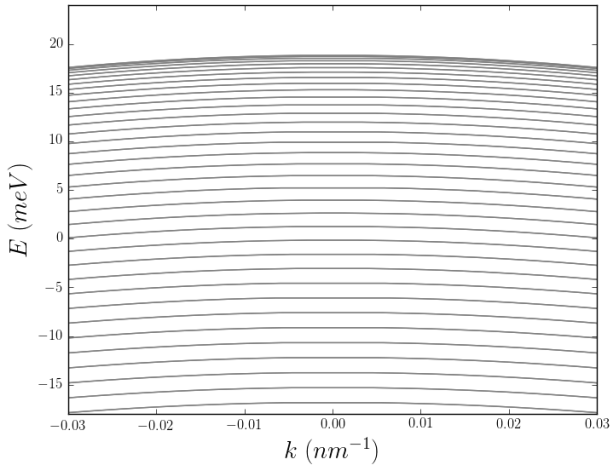

Figure **3.2.4.h:** $M = 1\ meV,\ \ U_0 = 340\ meV$

Figure 3.2.4: The plots show the band structure for different disorder strengths. The Hamiltonian is the BHZ model and the disorder is taken into account through application of the first order self-consistent Born approximation. The value of M is 1 meV (insulating phase) and the lattice constant is 5 nm.

Figure 3.2.4.a shows the clean band structure. The band gap is $2M = 2\ meV$ and there are no edge states in the gap. When the disorder strength, U_0, is increased to 30 meV, the band gap decreases. At roughly 50 meV the gap closes and by further increasing the disorder strength the gap opens again. After the gap re-opening there are edge states that lie inside the bulk insulating gap. Figure 3.2.4.d looks qualitatively similar to the clean topological band structure (figure 3.2.1.c). The disorder has turned the ordinary insulator band structure into that of a topological one. After the disorder strength is increased further, the bulk gap becomes larger and hole bands rise from the bottom of the figure upwards. Eventually at high disorder strengths the whole analysed energy range gets covered by the risen hole bands.

The process displayed in the plots of figure 3.2.4 agrees with the transport calculation results of figure 3.2.2.a. When the Fermi level is set to $-17.4\ meV$, the conductance goes to zero as U_0 is increased (green line in figure 3.2.2.a). The Fermi level never solely crosses the edge states and already before 100 meV the to disorder susceptible hole bands interfere with the transmission. When the Fermi level is set to 20 meV, the conductance initially decreases, but then forms the TAI plateau and eventually decreases to zero (blue line in figure 3.2.2.a). This behaviour agrees with the band structures of figure 3.2.4. In the clean limit, the Fermi level crosses with 8 electron bands. By taking the Kramers degeneracy into account the clean limit conductance is indeed equal to 16 conductance quantums. When the disorder strength is increased, the electron bands move upwards, the Fermi level crosses with less electron bands and the conductance decreases. At a certain disorder strength the Fermi level only crosses with the edge states (see figure 3.2.4.g). The system in the topological Anderson insulator regime. When U_0 is increased further, the edge states get 'buried' by the rising hole bands and the conductance goes to zero.

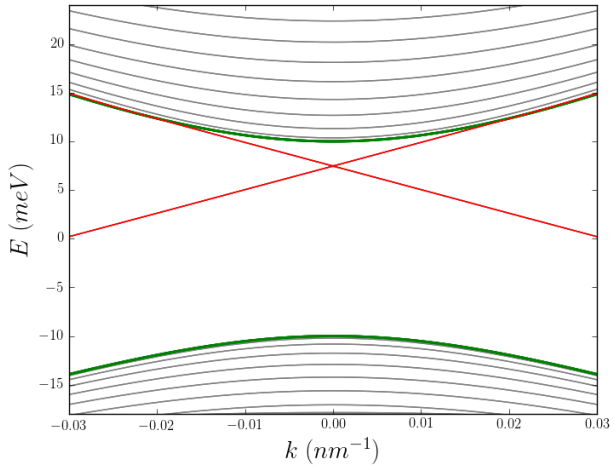

Figure **3.2.5.a:** $M = -10\ meV,\ \ U_0 = 0\ meV$

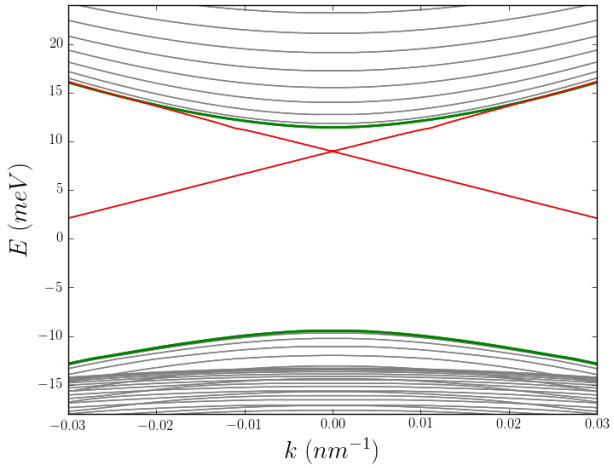

Figure **3.2.5.b:** $M = -10\ meV,\ \ U_0 = 50\ meV$

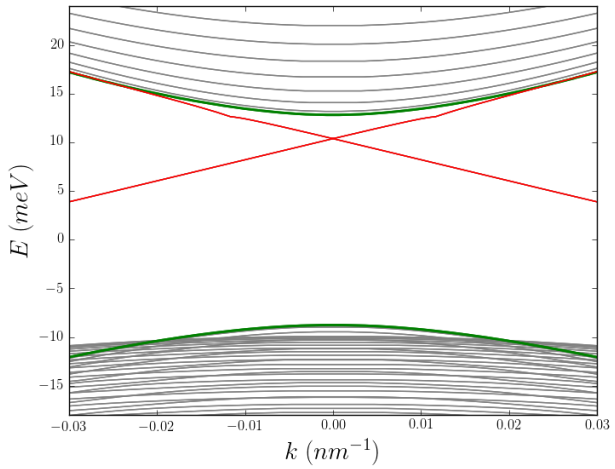

Figure **3.2.5.c:** $M = -10\ meV,\ \ U_0 = 70\ meV$

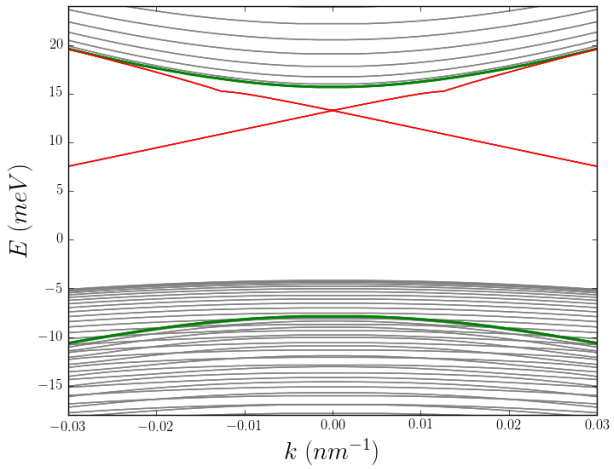

Figure **3.2.5.d:** $M = -10\ meV,\ \ U_0 = 100\ meV$

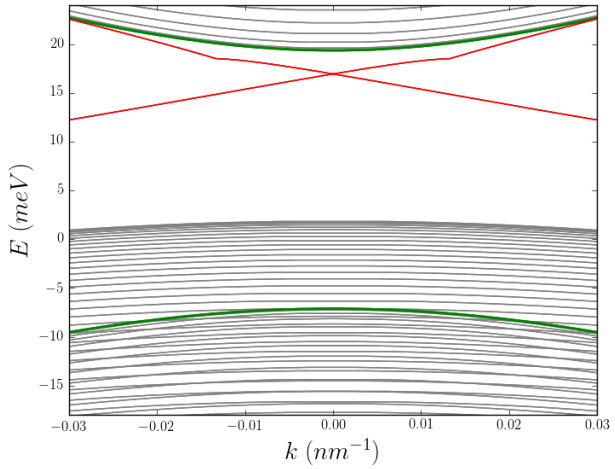

Figure **3.2.5.e:** $M = -10\ meV,\ \ U_0 = 130\ meV$

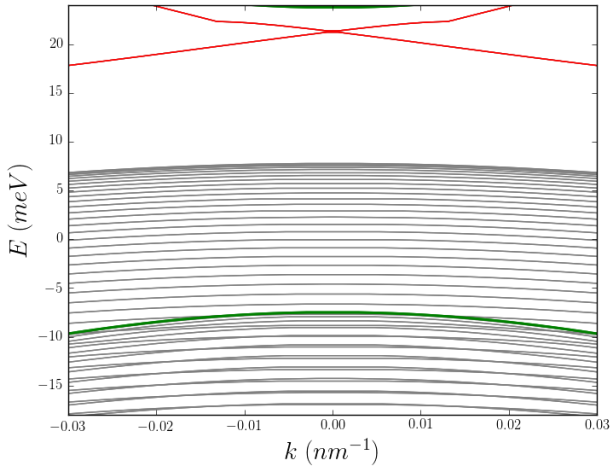

Figure **3.2.5.f:** $M = -10\ meV,\ \ U_0 = 160\ meV$

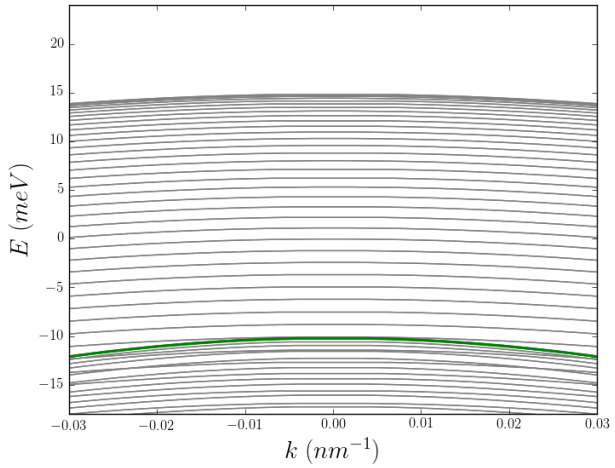

Figure **3.2.5.g:** $M = -10\ meV,\ \ U_0 = 200\ meV$

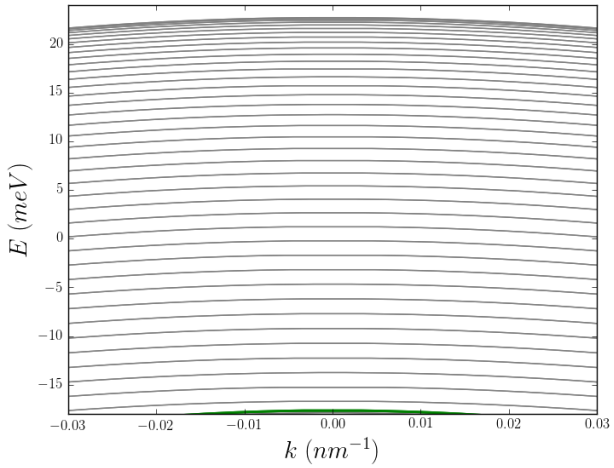

Figure **3.2.5.h:** $M = -10\ meV,\ \ U_0 = 260\ meV$

Figure 3.2.5: The plots show the band structure for different disorder strengths. The Hamiltonian is the BHZ model and the effect of disorder on the band structure is taken into account through application of the first order self-consistent Born approximation. The value of M is $-10\ meV$ (topological phase) and the lattice constant is 5 nm.

Figure 3.2.5.a shows the clean band structure. As the disorder strength, U_0, is increased the green electron band and red edge states move upwards, while the green hole band moves downwards. Also hole bands move upwards from the bottom of the analysed energy range. At very high disorder strengths the whole analysed energy range gets covered by hole bands.

The band structures of figure 3.2.5 agree with the transport calculation (figure 3.2.2.c). When the Fermi level is fixed at $-17.4\ meV$, the rising hole bands make the conductance decrease to zero. The clean-limit metal transitions into an Anderson insulator. When the the Fermi level is fixed at 9 meV, it crosses the edge states in the clean limit. As the disorder strength is increased, the Fermi level only crosses with the edge states for quite high disorder strengths. For $U_0 = 160\ meV$, figure 3.2.5.f, the Fermi level sill only crosses with the edge states, although this can not be seen in the figure due to the limited range of k-values. Somewhere between $U_0 = 160\ meV$ and $U_0 = 200\ meV$ the rising hole bands cross the 9 meV energy level and the conductance decreases to zero. When the Fermi level is set to 20 meV, it crosses with 7 electron bands and because of Kramers degeneracy the clean limit conductance is equal to 14 conductance quantums. When he disorder strength is increased, the electron bands move upwards and the conductance goes down. At some disorder strength the Fermi level only crosses the edge states and the system is in the TAI phase (figures 3.2.5.f and 3.2.5.g). When the disorder strength is increased further the rising hole bands cross the Fermi level and the conductance goes to zero (figure 3.2.5.h).

Besides the band structures, where for every plot U_0 was fixed and the energy was varied, it is also interesting to keep the energy fixed and vary U_0. Figures 3.2.6.c and 3.2.6.d show $E(k = 0)$ versus U_0 for the Fermi levels 20 and $-17.4\ meV$ respectively and $M = 1\ meV$ (insulating phase). The plots are only valid along the dashed line due to the energy dependence of the self-energy. Figures 3.2.6.c and 3.2.6.d agree with the conductance plot (figure 3.2.6.a). Comparison however cannot be fully made because the band structure does not incorporate the length of the sample and back scattering from the leads. Also $E(k = 0)$ is plotted and it can not be seen what the energies are for larger k-values.

As U_0 increases in figure 3.2.6.c, more and more electron bands cross the Fermi level, which corresponds with the lowering of the conductance. The TAI regime is identifiable, namely the U_0-range between the crossing of the last grey band with the blue dashed line (so before the red curve crosses with the blue dashed line) and the crossing of the rising hole bands with the blue dashed line. Also figure 3.2.6.d agrees with the conductance plot. As U_0 increases, more and more electron bands cross the Fermi level, which

corresponds with the lowering of the conductance. When the rising hole bands cross the green dashed line, the conductance becomes zero.

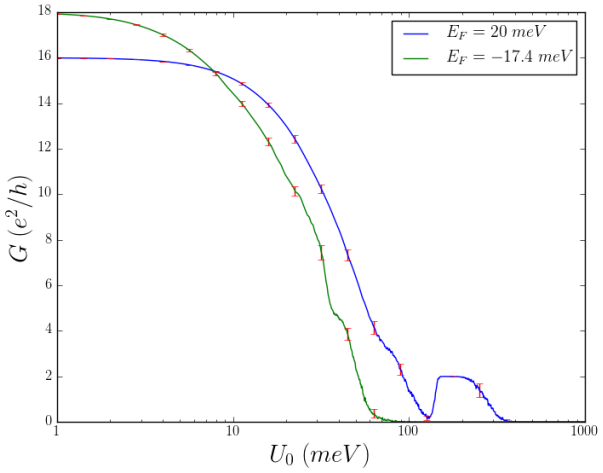

Figure **3.2.6.a:** Conductance, insulating phase

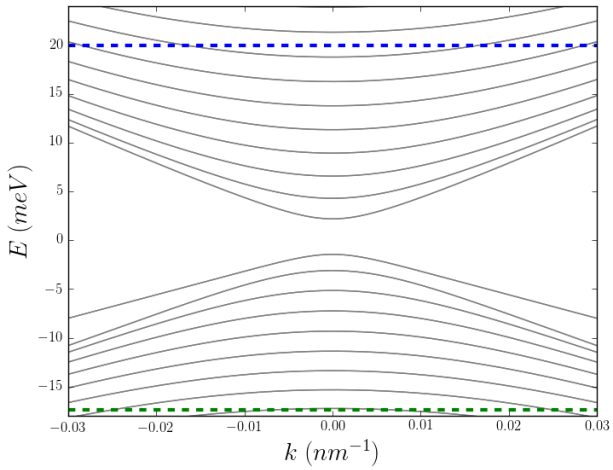

Figure **3.2.6.b:** Band structure, insulating phase

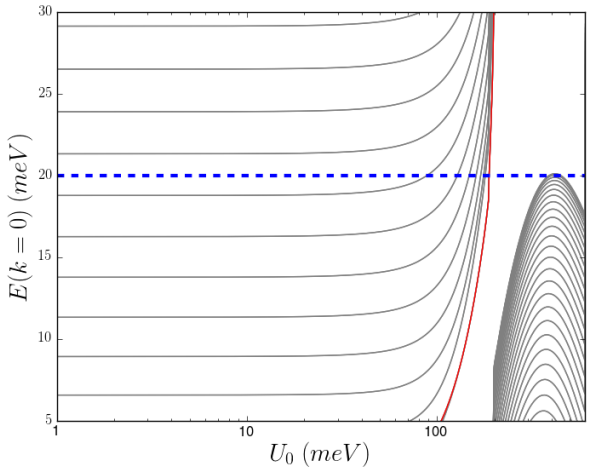

Figure **3.2.6.c:** $E(k=0)$, $E_F = 20\ meV$

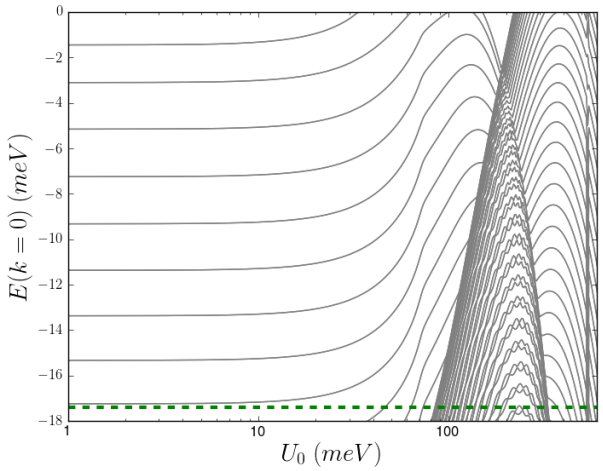

Figure **3.2.6.d:** $E(k=0)$, $E_F = 20\ meV$

Figure 3.2.6: The top left figure is a copy of figure 3.2.2.a and shows the conductance plotted versus the disorder strength. The top right figure shows the clean band structure with the relevant Fermi levels as dashed lines. In the bottom left image $E(k=0)$ is plotted versus the disorder strength for $E_F = 20\ meV$ and in the bottom right figure for $E_F = -17.4\ meV$. The Hamiltonian is the BHZ model and the 1SBA is the method used to simulate the effect of disorder.

The same kind of figure as 3.2.6 is made for the topological phase ($M = -10\ meV$).

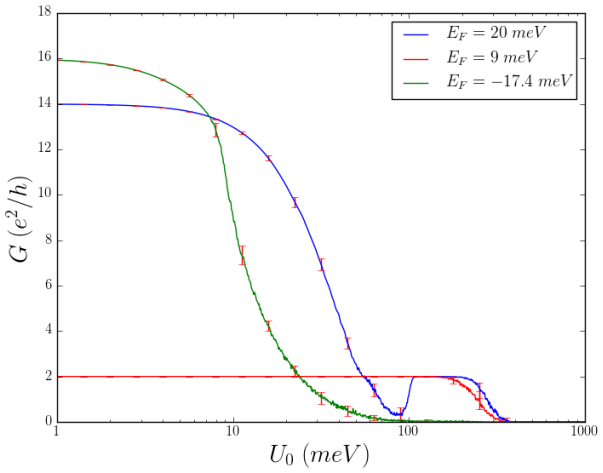

Figure **3.2.7.a:** Conductance, topological phase

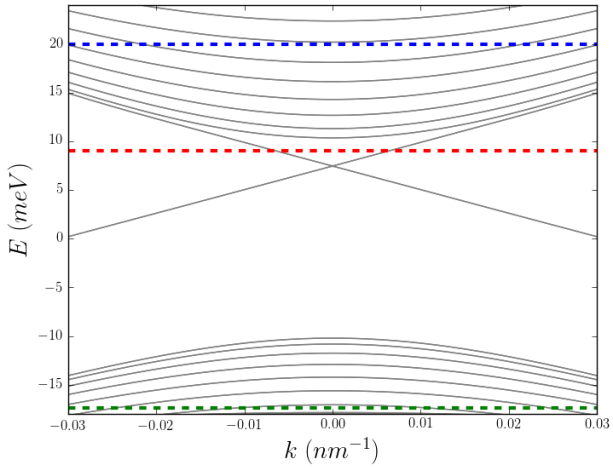

Figure **3.2.7.b:** Band structure, topological phase

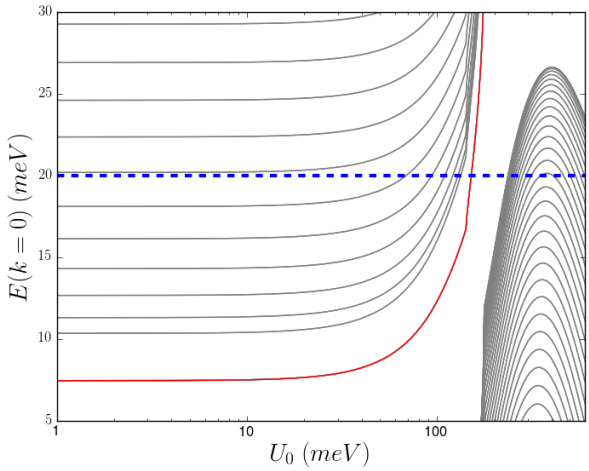

Figure **3.2.7.c:** $E(k=0)$, $E_F = 20\ meV$

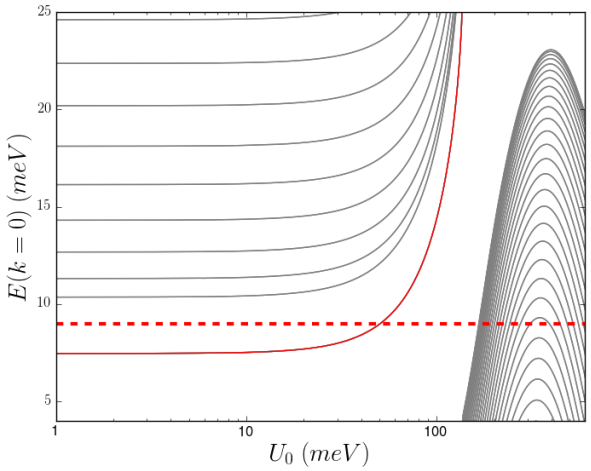

Figure **3.2.7.d:** $E(k=0)$, $E_F = 9\ meV$

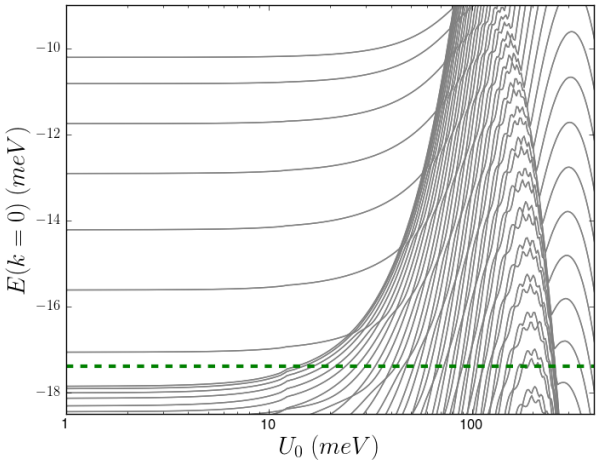

Figure **3.2.7.e:** $E(k=0)$, $E_F = -17.4\ meV$

Figure 3.2.7: The top left figure is a copy of figure 3.2.2.c and shows the conductance plotted versus the disorder strength. The top right figure shows the clean band structure with the relevant Fermi levels as dashed lines. In the other images $E(k=0)$ is plotted versus the disorder strength for the Fermi levels $E_F = 20\ meV$, $E_F = 9\ meV$ and $E_F = -17.4\ meV$. The Hamiltonian is the BHZ model and the method used to take the disorder into account is the 1SBA.

Figures 3.2.7.c, 3.2.7.d and 3.2.7.e agree with the conductance plot (figure 3.2.7.a). As U_0 increases in figure 3.2.7.c, more and more electron bands cross the Fermi level, which corresponds with the lowering of the conductance. Also in figure 3.2.7.c the TAI regime can be identified, namely the U_0-range after the last crossing of the bulk electron bands with the Fermi level (but before the red curve crosses) till the rising hole bands cross the blue dashed line. In figure 3.2.7.d $E(k = 0)$ is plotted versus U_0 with $E_F = 9\ meV$. Also this figure agrees with the conductance plot of figure 3.2.7.a. For low disorder strengths only the edge band (red colored) lies below the Fermi level and the conductance is equal to two conductance quanta. At a certain U_0-value, the the edge band crosses the Fermi level (figure 3.2.5.c shows this stage approximately). After the crossing, the Fermi level still crosses with the edge states in the band structure (but not at $k = 0$). When the rising hole bands start crossing the Fermi level, the conductance goes from $2G_0$ to zero. Lastly, figure 3.2.7.e also agrees with the conductance plot. As U_0 increases, more and more electron bands cross the Fermi level, which corresponds with the lowering of the conductance. When the rising hole bands cross the green dashed line, the conductance becomes zero.

3.2.2 Extended BHZ model

By using quasi-degenerate perturbation theory and considering symmetries (see [7]), the BHZ model can be extended to

$$\hat{H}_{BHZ,ext} = \begin{pmatrix} h(\bar{k}) & 0 \\ 0 & h^*(-\bar{k}) \end{pmatrix}, \text{ with}$$

$$h(\bar{k}) = \begin{pmatrix} r_1 + r_4 k^2 & c_1 k_+ & c_2 k_-^2 \\ c_1^* k_- & r_2 + r_5 k^2 & 0 \\ c_2^* k_+^2 & 0 & r_3 + r_6 k^2 \end{pmatrix},$$

$$k^2 = k_x^2 + k_y^2, \tag{3.2.8}$$

$$k_+ = k_x + i k_y,$$

$$k_- = k_x - i k_y,$$

$$\bar{k} = [k_x, k_y]\,.$$

In an experiment, the values of the parameters r_1, ..., r_6, c_1 and c_2 depend on the material, geometry and presence of gate voltages. In this work the values for r_i and c_i are somewhat arbitrarily chosen. However, r_4 is positive, while both r_5 and r_6 are negative. The parameters r_1 and r_2 determine if the system is in the

insulating phase ($r_1 > r_2$), at the transition point ($r_1 = r_2$) or in the topological phase ($r_1 < r_2$).

$$\begin{gathered}
\text{insulating:} \\
r_1 = 0.02\ eV \\
r_2 = -0.03\ eV \\
\\
\text{transition point:} \\
r_2 = r_2 = 0\ eV \\
\\
\text{topological:} \\
r_1 = -0.03\ eV \\
r_2 = 0.02\ eV \\
\\
r_3 = 0\ eV \\
r_4 = 20\ eVnm^2 \\
r_5 = -20\ eVnm^2 \\
r_6 = -25\ eVnm^2 \\
c_1 = 2\ eVnm \\
c_2 = 80\ eVnm^2
\end{gathered} \tag{3.2.9}$$

The parameters r_1 and r_2 are adjusted based on the desired state of the system. The other parameters r_3, ..., r_6, c_1 and c_2 are always equal to the values given by equation (3.2.9).

A lattice is build using the software package Kwant[8] and the hopping and on-site energies are obtained by using the Discretizer module. The lattice constant is 5 nm and is not changed throughout this section. Firstly, the system is made infinite in the x and y direction and the band structure is calculated. The result is six bulk bands of which only three are visible in a plot due the Kramers degeneracy. In figure 3.2.8 these bands are given a green color. Secondly, the system is made infinite in the x direction and finite in the y direction. Due to the confinement many bands appear, namely $L_y/a \cdot 6$ of which $L_y/a \cdot 3$ are visible in a plot due to Kramers degeneracy. In figure 3.2.8 these bands are grey colored, except for the outermost of these bands, which correspond to the edges of the system and are given a red color. The width of the well in the y direction, L_y, is set to 500 nm. For the infinite system the x-axis corresponds to the total wave vector, in which k_x and k_y have an equal weight and which runs from -0.05 to 0.05 nm^{-1}. For the finite system the x-axis corresponds to k_x, which in the plot is shown as k and which also runs from -0.05 to 0.05 nm^{-1}.

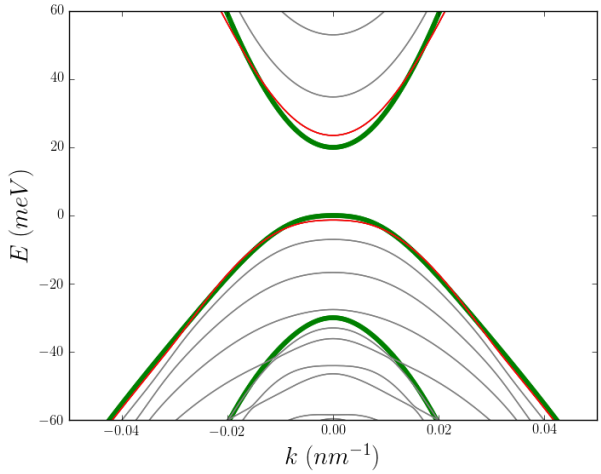

Figure **3.2.8.a:** insulating phase

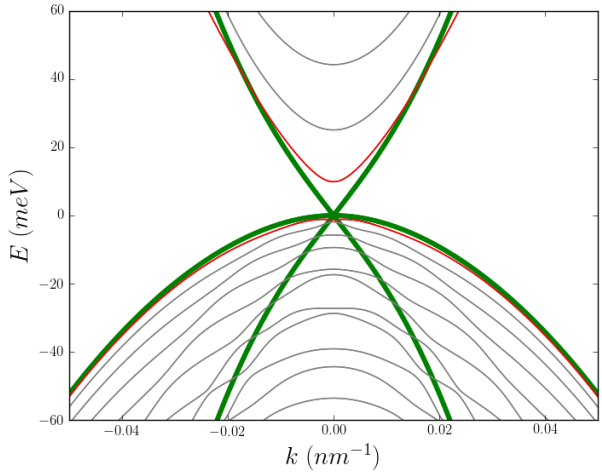

Figure **3.2.8.b:** transition point

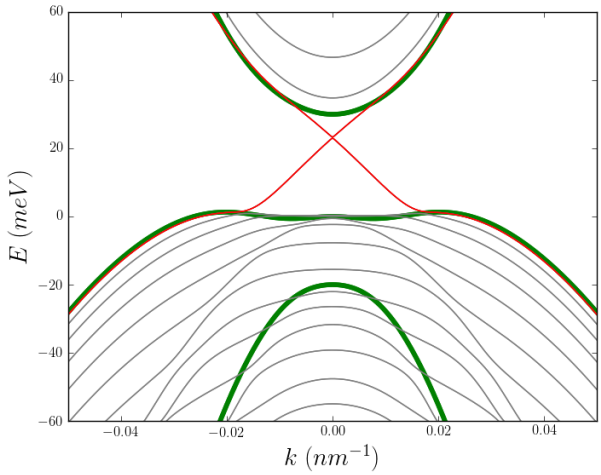

Figure **3.2.8.c:** topological phase

Figure 3.2.8: Band structure for different values of r_1 and r_2 (see equation (3.2.9)). The Hamiltonian is the extended BHZ Hamiltonian. The lattice constant is set to 5 nm and for the calculation concerning the finite system, the width of the quantum well is set to 500 nm. The green bands mark the boundary of the bulk states. The rest of the bands have a grey color, except for the edge bands which are red colored.

The effect of average disorder on the band structure is studied by applying the first order self-consistent Born approximation (see section 2.3.4), which is mathematically presented by

$$\Sigma^{+}(E) = a^4 n \tilde{U}_2' \lim_{\epsilon \to 0} \int \frac{d^2\bar{k}}{(2\pi)^2} \cdot \frac{1}{E + i\epsilon - H_0(\bar{k}) - \Sigma^{+}(E)}. \tag{3.2.10}$$

Equation (3.2.10) can be rewritten using the the Fourier transform (see equation (2.3.66b)). Further the impurity density, n, is equal to $1/a^2$ and the $\tilde{U}_2'$ is equal to $U_0^2/12$ (second moment of the uniform distribution).

Using the aforementioned information allows rewriting to

$$\Sigma^{+}(E) = \frac{(aU_0)^2}{24\pi} \int_{-\pi/a}^{\pi/a} dk_y G(x=0, k_y, E). \tag{3.2.11}$$

The method used to calculate the disordered band structure is summarized. The Discretizer module for Kwant[8] is used to determine the tight-binding version of the extended BHZ Hamiltonian (on-site and hopping energies). The next step is to use Kwant to build an infinite one dimensional chain for which the sites are spaced by the lattice constant and with the calculated on-site and hopping energies. The next step is to make an initial guess for Σ^{+} and add it to the on-site energies of the sites. Subsequently Kwant is used to calculate the Green's function at the origin for different values of k_y in the interval $[-\pi/a, \pi/a]$. With these values the integral can be approximated and after multiplication with the pre-factor $(aU_0)^2/24\pi$, the result is the self-energy. The previous self-energy value is overwritten by the newly calculated one. An Anderson mixing scheme is used and only a few iterations are required to obtain a high precision solution for the self-energy. Unfortunately for some energies the algorithm fails to converge and thus for some energies there is no self-energy available. The Hermitian part of the self-energy, which is evaluated at a certain energy, is added to the Hamiltonian. After diagonalisation disordered bands are obtained of which only the states are kept at the energy for which the self-energy was calculated. Every point on the disordered bands satisfies

$$E(k_{dis}) - E_0 = 0, \tag{3.2.12}$$

where E_0 is the energy at which Σ^{+} was calculated and $E(k_{dis})$ the band structure that corresponds with $\hat{H} + Re(\Sigma^{+})$. By repeating the process for a wide range of energies, the disordered bulk and edge bands are constructed for the insulating and topological phase.

The plots in figure 3.2.9 correspond to the insulating phase. In contrast to section 3.2.1 the computation method is slightly different. In order to plot the bands smoothly (see for example figures 3.2.4 and 3.2.5) it is necessary to do the calculation for every band separately, because then it is known which disordered states belong in which band. A computationally less intensive way of calculating the disordered band structure is to find all the corresponding k-values at a given energy E_0 at the same time. The disadvantage of this method is however that it can not be determined which states belong in the same band and the plots will therefore be scatter plots. Also the edge states can not be given a red color as was done in previous figures.

Once a self-energy, $\Sigma(E_0)$, has been calculated a system is build that is infinite in the both the positive and negative x-direction, but finite in the y-direction. The on-site and hopping energies of $\hat{H} + \Sigma(E_0)$ are calculated and assigned to the sites. As mentioned before $L_y = 500\ nm$ and $a = 5\ nm$. The system has translation symmetry in the x-direction. Calculating the eigenvalues of the translation operator will yield the sought after k-values. The translation operator has the property

$$\hat{T}_a \psi(x) = \psi(x + a) \tag{3.2.13}$$

and the equation for the eigenfunctions and eigenvalues is

$$\hat{T}_a u(x) = \lambda u(x). \tag{3.2.14}$$

Eigenfunctions are of the form

$$u(x) = e^{ikx} f(x), \tag{3.2.15}$$

where $f(x)$ is a function that is periodic in a (thus $f(x) = f(x + a)$). This comes from Bloch's theorem and the fact that the translation operator commutes with the Hamiltonian. In order to find the eigenvalues, $\hat{T}_a$ is set to operate on $u(x)$, giving

$$\hat{T}_a u(x) = \hat{T}_a \left(e^{ikx} f(x)\right) = e^{ik(x+a)} f(x + a) = e^{ika} e^{ikx} f(x) = e^{ika} u(x),$$

$$\hat{T}_a u(x) = e^{ika} u(x). \tag{3.2.16}$$

The eigenvalues are thus equal to e^{ika}. By letting Kwant solve the eigenvalue problem for the translation operator, the k-values can be found for different energies and the band diagram can be plotted.

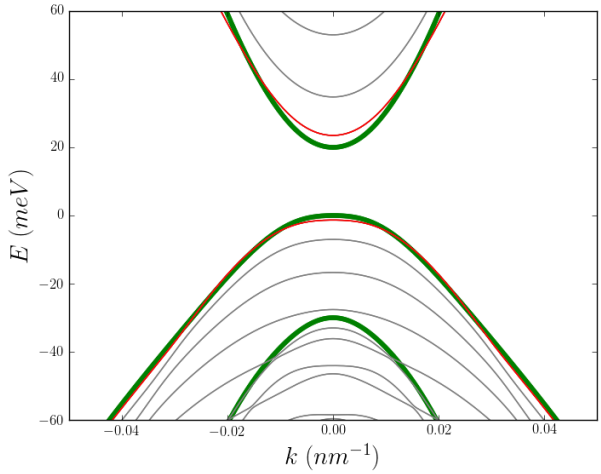

Figure **3.2.9.a:** $U_0 = 0\ eV$

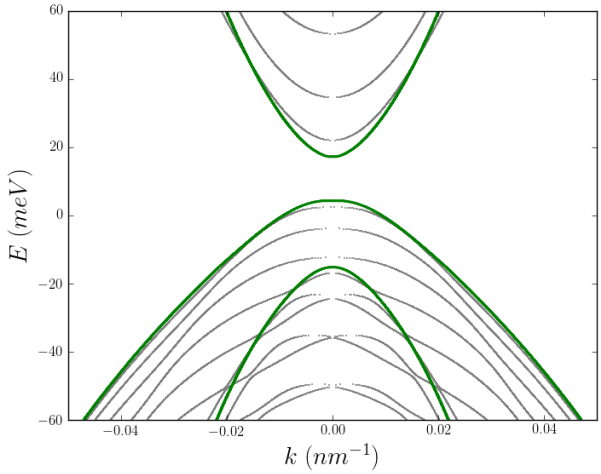

Figure **3.2.9.b:** $U_0 = 0.5\ eV$

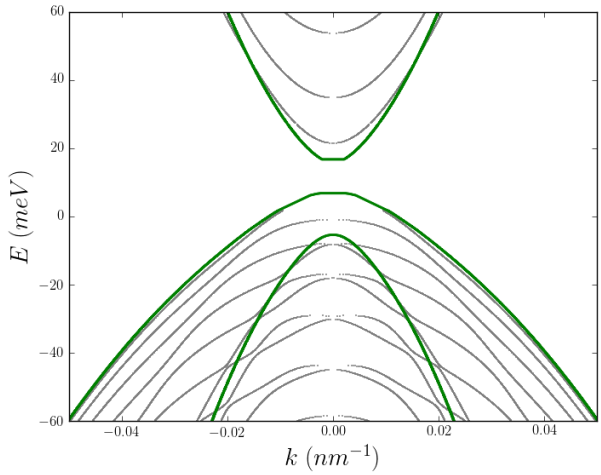

Figure **3.2.9.c:** $U_0 = 0.65\ eV$

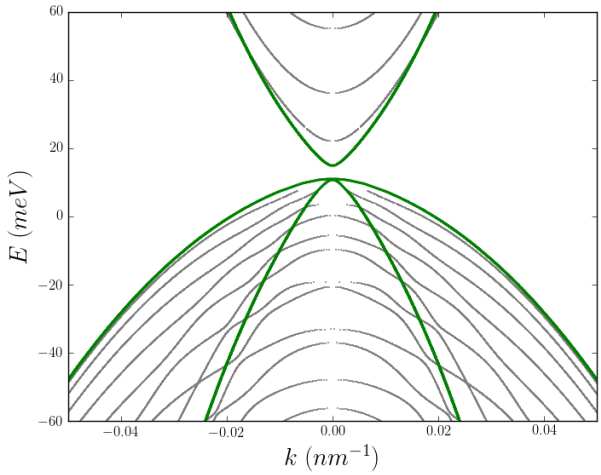

Figure **3.2.9.d:** $U_0 = 0.85\ eV$

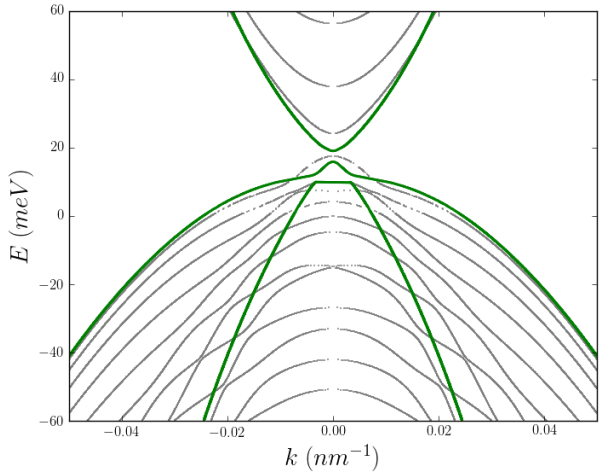

Figure **3.2.9.e:** $U_0 = 0.95\ eV$

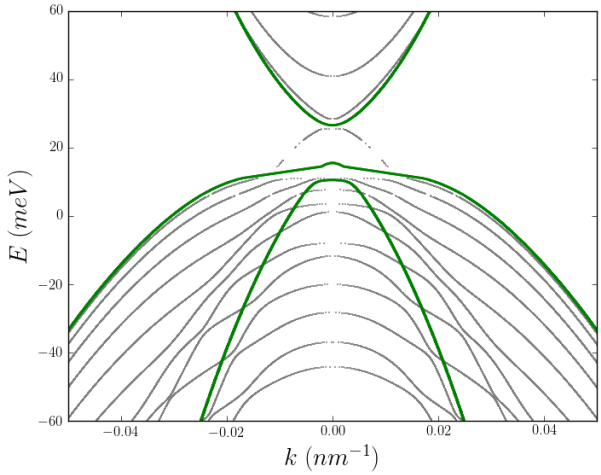

Figure **3.2.9.f:** $U_0 = 1.05\ eV$

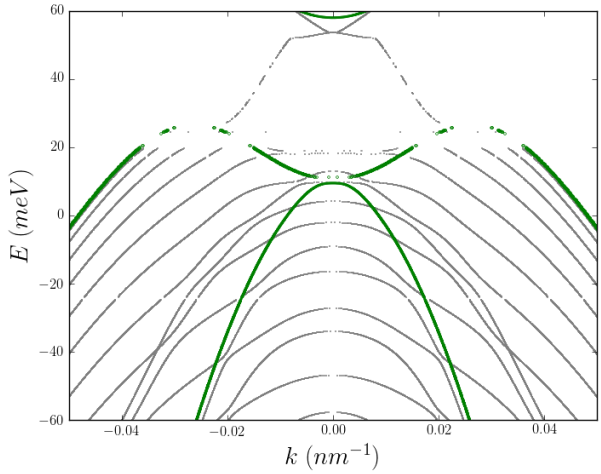

Figure **3.2.9.g:** $U_0 = 1.38\ eV$

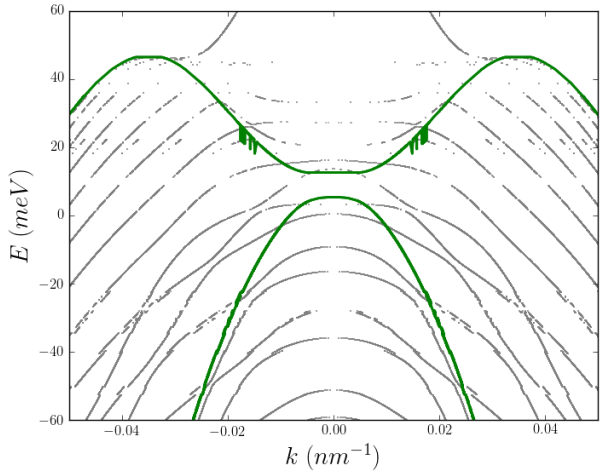

Figure **3.2.9.h:** $U_0 = 1.68\ eV$

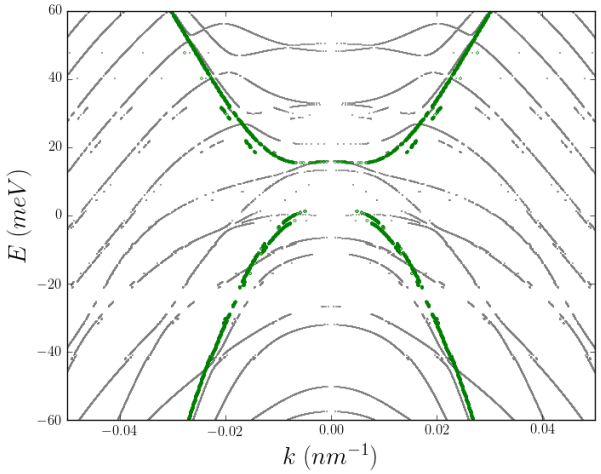

Figure **3.2.9.i:** $U_0 = 2.06\ eV$

Figure 3.2.9: The plots show the band structure for different disorder strengths. The Hamiltonian is the extended BHZ Hamiltonian in the insulating phase (see equations (3.2.8) and (3.2.9)) and the lattice constant is 5 nm. The first order self-consistent Born approximation is the method used to simulate the effect of disorder.

Figure 3.2.9 shows the band structures for different disordered strengths of the extended BHZ Hamiltonian. The points in the energy direction are evenly spaced, which can cause the top and bottom of the bands appear to be a bit limited in points. Further the algorithm to calculate the self-energy does not always converge causing some white gaps and off track points.

The process seen in figure 3.2.9 is similar to that of figure 3.2.4. In the clean limit there are no edge states in the gap. When the disorder strength increases, the band gap decreases. At a U_0-value a bit higher than 0.85 eV the gap closes and by further increasing the disorder strength the gap opens again. After the gap-reopening there are edge states that lie inside the bulk insulating gap. The disorder has turned the ordinary insulator band structure into that of a topological one. After the disorder strength becomes larger the green electron band (the upper band) moves out of the picture while the middle green band stretches;

the hole-like parts move upwards while the electron-like part hardly moves. As U_0 increases the grey hole bands rise. Lastly, the green hole band (bottom band) moves downwards.

From the band structures the behaviour of conduction plots (G versus U_0), which could be made with a transport calculation, can be predicted. Such a prediction is qualitative, because the band structure does not incorporate the length of the sample and back scattering from the leads, which would influence transport. It is expected that the conduction plot would look similar to figure 3.2.2.a. For example, when the Fermi level is placed in the upper region of the band structure (e.g. $E_F = 40\ meV$), the conductance is equal to a certain number times the conductance quantum in the clean limit. It is expected that the conductance then decreases as U_0 increases, but a plateau is formed for a certain U_0-interval and finally the conductance decays to zero due to the rising hole bands as U_0 is increased further.

Similar figures as in figure 3.2.9 are made for the topological phase.

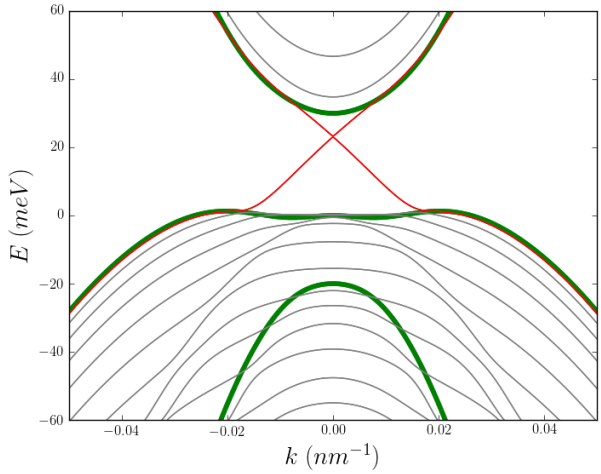

Figure **3.2.10.a:** $U_0 = 0\ eV$

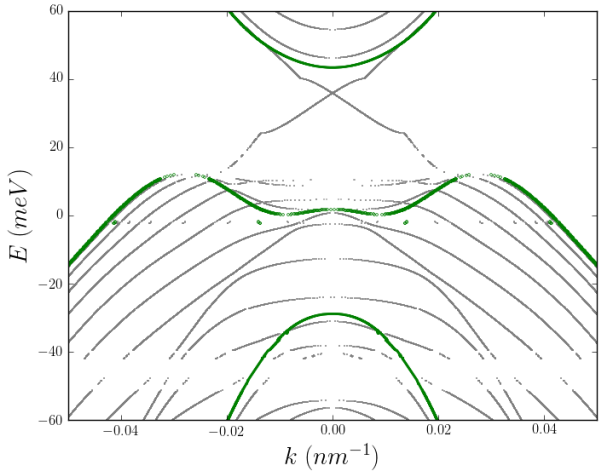

Figure **3.2.10.b:** $U_0 = 0.75\ eV$

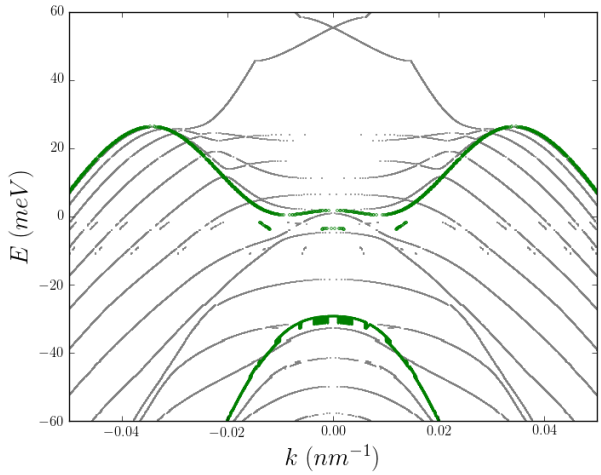

Figure **3.2.10.c:** $U_0 = 1.05\ eV$

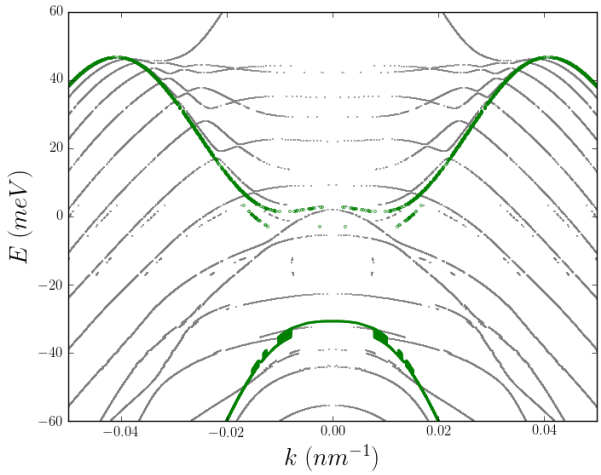

Figure **3.2.10.d:** $U_0 = 1.38\ eV$

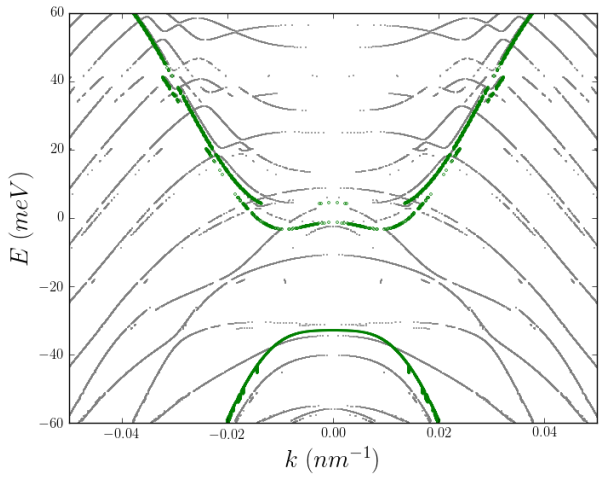

Figure **3.2.10.e:** $U_0 = 1.68\ eV$

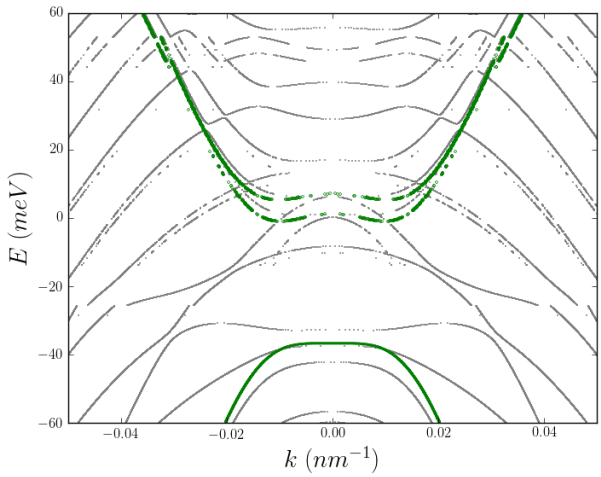

Figure **3.2.10.f:** $U_0 = 2.06\ eV$

Figure 3.2.10: The plots show the band structure for different disorder strengths. The Hamiltonian is the extended BHZ Hamiltonian in the topological phase (see equations (3.2.8) and (3.2.9)) and the lattice constant is 5 nm. The effect of disorder is taken into account through application of the 1SBA and by calculating the eigenvalues of the translation operator.

Figure 3.2.10.a shows the clean band structure for the topological phase. The edge states have been given a red color and the green bands mark the boundary of the bulk states. As the disorder strength, U_0, is increased the green electron band (the upper band) moves upwards, while the green hole band (the lower band) moves downwards. The middle green band stretches as the hole like parts move upwards and the middle part hardly moves.

Similar to the insulating phase (see figure 3.2.9), the behaviour of conduction plots can be predicted. This prediction is qualitative, because effects such as the length of the sample in the transport direction and back scattering from the leads are not incorporated in the band structure, but these effects do influence the transport calculation. It is expected that the conduction plot would look similar to figure 3.2.2.c. For example, when the Fermi level is placed such that it crosses with the edge states in the clean limit (e.g. $E_F = 20\ meV$), the conductance is equal to two conductance quanta for $U_0 = 0\ eV$. When U_0 increases, the conductance is expected to remain robust at $2G_0$ over a large range of U_0-values until it decays to zero at high disorder strengths due to the rising hole bands.

4 Conclusion and discussion

In this research the effect of disorder was investigated. A material is often not clean, but instead has many impurities. These defects give rise to potentials that scatter the electrons. In practice, the exact disorder configuration of a material is almost always unknown. For this reason, are experimental observations often best represented by ensemble averages. The members of an ensemble, which typically all have a different realisation of the disorder configuration, are averaged. In order to create the members of the ensemble and subsequently derive equations and make simulations, assumptions were made about the impurities. In the larger part of this work, the impurities are assumed to have a delta shape. The impurity amplitudes were often defined to have a zero mean and delta-correlation.

One of the mathematical tools needed were Green's functions. The (retarded) Green's function could be written as a series, called the Born series, in which every term represented how many times an electron scatters off the impurities. The Green's function could be averaged analytically over the disorder realisations, giving the impurity averaged Green's function. Defining the self-energy simplified the formula's and resulted in a short equation for the impurity averaged Green's function, which was

$$G^+(\bar{k}, E) = \frac{1}{E + i\epsilon - H_0(\bar{k}) - \Sigma^+(E)}. \tag{4.1}$$

A first order approximation of the self-energy led to a self-consistent equation,

$$\Sigma^+(E) = a^6 n \tilde{U}_2' \lim_{\epsilon \to 0} \int \frac{d^3\bar{k}}{(2\pi)^3} \cdot \frac{1}{E + i\epsilon - H_0(\bar{k}) - \Sigma^+(E)}, \tag{4.2}$$

which was called the first order self-consistent Born approximation (1SBA). In this work $\Sigma^+(E)$ was calculated for different Hamiltonians. By adding the Hermitian part of $\Sigma^+(E)$ to the Hamiltonian, it could be observed how the band structure changed as a result of the disorder.

The calculation of the self-energy was facilitated by the Python software package Kwant[8]. The algorithm is repeated here, because it is at the core of this work. The Discretizer module for Kwant was used to determine the tight-binding versions of Hamiltonians. By using this software, the on-site and hopping energies can be found in an easy manner without going through elaborate work by hand. The next step was to use Kwant to build an infinite one dimensional chain. After making an initial guess for the self-energy and adding it to the on-site energies of the sites, the Green's function in real space was calculated at the origin. Depending on the dimensionality of the problem at hand, the next step is to carry out an integral or multiple integrals, but by using the 'trick', where you calculate the Green's function in real space at the origin, the evaluation of a rather difficult integral is circumvented and the problem is made much easier to solve. If equation (4.2) would be solved directly, which was also done as a verification for some Hamiltonians, one has to worry about the poles in the complex plane. Because equation (4.2) is self-consistent, the previously calculated $\Sigma^+(E)$ is replaced by the new one. By using an Anderson mixing scheme, often only a few iterations are typically necessary to find the self-energy. By using Discretizer and Kwant, it is often straightforward to make the algorithm work for many Hamiltonians. Inputs of the algorithm were typically a Hamiltonian, the disorder strength and a lattice constant. The Hermitian part of the self-energy was added to the Hamiltonian, however it should be kept in mind that the self-energy is energy-dependent and therefore the 'net' Hamiltonian is only valid at a certain energy. After diagonalisation only the states are kept at the energy at which the self-energy was evaluated. The results consisted of disordered band structures that revealed relevant physical insights.

The first Hamiltonian that was investigated, is the most simple one, namely that for a free particle in a 1D infinite space. The disorder caused the band to move downwards, but due to the energy dependence of the self-energy, this shift was largest at the lowest energy and negligible for high energies. The disorder created states below the original band.

The second studied system was a particle in a 1D infinite well. The results were similar to the first Hamiltonian, but the finiteness of the system allowed for comparison between the 1SBA and numerical

averaging. At low energies the numerical one showed an exponential tail, which could not be fabricated with the 1SBA, showing that the 1SBA is a rather crude approximation.

Next, two more complicated 1D Hamiltonians were analysed, displaying among other things that disorder can cause a band gap closing.

The last relatively simple Hamiltonian was for a particle in a 2D infinite system. The results were similar to that of a free particle in 1D infinite system. The band moved downwards with the largest shift at $k_x = k_y = 0$.

In the theory section is was attempted to find out how the disorder strength scales with the lattice constant. The approach was to scale the disorder strength, such that the mean free path length did not depend on the lattice constant. The result seemed logical and gave the expected results for 1D systems, but failed to show sensible results for 2D systems. Unfortunately, this matter remains unresolved in this work.

To make a step to more relevant physical systems, the BHZ Hamiltonian was introduced. The Hamiltonian is in the insulating phase, at the transition point or in the topological phase depending on the value of a parameter in the Hamiltonian. Disordered band structures were made for the insulating and topological phase. By constructing the band structure for several different disorder strengths, it could be visualised how the bands evolved under increasing disorder. Globally, for the bulk bands (green color in plots) it can be said that the electron band moved in the upwards direction (to higher energies), while the hole band moved downwards (to lower energies). Further, it became clear that when the Hamiltonian was set to the insulating phase and the disorder strength was increased, the insulating band structure turned into that of a topological one. It was seen that as the disorder strength increased, the band gap closed and reopened. After the reopening, there were edge states in the bulk insulating gap. Additionally, a transport calculation was done, where the sample had a rectangular shape. The most interesting feature of the conduction versus disorder strength plot was that when the Fermi level and disorder strength are placed within a certain range, the system is in the TAI phase. In this situation transport is along the edges, which was also confirmed by executing the transport calculation for different widths. The absence of width-dependence, when the system was in the TAI regime, indicated that transport was along the edges and not through the bulk. By repeating the transport calculation many times and plotting the variance of the conduction versus the disorder strength, it was concluded that the electrons, at the edge states, do not backscatter at all in the TAI phase, because the variance was nearly zero in this regime. The disordered band structures were in agreement with the transport calculation. The comparison could only be made qualitatively due to the fact that certain effects such as the sample length and back scattering from the leads are not incorporated in the band structure. However, based on the band structure alone, the shape of the conduction versus disorder strength plot could have been predicted. It was also observed that hole bands, rising from low to higher energies as the disorder strength was increased, caused the conduction to eventually go to zero. For example, when the parameters in the Hamiltonian were set to values such that the system was in the topological phase and the Fermi level was set such that it crossed with the edge states, one would expect that impurities, which do not break time reversal symmetry, have no effect on the conduction by the edge states. However, it was observed in the conduction versus disorder strength plot, that this robust conduction breaks down at high disorder strengths. The reason that this happened, could be seen in the disordered band structures. The edge states got 'buried' by the rising hole bands. Lastly, in this section $E(k = 0)$ was plotted versus the disorder strength. In these plots the TAI regime could be identified. The features of the $E(k = 0)$ versus disorder strength plots agreed with the transport calculation.

The last Hamiltonian that was studied, was the extended BHZ Hamiltonian. Just as for the BHZ Hamiltonian, the parameters of the extended Hamiltonian can be chosen such that the system is in the insulation phase, at the transition point or in the topological phase. The algorithm to calculate the disordered band structures is the same as for the previous Hamiltonians, but in order to speed up the calculations all the disordered states at a certain energy were found at once instead of doing the calculation per band. The disadvantage of this method is, that it is impossible to know which disordered states belong in which band. For this reason, the disordered band structures were displayed as scatter plots instead of line plots. Globally, for the bulk bands (green color in plots), it can be said that the electron band (top band) moved in the upwards direction to higher energies, the hole band (lower band) moved in the downwards direction and the

middle band stretched. The hole like parts moved upwards, while the middle part of the band hardly moved or moved slightly downwards. Further the behaviour of the disordered band structures of the extended BHZ Hamiltonian were similar to that of the BHZ Hamiltonian. When the Hamiltonian was set to the insulating phase and the disorder strength was increased, the band gap closed and reopened. After the reopening there were edge states in the bulk insulating gap. Thus, the disorder transformed the band structure from an ordinary state into a topological one.

The method used in this research, to calculate disordered band structures, is very general. It can be applied to other Hamiltonians (also 3D), which can possibly reveal interesting physical phenomena. As was demonstrated in this work, it is useful to visualize what happens to the band structure when disorder is turned on and its strength is varied.

References

[1] König, M., Buhmann, H., Molenkamp, L.W., Huhghes, T., Liu, C., Qi, X., Zhang, S., *The Quantum Spin Hall Effect: Theory and Experiment*, J. Phys. Soc. Jpn. **77** (2008)

[2] Ando, T., Matsumoto, Y., Uemura, Y., *Theory of Hall effect in a two-dimensional electron system*, J. Phys. Soc. Jpn. **39** (1975)

[3] Wakabayashi, J., Kawaji, S., *Hall effect in silicon MOS inversion layers under strong magnetic fields*, J. Phys. Soc. Jpn. **44** (1978)

[4] v. Klitzing, K., Dorda, G., Pepper, M., *New method for high-accuracy determination of the fine-structure constant based on quantized Hall resistance*, Phys. Rev. Lett. **45** (1980)

[5] Laughlin, R., *Quantized Hall conductivity in two dimensions*, Phys. Rev. B., **23** (1981)

[6] Bernevig, A., Hughes, T.L., Zhang, S., *Quantum Spin Hall Effect and Topological Phase Transition in HgTe Quantum Wells*, Science **314** (2006)

[7] Kreeft, M.B., *3 Band BHZ*, (2017)

[8] Groth, C.W., Wimmer, M., Akhmerov, A.R., Waintal, X., *Kwant: a software package for quantum transport*, New Journal of Physics **16** (2014)

[9] Haberman, R., *Applied Partial Differential Equations with Fourier Series and Boundary Value Problems*, 5th edition, (2014)

[10] Ventra, M.D., *Electrical Transport in Nanoscale systems*, (2008)

[11] Datta, S., *Electronic transport in mesoscopic systems*, (1995)

[12] Rammer, J., *Quantum Transport Theory*, (1998)

[13] Groth, C.W., Wimmer, M., Akhmerov, A.R., Tworzydło, J., Beenakker, C.W.J., *Theory of the Topological Anderson Insulator*, Phys. Rev. Lett. **103** (2009)

[14] Li, J., Chu, R., Jain, J.K., Shen, S., *Topological Anderson Insulator*, Phys. Rev. Lett. **102** (2009)

[15] Zhou, B., Lu, H., Chu, R., Shen, S., Niu, Q., *Finite Size Effects on Helical Edge States in a Quantum Spin-Hall System*, Phys. Rev. Lett. **101** (2008)

Appendices

Appendix A

Appendix A.1

In this appendix is shown for the time-independent case that interchanging the position of excitation with the position of measurement does not alter the Green's function; $G(\bar{r};\bar{r}') = G(\bar{r}';\bar{r})$. This also holds in the time-dependent case, although this is not proven here. The symmetry of interchanging the two positions is called Maxwell's reciprocity.

In order to proof this symmetry, Green's second identity is used, where the two functions in this identity are chosen to be $G(\bar{r};\bar{r}_1)$ and $G(\bar{r};\bar{r}_2)$, which gives

$$\int_V \left[u\hat{\mathcal{L}}\{w\} - w\hat{\mathcal{L}}\{u\}\right] d^3\bar{r} = \int_V \left[G(\bar{r};\bar{r}_1)\hat{\mathcal{L}}\{G(\bar{r};\bar{r}_2)\} - G(\bar{r};\bar{r}_2)\hat{\mathcal{L}}\{G(\bar{r};\bar{r}_1)\}\right] d^3\bar{r} = 0. \tag{A.1.1}$$

Because the Green's function satisfies homogeneous boundary conditions, the right hand side of equation (A.1.1) will be zero for any linear operator and any boundary conditions.

Using $\hat{\mathcal{L}}\{G(\bar{r};\bar{r}_1)\} = \delta(\bar{r}-\bar{r}_1)$ and $\hat{\mathcal{L}}\{G(\bar{r};\bar{r}_2)\} = \delta(\bar{r}-\bar{r}_2)$,

$$\int_V \left[G(\bar{r};\bar{r}_1)\delta(\bar{r}-\bar{r}_2) - G(\bar{r};\bar{r}_2)\delta(\bar{r}-\bar{r}_1)\right] d^3\bar{r} = G(\bar{r}_2;\bar{r}_1) - G(\bar{r}_1;\bar{r}_2) = 0,$$

$$G(\bar{r}_2;\bar{r}_1) = G(\bar{r}_1;\bar{r}_2).$$

After renaming the end result is

$$G(\bar{r};\bar{r}') = G(\bar{r}';\bar{r}). \tag{A.1.2}$$

Appendix A.2

In this appendix is shown how the solution for the three dimensional non-homogeneous wave equation is expressed in terms of integrals over the Green's function.

The three dimensional non-homogenous wave equation is

$$\frac{\partial^2\psi(\bar{r},t)}{\partial t^2} - c^2\nabla^2\psi(\bar{r},t) = f(\bar{r},t). \tag{A.2.1}$$

The solution is subject to $\psi(\bar{r},0) = I(\bar{r})$ and $\left.\frac{\partial\psi(\bar{r},t)}{\partial t}\right|_{t=0} = v(\bar{r})$. The operator $\hat{\mathcal{L}}$ is identified as

$$\hat{\mathcal{L}} = \frac{\partial^2}{\partial t^2} - c^2\nabla^2. \tag{A.2.2}$$

It is straightforward to verify that $\hat{\mathcal{L}}$ is a linear operator. Further it is easier to use the source varying Green's function, which means that t and t' are interchanged and thus

$$\hat{\mathcal{L}}\{G(\bar{r},t';\bar{r}',t)\} = \frac{\partial^2 G(\bar{r},t';\bar{r}',t)}{\partial t^2} - c^2\nabla^2\ G(\bar{r},t';\bar{r}',t) = \delta(\bar{r}-\bar{r}')\delta(t-t'). \tag{A.2.3}$$

$G(\bar{r},t';\bar{r}',t) = 0$ for $t > t'$, because the Green's function can physically only take on non-zero values for times after the delta forcing has taken place (causality). Let $t_{initial} = 0$ and $t_{final} = t'+$, where $t'+$ means

a time larger than t'. Green's second identity for the wave equation can be worked out

$$\int_0^{t'+}\int_V \left[u\hat{\mathcal{L}}\{w\} - w\hat{\mathcal{L}}\{u\}\right] d^3\bar{r}dt = \int_0^{t'+}\int_V \left[u\frac{\partial^2 w}{\partial t^2} - w\frac{\partial^2 u}{\partial t^2}\right] d^3\bar{r}dt - c^2\int_0^{t'+}\int_V \left[u\nabla^2 w - w\nabla^2 u\right] d^3\bar{r}dt =$$
$$\int_V \left[u\frac{\partial w}{\partial t} - w\frac{\partial u}{\partial t}\right]_0^{t'+} - c^2\int_0^{t'+}\oiint \left[u\nabla w - w\nabla u\right]\cdot\hat{n}dSdt.$$

Now let $u = \psi(\bar{r},t)$ and $w = G(\bar{r},t';\bar{r}',t)$. Substituting this in the equation above gives

$$\psi(\bar{r}',t') = \int_0^{t'}\int_V G(\bar{r},t';\bar{r}',t)f(\bar{r},t)d^3\bar{r}dt + \int_V \left[v(\bar{r})G(\bar{r},t';\bar{r}',0) - I(\bar{r})\left.\frac{\partial G(\bar{r},t';\bar{r}',t)}{\partial t}\right|_{t=0} d^3\bar{r}\right] - c^2\cdot$$
$$\int_0^{t'}\oiint \left[\psi(\bar{r},t)\nabla G(\bar{r},t';\bar{r}',t) - G(\bar{r},t';\bar{r}',t)\nabla\psi(\bar{r},t)\right]\cdot\hat{n}dSdt.$$

Renaming the integration variables $\bar{r}$ and t to $\bar{r}'$ and t' and using the symmetry of the Green's function, $G(\bar{r},t;\bar{r}',t') = G(\bar{r}',t;\bar{r},t')$, gives

$$\psi(\bar{r},t) = \int_0^{t}\int_V G(\bar{r},t;\bar{r}',t')f(\bar{r}',t')d^3\bar{r}'dt' + \int_V \left[v(\bar{r}')G(\bar{r},t;\bar{r}',0) - I(\bar{r}')\left.\frac{\partial G(\bar{r},t;\bar{r}',t')}{\partial t'}\right|_{t'=0} d^3\bar{r}'\right] -$$
$$c^2\int_0^{t}\oiint \left[\psi(\bar{r}',t')\nabla' G(\bar{r},t;\bar{r}',t') - G(\bar{r},t;\bar{r}',t')\nabla'\psi(\bar{r}',t')\right]\cdot\hat{n}dS'dt'. \tag{A.2.4}$$

The solution of the differential equation can indeed be expressed as integrals over the Green's function. Three forcing terms are identified: the first term represents forcing by the source term of differential equation, the second term represents forcing by the initial conditions and the third term represents forcing by the boundary conditions.

Appendix B

Appendix B.1

In this appendix the integral self-consistency relation as presented by equation (3.1.12) is solved. This equation is repeated:

$$\Sigma^+(E) = a^2 n\tilde{U}_2' \lim_{\epsilon\to 0}\int_{-\pi/a}^{\pi/a}\frac{dk_x}{2\pi}\cdot\frac{1}{E + i\epsilon - 2t(1-\cos(ak_x)) - \Sigma^+(E)}. \tag{B.1.1}$$

Introducing a change in variables, $w = ak_x$, simplifies the integral to

$$\Sigma^+(E) = \frac{an\tilde{U}_2'}{2\pi}\lim_{\epsilon\to 0}\int_{-\pi}^{\pi}\frac{dw}{E + i\epsilon - 2t(1-\cos(w)) - \Sigma^+(E)}. \tag{B.1.2}$$

If the limit $\epsilon\to 0$ would be taken before integrating, there could be a discontinuity on the integration path. Originally ϵ was added to guarantee convergence. The integral is divided into three parts: $[-\pi, -R-\Delta R]$, $[-R+\Delta R, R+\Delta R]$ and $[R+\Delta R,\pi]$. If necessary, the variables R and ΔR can be chosen such that the poles of the integrand are excluded from the integral. The integration path is modified, such that the singularities are avoided by construction. If the singularities are not bothersome, R and ΔR can be be put to zero. During the recursive process of solving equation (B.1.2), the poles will move and every iteration step the value of R is adjusted accordingly.

The impurity density amplitudes are generated from a uniform distribution in the interval $[-U_0/2, U_0/2]$ and therefore $\tilde{U}_2' = U_0^2/12$. In order to fairly compare self-energies evaluated for different lattice constants,

the second moment of the uniform distribution, $U_0^2/12$, is scaled according to equation (2.3.74): $\tilde{U}'_{2,s} = \tilde{U}'_2/a = U_0^2/12a$. The scaling with a however does not effect the units of the equation. Further the impurity density, n, is equal to $1/a$. Taking the aforementioned comments into account yields

$$\Sigma^+(E) = I_1 + I_2 + I_3 = \frac{U_0^2}{24\pi a}\left(\int_{-\pi}^{-R-\Delta R} \frac{dw}{E - 2t(1-\cos(w)) - \Sigma^+(E)} + \int_{-R+\Delta R}^{R-\Delta R} \frac{dz}{E + i\epsilon - 2t(1-\cos(z)) - \Sigma^+(E)} + \int_{R+\Delta R}^{\pi} \frac{dw}{E - 2t(1-\cos(w)) - \Sigma^+(E)} \right). \tag{B.1.3}$$

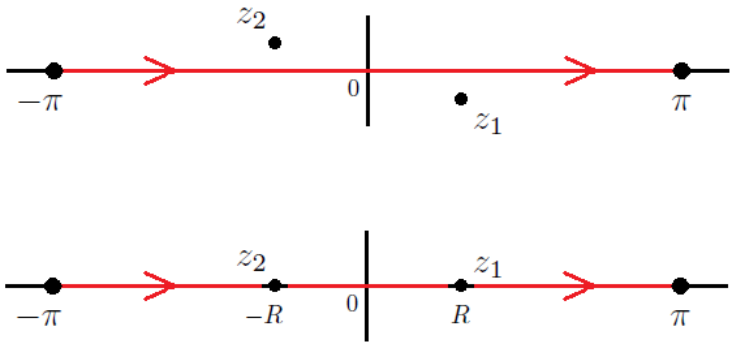

Figure B.1.1: The upper figure shows the case where the poles are in the complex plane and they pose no problem to the integration process. The lower figure shows the case where the poles are on the real axis and they disturb the integration progress.

For the first and the last integral the variable w is real and for a non-zero R and ΔR the integration variable $z = x + iy$, in the middle integral, is complex. The parameters E, ϵ, t, a and U_0 are real while Σ^+ is complex.

The coordinates of the possibly present poles are determined by equating the denominator of the integrand to zero:

$$E + i\epsilon - 2t(1-\cos(z)) - \Sigma^+ = 0,$$

$$E - 2t + 2t\ Re\{\cos(z)\} - Re\{\Sigma^+\} = 0 \quad \wedge \quad \epsilon + 2t\ Im\{\cos(z)\} - Im\{\Sigma^+\} = 0.$$

Rewriting, by using that $\cos(z) = \cos(x)\cosh(y) - i\sin(x)\sinh(y)$, where $x = Re(z)$ and $y = Im(z)$ gives

$$\cos(x)\cosh(y) = \frac{2t + Re\{\Sigma^+\} - E}{2t} \quad \wedge \quad \sin(x)\sinh(y) = \frac{\epsilon - Im\{\Sigma^+\}}{2t}. \tag{B.1.4}$$

The equations of (B.1.4) are rewritten into

$$y = \operatorname{arccosh}\left(\frac{A}{\cos(x)}\right) \quad \wedge \quad y = \operatorname{arcsinh}\left(\frac{B}{\sin(x)}\right), \tag{B.1.5}$$

where

$$A = \frac{2t + Re\{\Sigma^+\} - E}{2t} \quad \text{and} \quad B = \frac{\epsilon - Im\{\Sigma^+\}}{2t}. \tag{B.1.6}$$

It is known that $x, y \in \mathbb{R}$, but also that $x \in [-\pi, \pi]$ and that y does not have such a restriction. The strategy for numerics it is to scan x in the interval from $-\pi$ to π, then using the two equations of (B.1.5) to give two sets of possible y-values after which comparison will yield the solutions. From the cosine in the integrand and the fact that x runs from $-\pi$ to π, it is known that two or no poles will be found; furthermore if two poles are found that these poles are simple poles and that $z_2 = -z_1$.

If equation (B.1.4) has no solutions, there is no need to split the integral into three parts and the integrand is integrated from $-\pi$ to π with $\epsilon = 0$ and w is real. If equation (B.1.4) has two solutions, but the poles are far enough away from the real axis, there is no need to integrate around the singularities and $R = 0$ and $\Delta R = 0$; the integration path runs along the real axis. If equation (B.1.4) has two solutions and the poles are close to the real axis, the value for R is set to the real part of the pole in the right half plane and ΔR is set to some small real value.

In summary, values for a ($t = \hbar^2/2ma^2$), E and U_0 are chosen, $\epsilon = 0$ and a value for Σ^+ is guessed. Equation (B.1.5) is solved with these numbers resulting in no solutions or two solutions. If there are no solutions, equation (B.1.3) is applied with $R = 0$ and $\Delta R = 0$. If there are two solutions, but the absolute value of the imaginary part of the poles is large, R and ΔR are put to zero and the integration path runs along the real axis. If there are two solutions and the poles are close to the real axis, R is chosen to be equal to the real part of the pole in the right half plane and ΔR is set to a small real value. Subsequently equation (B.1.3) is applied with this non-zero value for R and ΔR. In all cases the value of Σ^+ is overwritten by the result of the integral and the process is repeated until the change in Σ^+ is below a reasonable threshold level. By using an Anderson mixing scheme, the solution is typically found after just a few iterations.

The results obtained with this algorithm agree with the method that involves equation (3.1.13) and the software package Kwant[8].

Appendix B.2

In this appendix the integral self-consistency relation as presented by equation (3.1.30) is solved. This equation is repeated:

$$\Sigma^+(E) = \frac{U_0^2}{48\pi^2} \lim_{\epsilon \to 0} \int_{-\pi/a}^{\pi/a} dk_y \int_{-\pi/a}^{\pi/a} dk_x \cdot \frac{1}{E + i\epsilon - H_0(k_x, k_y) - \Sigma^+(E)}, \tag{B.2.1}$$

with $H_0(k_x, k_y) = 2t(1 - \cos(ak_x)) + 2t(1 - \cos(ak_y))$ in which $t = \hbar^2/2ma^2$. Introducing the changes in variables $w = ak_x$ and $s = ak_y$ simplifies equation (B.2.1) to

$$\Sigma^+(E) = \frac{U_0^2}{48\pi^2 a^2} \lim_{\epsilon \to 0} \int_{-\pi}^{\pi} ds \int_{-\pi}^{\pi} dw \cdot \frac{1}{E + i\epsilon - 4t + 2t(\cos(w) + \cos(s)) - \Sigma^+(E)}. \tag{B.2.2}$$

The ϵ guarantees there is no singularity on the integration path. The inner integral is evaluated for different values of s in the interval $[-\pi, \pi]$ after which the outer integral can be calculated as a Riemann sum. Similar to Appendix B.1 the integral over w is divided into three parts: $[-\pi, -R - \Delta R]$, $[-R + \Delta R, R - \Delta R]$ and $[R + \Delta R, \pi]$. The integral is rewritten into

$$\begin{aligned} I_w = I_{w,1} + I_{w,2} + I_{w,3} = & \int_{-\pi}^{-R-\Delta R} \frac{dw}{E + i\epsilon - 4t + 2t(\cos(w) + \cos(s)) - \Sigma^+(E)} + \\ & \int_{-R+\Delta R}^{R-\Delta R} \frac{dz}{E + i\epsilon - 4t + 2t(\cos(z) + \cos(s)) - \Sigma^+(E)} + \int_{R+\Delta R}^{\pi} \frac{dw}{E + i\epsilon - 4t + 2t(\cos(w) + \cos(s)) - \Sigma^+(E)}. \end{aligned} \tag{B.2.3}$$

If necessary, the variable R and ΔR can be chosen such that the integration path is modified and the poles are avoided by construction. If the singularities are not on the original integration path, R and ΔR can be put to zero. During the recursive process of solving equation (B.2.2), the poles will move and every iteration step the value of R is adjusted accordingly.

For $I_{w,1}$ and $I_{w,3}$ the variable w is real and for $I_{w,2}$, if R and ΔR are non-zero, the integration variable $z = x + iy$ is complex. The parameters E, ϵ and t are real while Σ^+ is complex. Further the variable s has a real value in the interval $[-\pi, \pi]$. The picture that corresponds with I_w is the same as figure B.1.1.

The coordinates of the poles are determined by equating the denominator of the integrand to zero:

$$E + i\epsilon - 4t + 2t(\cos(z) + \cos(s)) - \Sigma^+ = 0,$$

$$E - 4t + 2t\ Re\left\{\cos(z)\right\} + 2t\cos(s) - Re\left\{\Sigma^+\right\} = 0 \quad \wedge \quad \epsilon + 2t\ Im\left\{\cos(z)\right\} - Im\left\{\Sigma^+\right\} = 0.$$

Rewriting, by using that $\cos(z) = \cos(x)\cosh(y) - i\sin(x)\sinh(y)$, where $x = Re(z)$ and $y = Im(z)$ gives

$$\cos(x)\cosh(y) = \frac{4t + Re\left\{\Sigma^+\right\} - E - 2t\cos(s)}{2t} \quad \wedge \quad \sin(x)\sinh(y) = \frac{\epsilon - Im\left\{\Sigma^+\right\}}{2t}. \tag{B.2.4}$$

The equations of (B.2.4) are rewritten into

$$y = \operatorname{arccosh}\left(\frac{A}{\cos(x)}\right) \quad \wedge \quad y = \operatorname{arcsinh}\left(\frac{B}{\sin(x)}\right), \tag{B.2.5}$$

where

$$A = \frac{4t + Re\left\{\Sigma^+\right\} - E - 2t\cos(s)}{2t} \quad \text{and} \quad B = \frac{\epsilon - Im\left\{\Sigma^+\right\}}{2t}. \tag{B.2.6}$$

It is known that $x \in [-\pi, \pi]$ and that y does not have such a restriction. The variable x is scanned in the interval from $-\pi$ to π, then using the two equations of (B.2.5) to give two sets of possible y-values after which comparison will yield the solutions. From the cosine in the integrand and the fact that x runs from $-\pi$ to π, it is known that two or no poles will be found; furthermore if two poles are found that these poles are simple poles and that $z_1 = -z_2$.

If equation (B.2.5) has no solutions, there is no need to split the integral into three parts; R and ΔR are put to zero and the integrand is integrated from $-\pi$ to π with $\epsilon = 0$ and w is real. If equation (B.2.5) has two solutions, but the poles are far enough away from the real axis, there is no need to modify the integration path and R and ΔR are zero. If equation (B.2.5) has two solutions and the poles are close to the real axis, the value of R is set equal to the real part of the pole in the right half plane and ΔR is set to a small real value, consequently the integration path runs along the real axis avoiding the singularities.

In summary, values for a ($t = \hbar^2/2ma^2$), E and U_0 are chosen, $\epsilon = 0$ and a value for Σ^+ is guessed. Further a value of s between $-\pi$ and π is picked. Equation (B.2.5) is solved with these numbers resulting in no solutions or two solutions. If there are no solutions, equation (B.2.3) is applied with R and ΔR equal to zero. If there are two solutions, but the absolute value of the imaginary part of the poles is large, R and ΔR are put to zero and the integration path runs along the real axis. If there are two solutions and the poles are close to the real axis, R is chosen to be equal to the real part of the pole in the right half plane and ΔR is set equal to a small real number. Subsequently equation (B.2.3) is applied with this non-zero value for R and ΔR. In all cases the value of I_w is stored and the process is repeated with a different value of s. When a reasonable amount of I_w-values for different s-values has been calculated, the self-energy can be found by

$$\Sigma^+(E) = \frac{U_0^2}{48\pi^2 a^2} \sum_{s=-\pi}^{\pi-\Delta s} \frac{I_w(s + \Delta s, \Sigma^+(E)) + I_w(s, \Sigma^+(E))}{2}\ \Delta s. \tag{B.2.11}$$

The value of Σ^+ is overwritten by the result and the process is repeated until the change in Σ^+ is below a threshold level. By using an Anderson mixing scheme, the solution is typically found after just a few iterations.

The results obtained with this algorithm are the same as with the method that involves equation (3.1.32) and the software package Kwant[8].

Appendix C

In this appendix the mean free path length is estimated for a continuous volume of arbitrary dimension in which a fixed number of delta impurities have been placed.

The starting point is Fermi's golden rule, which is equal to

$$\Gamma_{i\to f} = \frac{2\pi}{\hbar}\sum_f \left|\langle f|\,\hat{H}_{int}\,|i\rangle\right|^2 \delta(E_i - E_f). \tag{C.1}$$

The initial and final state are plane waves with wave vectors $\bar{k}$ and $\bar{k}'$ respectively, thus $\psi_i = \frac{1}{\sqrt{L^d}} e^{i\bar{k}\cdot\bar{r}}$ and $\psi_f = \frac{1}{\sqrt{L^d}} e^{i\bar{k}'\cdot\bar{r}}$, where d is the dimension. The matrix element is now calculated with $\hat{H}_{imp} = \sum_p \alpha_p \delta(\bar{r} - \bar{r}_p)$, giving

$$\left|\langle f|\,\hat{H}_{int}\,|i\rangle\right|^2 = \langle f|\,\hat{H}_{int}\,|i\rangle\,\langle i|\,\hat{H}_{int}\,|f\rangle = \frac{1}{L^{2d}}\left[\int e^{-i\bar{k}'\cdot\bar{r}}\left(\sum_p \alpha_p\delta(\bar{r}-\bar{r}_p)\right)e^{i\bar{k}\cdot\bar{r}}d^d\bar{r}\right]\cdot$$
$$\left[\int e^{-i\bar{k}\cdot\bar{r}}\left(\sum_q \alpha_q\delta(\bar{r}-\bar{r}_q)\right)e^{i\bar{k}'\cdot\bar{r}}d^d\bar{r}\right] = \frac{1}{L^{2d}}\sum_{p,q}\alpha_p\alpha_q e^{i(k-k')\cdot\bar{r}_p}e^{-i(k-k')\cdot\bar{r}_q}.$$

The impurity average of the matrix element is taken. Using that $\mathbb{E}\left[\alpha_p\alpha_q\right] = 0$ if $p \neq q$ and $\mathbb{E}\left[\alpha_p^2\right] = \tilde{U}_2$ leads to

$$\left\langle\left|\langle f|\,\hat{H}_{int}\,|i\rangle\right|^2\right\rangle_{imp} = \frac{\tilde{U}_2}{L^{2d}}\cdot N,$$

$$\left\langle\left|\langle f|\,\hat{H}_{int}\,|i\rangle\right|^2\right\rangle_{imp} = \frac{n\tilde{U}_2}{L^d}. \tag{C.2}$$

The calculated matrix element is put into equation (C.1), giving

$$\Gamma = \frac{2\pi n\tilde{U}_2}{\hbar L^d}\sum_{k'}\delta(E_k - E_{k'}). \tag{C.3}$$

The density of states is defined as

$$D(E_k) = \frac{1}{L^d}\sum_{k'}\delta(E_k - E_{k'}). \tag{C.4}$$

Therefore:

$$\Gamma = \frac{2\pi n\tilde{U}_2}{\hbar}D(E_k). \tag{C.5}$$

The mean free path length can be calculated with

$$l_{free} = v_F\cdot\tau_{free} = \frac{v_F}{\Gamma} = \frac{v_F\hbar}{2\pi n\tilde{U}_2}\frac{1}{D(E_k)}.$$

Rewriting, by using that $v_F = \sqrt{\frac{2E_F}{m}}$, yields

$$l_{free} = \frac{\hbar}{2\pi n\tilde{U}_2}\sqrt{\frac{2E_F}{m}}\frac{1}{D(E_k)}. \tag{C.6}$$

The mean free path length is inversely proportional with the second moment of the disorder amplitude distribution and inversely proportional with the impurity density.